STUDY OF FLUX TRANSFER EVENTS OBSERVED AT THE EARTH'S MAGNETOPAUSE BY THEMIS SATELLITES

Marcos Vinicius Dias Silveira

Doctorate Thesis of the Graduate Course in Space Geophysics, guided by Drs. Daiki Koga, and Walter Demetrio Gonzalez Alarcon, approved in march 03, 2015.

URL of the original document:
<http://urlib.net/8JMKD3MGP3W34P/3HTKPG5>

INPE

São José dos Campos

2015

STUDY OF FLUX TRANSFER EVENTS OBSERVED AT THE EARTH'S MAGNETOPAUSE BY THEMIS SATELLITES

Marcos Vinicius Dias Silveira

Doctorate Thesis of the Graduate Course in Space Geophysics, guided by Drs. Daiki Koga, and Walter Demetrio Gonzalez Alarcon, approved in march 03, 2015.

URL of the original document:
<http://urlib.net/8JMKD3MGP3W34P/3HTKPG5>

INPE

São José dos Campos

2015

Aprovado (a) pela Banca Examinadora em cumprimento ao requisito exigido para obtenção do Título de *Doutor(a)* em

Geofísica Espacial/Ciências do Ambiente Solar-Terrestre

Dr.   Alisson Dal Lago

Presidente / INPE / São José dos Campos - SP

Dr.   Daiki Koga
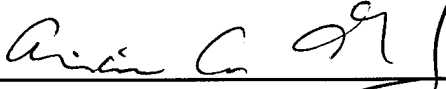
Orientador(a) / INPE / São José dos Campos - SP

Dr.   Walter Demetrio Gonzalez Alarcon
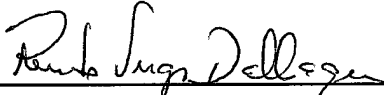
Orientador(a) / INPE / SJCampos - SP

Dra.   Alícia Luisa Clúa de Gonzalez Alarcon

Membro da Banca / INPE / SJCampos - SP

Dr.   Renato Sérgio Dallaqua

Membro da Banca / INPE / São José dos Campos - SP

Dr.   Fernando Jaques Ruiz Simões Junior

Convidado(a) / UFPEL / Pelotas - RS

Dra.   Flávia Reis Cardoso

Convidado(a) / EEL - USP / Lorena - SP

Este trabalho foi aprovado por:

( ) maioria simples

(✓) unanimidade

Aluno (a):   *Marcos Vinicius Dias Silveira*

São José dos Campos, 03 de Março de 2015

To the memory of my mother Venilda Dias Silveira.

ACKNOWLEDGEMENTS

ABSTRACT

Magnetic reconnection is a fundamental plasma process defined as topological restructuring of magnetic fields due to changes in the connectivity of magnetic field lines. Although other phenomena, e.g., particle acceleration and heating, can happen concurrently associated with reconnection, it is the most important process because it allows the fast magnetic energy release in large scales. Flux transfer events (FTEs) are considered as a result of transient magnetic reconnection and are often observed in the vicinity of the Earth's magnetopause. Thus, the study on magnetic reconnection is one of the important issues for the solar wind-magnetospheric coupling process. The space physics community has been interested in FTEs since their discovery. Recently, computational simulations, and multi-point observations have provided advances to FTE generation and structure formation studies. In this work data collected by the THEMIS mission was used to investigate flux transfer events under multi-points observations, which allows to investigate the structure itself, how it influences external plasma dynamics and analyze their dynamics under magnetic reconnection location. Although the techniques presented here had been employed in previous studies, we believe that the analysis of equatorial FTEs using multi-point observations and of its subsequent motion have a big importance to better understand magnetic reconnection at the Earth's magnetopause. It was created a list of flux transfer events observed by THEMIS probes at the dayside of the magnetopause and characterized these events according to the solar wind parameters and magnetic reconnection locations. Also are presented case studies of FTEs observed at multi-point observations including representative signatures observed in dataset in this thesis.

Keywords: Flux transfer events. Magnetic field reconnection. Transient event. Magnetopause. Magnetosphere.

ESTUDO DE EVENTOS DE TRANSFERÊNCIA DE FLUXO OBSERVADOS NA MAGNETOPAUSA TERRESTRE PELOS SATÉLITES THEMIS

RESUMO

Reconexão magnética é um processo fundemantal de plasma definido como uma reestruturação topológica do campo magnético devido à mudanças na conectividade das linhas do campo magnético. Embora fenômenos como aceleração e aquecimento de partículas também ocorram no plasma, a reconexão magnética é o mais importante pois permite a rápida conversão de energia magética em grande escala. Eventos de tranferência de fluxo são considerados o resultado da reconexão magnética transiente e são frequentemente observados na vizinhança da magnetopausa terrestre. Portanto, estudos sobre a reconexão magnética são tópicos muito importantes sobre o acoplamento do sistema vento solar-magnetosfera. A comunidade da geofísica espacial têm interesse sobre os FTEs desde a sua descoberta. Recentemente, a simulação computacional e multi-observação de satélites têm permitido avanços na pesquisa sobre modelos de geração e estrutura dos FTEs. Neste trabalho, usou-se dados obtidos pelos satélites da missão THEMIS para investigar os FTEs sob aspectos da reconexão magnética. Emboras as técnicas apresentadas neste trabalho tenham sido empregadas em outros trabalhos, acredita-se que a análise de FTEs equatoriais através de multi-observações e o seu movimento subsequente sejam muito importantes para o entendimento da reconexão na magnetopausa terresetre. Portanto, foi analisada uma lista de FTEs no lado diurno da mangetopausa. Os eventos foram caracterizados de acordo com parâmetros do vento solar e de reconexão magnética.

Palavras-chave: Eventos de transferência de fluxo. Reconexão magnética. Eventos transientes. Magnetopausa. Magnetofera.

LIST OF TABLES

Page

LIST OF ABBREVIATIONS

ACE	–	Advanced Composition Explorer
ARTEMIS	–	Acceleration, Reconnection, Turbulence, and Electrodynamics of the Moon's Interaction with the Sun
BL	–	Boundary Layer
CME	–	Coronal Mass Ejection
DSL	–	Despun spacecraft
EFI	–	Electric field instruments
ESA	–	Ion and Electron Electrostatic Analyzers
FGM	–	Fluxgate Magnetometer
FTE	–	Flux Transfer Event
GSE	–	Geocentric solar ecliptic
GSFC	–	Goddard Space Flight Center
GSM	–	Geocentric Solar Magnetospheric
IMF	–	Interplanetary Magnetic Field
ISEE	–	International Sun-Earth Explorer
LLBL	–	Low Latitude Boundary Layer
MHD	–	Magnetohydrodynamic Theory
NASA	–	National Aeronautics and Space Administration
OMNI	–	Operating Missions as a Node on the Internet
SCM	–	Search Coil Magnetometer
SPFD	–	Space Physics Data Facilities
SST	–	Solid State Telescope
THEMIS	–	Time History of Events and Macroscale Interactions During Substorms
WIND	–	Understanding Interplanetary Dynamics

CONTENTS

1 INTRODUCTION

Most of the known matter in the universe is in ionized state (the so-called plasma), and plasma in nature, such as the Sun, interstellar gas clouds and the Earth's magnetosphere exhibit different dynamical phenomena arising from the effects of electric and magnetic forces. In the Earth's vicinity most of the charged particles derive their energy ultimately from the Sun or from local processes in the Earth's magnetosphere, these process are investigated by solar-terrestrial physics. There is a common characteristic of plasma phenomenona in laboratory experiments, the solar system and other regions of the universe. It is a mixture of two different regions of plasma and magnetic fields due to a phenomenon known as magnetic reconnection.

Magnetic reconnection is a fundamental plasma process defined as topological restructuring of magnetic fields due to changes in the connectivity of magnetic field lines[1] (PRIEST; FORBES, 2000). Magnetic reconnection is the most important process, because it allows the fast magnetic energy release in large scales.

In the Earth's magnetosphere, reconnection is responsible for mass, energy, and momentum exchange between magnetosphere and solar wind. Its consequence can be observed as a disturbance of plasma convection, injection of particles into high-latitude ionosphere, and magnetic field variations observed on the ground. The first model for magnetic reconnection in the magnetosphere was proposed by Dungey (1961). In this model the interaction between Earth's magnetosphere and southward interplanetary magnetic fields results in two null points of magnetic field at the dayside and night side of magnetosphere. The interaction efficiency (geoeffectiveness) depends on north/south interplanetary magnetic field orientation.

Although magnetic reconnection described by Dungey's model was confirmed directly by Paschmann et al. (1979) observations, the frequency of ocurrence of global and steady reconnection to the magnetopause crossings was much smaller than expected (PRIEST; FORBES, 2000). However, Haerendel et al. (1978) which studied high-latitude magnetopause measurements from HEOS 2 suggested that reconnection could occur in a "burst" mode. Meanwhile, Russell and Elphic (1978) observed a flux tube like structure interconnecting the magnetosphere and magnetosheath. Russell and Elphic dubbed these structures flux transfer events (FTE).

---

[1]Although there is no experiment to prove the existence of magnetic field lines, this concept helps to understand the magnetic field geometry and it is largely employed in the magnetic reconnection theory.

Space physics community has been interested in FTEs since their discovery. Recently, computational simulations and multi-point observations have provided advances to FTE generation and structure formation. Thus, the THEMIS mission was used to investigate flux transfer events under multi-point observations. Multi-point observations provide observations of different layers of an FTE, which allows to study the FTE's structure. Other possibility is to study how the FTE motion affects the ambient plasma and mangetic field.

1.1 Objectives

The Earth's magnetopause is an interesting laboratory to study space physics. The magnetopause magnetic reconnection process allows the transference of particles, momentum and energy from the solar wind to the magnetosphere. The consequent effects of reconnection is the disturbance in the magnetospheric plasma dynamics. Flux transfer events, which result from burst reconnection, also have an important role in local plasma dynamics. The THEMIS mission is a great tool to investigate structures like flux transfer events under multi-point observations, which allows to investigate the structure itself and how it influences external plasma dynamics. According to these facts the main objective of this thesis is to analyze the dynamics of flux transfer events observed at the Earth's magnetopause by THEMIS satellites under magnetic reconnection aspects.

Based on the main objectives here is possible list of specific objectives to be reached in this work.

- Obtain a list of flux transfer events with magnetic field and plasma parameters well defined;

- Investigate the relation of flux transfer events and solar wind parameters to understand the scenario where they occur;

- Compare tendency of flux transfer events' motion with predictions of Cooling model associated with the component reconnection model;

- Analyze plasma flow associated with flux transfer events' motion.

2 THEORETIC BACKGROUND

2.1 Plasma Concept

Plasma constitutes most of matter known in the universe. It is defined as a quasi-neutral gas composed of charged particles which exhibit a collective behavior. To satisfy the quasi-neutrality requirement the plasma must have about equal number of positive and negative charges per volume element. Such a volume must be large enough to contain a sufficient number of particles, yet small enough to not be affected for variation of macroscopic parameters such as density and temperature (BAUMJOHANN; TREUMANN, 1996). Thus, a particle, which has a Coulomb potential associated with its charge q,

$$\phi_C = \frac{q}{4\pi\epsilon_0 r}, \tag{2.1}$$

is shielded by the other charges in the plasma and assumes the Debye form,

$$\phi_D = \frac{q}{4\pi\epsilon_0 r} \exp\left(-\frac{r}{\lambda_D}\right), \tag{2.2}$$

where ϵ_0 is the free space permittivity and λ_D is the Debye length, i.e., it is the distance over which a balance is obtained between the thermal particle energy and the electrostatic potential energy resulting from any charge separation. The Debye length is a function of the particles temperature, T_ℓ, and the plasma density, $n_e \simeq n_i$,

$$\lambda_D = \left(\frac{\epsilon_0 \kappa_B T_\ell}{n_e e^2}\right)^{1/2}, \tag{2.3}$$

where $\ell = e, i$ means electrons and ions respectively. The temperatures are assumed $T_e \simeq Ti$, κ_B is the Boltzmann constant, and e is the electron charge. The Debye shielding effect is a characteristic of all plasmas, although it does not always occur in every media with charged particles. To be a plasma it is necessary that the physical dimensions of the system is large enough so that the particles exhibit a collective behavior. So, if L is a characteristic dimension of the plasma it must be,

$$L \gg \lambda_D, \tag{2.4}$$

which is called the first plasma criterion. Since the shielding effect is the result of the collective behavior inside a Debye sphere, it is also necessary a large number of particles. This is the second plasma criterion,

$$n_e \lambda_D^3 \gg 1. \tag{2.5}$$

When the medium contains neutral particles, they collide to charged particles and the medium reaches the equilibrium. For the electrons to remain unaffected, the average time between two collisions of electron-neutral particle, τ_n, must be larger than plasma frequency. This condition is the third condition for an ionized medium to behave as a plasma:

$$\omega_{pe} \tau_n \gg 1, \tag{2.6}$$

where e means electrons species. As mentioned previously, plasma constitutes most of the matter known in the universe. Of course, this could not be different in our solar system. In the Earth's neighborhood all matter above about 100 km altitude, in the ionosphere, the interplanetary space, and the Sun itself are in plasma state (BAUMJOHANN; TREUMANN, 1996).

2.2 Theoretical Approaches

In general the plasma dynamics can be described by solving the motion equation to each particle considering the electric and magnetic fields, together with other forces involved in the system. It is possible to solve plasma motions, but it is not practical, because of the big number of particles and sometimes it is more interesting to know the average quantities like density and temperature rather than individual velocity of each particle. Therefore, several theories have been used to study plasma dynamics, their approximations are dependent on the problem to be solved.

The single particle motion is the simplest approach description of plasma. It describes the motion of a single charged particle under the influence of external electric and magnetic fields. In this case the collective behavior is neglected.

On the other hand the magnetohydrodynamic (MHD) approach neglects the single particle aspects. The approach assumes the local plasma equilibrium and the plasma as a conducting fluid with macroscopic variable, i.e. average density, velocity, and

temperature.

The multi-fluid approach is similar to MHD theory, but one improvement is the consideration of different particle species, where electron, proton and heavier ions are taken into account. It has advantage that the different particle species with different masses lead to charge separation field and high-frequency wave propagation.

One more complete approach is the kinetic theory. This approach describes at the development of the distribution function of the particles in phase space for the system under consideration, instead of solving the equation of motion for each charged particle.

2.3 Magnetic Reconnection

Magnetic reconnection is a fundamental plasma process defined as topological restructuring of magnetic fields due to changes in the connectivity of magnetic field lines. In MHD theory, the process of conversion and transference of energy can be classified as ideal or non-ideal. The ideal processes, as kink instability, convert magnetic energy into kinetic energy without magnetic dissipation, while non-ideal processes, i.e. magnetic reconnection can convert magnetic energy into kinetic energy and heat (PRIEST; FORBES, 2000).

The MHD theory is based on conservation principles and state equation, where electric and magnetic fields must satisfy the Maxwell's equations. The first MHD equation is the continuity equation, which guarantees the mass conservation for a classical plasma,

$$\frac{\partial n}{\partial t} + \nabla \cdot (n \, \mathbf{v}) = 0, \tag{2.7}$$

where n is the numerical density and $\mathbf{v}$ is the plasma flow velocity.

The second MHD equation is the momentum conservation equation, which considers the plasma velocity, particle density, and the electromagnetic force which act in the plasma.

$$\frac{\partial (n \, m \, \mathbf{v})}{\partial t} + \nabla \cdot (n \, m \, \mathbf{v} \, \mathbf{v}) = -\nabla \cdot \mathcal{P} + \rho \, \mathbf{E} + \mathbf{j} \times \mathbf{B}, \tag{2.8}$$

where $\mathcal{P}$ is the plasma pressure tensor, ρ is the electric charge density, m is the fluid

mass, $\mathbf{E}$ is the electric field, $\mathbf{B}$ is the magnetic field, and $\mathbf{j}$ is the electric current density.

The third MHD equation is energy conservation equation,

$$\frac{\partial}{\partial t}\left[n\,m\left(\frac{1}{2}v^2 + w\right) + \frac{B^2}{2\,\mu_0}\right] = -\nabla \cdot \mathbf{q}, \tag{2.9}$$

where v is flow speed, B is the magnetic field strength, w is the enthalpy of the fluid, and $\mathbf{q}$ is the heat flux density vector (BAUMJOHANN; TREUMANN, 1996).

Manipulating these equations together with Maxwell's laws and neglecting small current densities and quadratic terms in velocity it leads to the Generalised Ohm's law:

$$\mathbf{E} + \mathbf{v} \times \mathbf{B} = \eta\mathbf{j} + \frac{1}{n\,e}\mathbf{j} \times \mathbf{B} - \frac{1}{n\,e}\nabla \cdot \mathcal{P}_e + \frac{m_e}{n\,e^2}\frac{\partial\mathbf{j}}{\partial t}, \tag{2.10}$$

where η is the electrical resistivity of the plasma which is considered as a scalar, the electron pressure tensor $\mathcal{P}_{\rceil}$, m_e and e are the electron mass and electron charge, respectively.

In general, several assumptions are done to simplify the Ohm's law. Assuming that $\mathbf{j}$ is stationary ($\partial\mathbf{j}/\partial t = 0$), the cyclotronic frequency of electrons (ω_{ce}) smaller than the collision rate between electron and ions (ν_{ei}) leads to $\mathbf{j} \times \mathbf{B} = 0$. Neglecting the electron pressure gradient ($\mathcal{P}_e = 0$), leads to more familiar Ohm's law,

$$\eta\mathbf{j} = \mathbf{E} + \mathbf{v} \times \mathbf{B}. \tag{2.11}$$

Through the Ohm's law in the form of Equation 2.11 it is possible to obtain an equation which characterizes the magnetic field embedded in plasma, that is called the general induction equation:

$$\frac{\partial\mathbf{B}}{\partial t} = \nabla \times (\mathbf{v} \times \mathbf{B}) + \frac{1}{\mu_0\,\sigma}\nabla^2\mathbf{B}, \tag{2.12}$$

where $\sigma = 1/\eta$. The plasma and magnetic field behaviors are described by relative importance of the terms in the right hand side. The first term in the equation tells

us about the convection of the plasma and the magnetic field and the second term tells us about the magnetic diffusion in the plasma.

In an ideal MHD the plasma conductivity is high, almost infinite, and the diffusion term can be neglected. In this case the magnetic field stays frozen in the plasma, that is, one element of plasma connected to a magneitc field line will remain connected to it in all subsequent instants (LAKHINA, 2000). This result also suggests that the magnetic induction in a closed circle will not change even though each point within the curve moves with different velocities. Thus, the induction equation is,

$$\frac{\partial \mathbf{B}}{\partial t} = \nabla \times (\mathbf{v} \times \mathbf{B}). \tag{2.13}$$

When the second term is dominant, the induction equation become a pure diffusion equation,

$$\frac{\partial \mathbf{B}}{\partial t} = \frac{1}{\mu_0\,\sigma}\nabla^2\mathbf{B}. \tag{2.14}$$

since the coefficient $1/\mu_0\sigma$ is inversely proportional to the electric conductivity. Thus, a magnetic field frozen in a not-high conductivity plasma, with finite σ, results in ohmic losses and the currents that are responsible for the magnetic decay away, implying the magnetic energy conversion into plasma energy (PARKS, 2004).

A dimensional analysis can be done in the diffusion equation, considering the characteristic length (L_B) and time which the magnetic field varies. With this assumption the solution of Equation 2.14 is

$$B = B_0\,\exp\left(\pm t/\tau_d\right), \tag{2.15}$$

where τ_d is the characteristic time for the magnetic field diffusion, which is defined as:

$$\tau_d = \mu_0\,\sigma\,L_B^2. \tag{2.16}$$

If either σ tends to be infinite or L_B is very large, the magnetic field decay will be longstanding and the diffusion will be inefficient process.

The Magnetic Reynolds number can be used to determine which term of induction

7

equation is more important. Reynolds number is defined as the ratio between the two terms as,

$$R_m = \frac{|\nabla \times (\mathbf{v} \times \mathbf{B})|}{\left|\frac{1}{\mu_0 \sigma}\nabla^2\mathbf{B}\right|} = \mu_0 \, \sigma \, L_B \, V,$$

where V is the average speed perpendicular to $\mathbf{B}$. In an extreme case, for $R_m \ll 1$, the diffusion term is dominant. In the other extreme, $R_m \gg 1$, the convection term is dominant and the magnetic field and plasma move together with froze-in condition. Even in non-extreme cases, could have a region which L_B is very small so that the characteristic time is comparable to the time which the field lines leave the diffusion region. In that region, diffusion process takes place and the froze-in concept becomes invalid. Thus the magnetic reconnection happens only in the diffusion region, outside of it the magnetic field and the plasma flow remain traveling together (LAKHINA, 2000).

2.4   The Sun and the Interplanetary Medium

The Sun, which is the nearest star from the Earth, is a body of hot plasma. The energy released from the Sun is derived from thermonuclear fusion reactions of protons forming helium ions in its interior. The Sun is in gas state, but its gravitational force due to large mass (2×10^{30} kg) prevent the escape of most energetic particles. Its visible part, the atmosphere, is divided in three regions: The photosphere, with 500 km thick that emits most of the Sun's light, density of the $10^{23}m^{-3}$, and temperature of about 6,000 K; The chromosphere, with 10,000 km thick, a density of $10^{17}m^{-3}$, and temperatures of the order of 100,000 K; The outermost layer, the corona, which extends to millions of kilometers into space. The density is typically $10^{15}m^{-3}$ near the Sun and 10^7m^{-3} in the Earth's orbit. The Sun's magnetic field is due to the electrical currents in its internal layers. This magnetic field also extends into space traveling together with the plasma, it is often mentioned as interplanetary magnetic field (IMF). In the Sun's surface the magnetic field is typically of the order of 10^{-4} T, but in sunspot regions it can rise to 0.1 T.

Energetic plasma can escape from the Sun's atmosphere, this plasma is called solar wind. The solar wind is a conducting tenuous plasma composed mainly by protons and electrons, it is continuously emitted by the Sun with high speeds into interplanetary space. The solar magnetic field remains frozen in the plasma flow due to its

high conductivity. At the Earth's orbit distance (1 AU) the solar wind parameters are typically: ion densities $n_i \simeq 5cm^{-3}$, electron temperature $T_e \simeq 10^5$ K, magnetic field $B \simeq 5$ nT and flow speed $V \simeq 500$ km/s.

When the solar wind hits on the Earth's magnetic field it cannot simply penetrate into the geomagnetic domain. The solar wind is slowed down and deflected around the Earth. Since the solar wind hits an obstacle with supersonic speed, a shock region, called bow shock, is generated where the plasma is slowed and a substantial fraction of the particles' kinetic energy is converted into the thermal energy. The region of thermalized subsonic plasma between the bow shock and the Earth's magnetic field is called magnetosheath. The plasma in this region is denser and hotter than solar wind plasma and the magnetic field strength has higher values in this region.

2.5 The Earth's Magnetosphere

The magnetosphere results from the interaction of the IMF and solar wind with the Earth's magnetic field. As it was discussed before, the solar wind cannot simply penetrate into the geomagnetic field region, thus it is deviated around it. In a perspective the Earth's magnetosphere is a cavity in the solar wind, and the dynamic pressure of the solar wind compressed the outer part of the magnetic field in the dayside and stretches it in the night side, called magnetotail.

Figure 2.1 shows the magnetosphere regions and magnetospheric currents. The magnetopause is the upper boundary of the magnetosphere, which separates the Earth's magnetic field and plasma originated in the Earth from the solar wind plasma. As in most of plasma boundaries a magnetopause current is generated in this layer due to rotation of the magnetic field.

Ring current is an electric current flowing toroidally around the Earth, centered at the equatorial plane and at altitudes of about 5 R_E. This is a very important current because during geomagnetic storms more particles than usual are injected from the tail region into the ring current.

Inner the magnetosphere there is plasmasphere, which is a region of dense cold-plasma population. It is located just outside the upper ionosphere. The plasmasphere coexists approximately in the same region as the radiation belts. There is no clear distinction between the radiation belts and ring-current particles. However, the radiation belts consist of particles in orbits around the Earth, from about 1000

km above the surface to a geocentric distance of about 6 R_E.

The magnetotail or magnetic tail is the region of the magnetosphere that stretches away from the sun behind Earth. The magnetotail acts as a reservoir of plasma and magnetic energy, and they can released into the inner magnetosphere during magnetic substorms. Plasma sheet current is in the center of the tail within a region of hot plasma that separates two regions with oppositely directed magnetic field called the tail lobes. The tail lobes are regions magnetically connected with the two polar regions of the Earth and are identified as north and south lobes.

Polar cusps and plasma mantles are regions directly adjacent and inward of the magnetopause. The polar cusp are regions where the magnetic field presents singularities and which the magnetosheath plasma has direct access to the ionosphere. The plasma mantle region represents a boundary to the magnetotail usually filled with solar wind plasma but with stretched magnetic field.
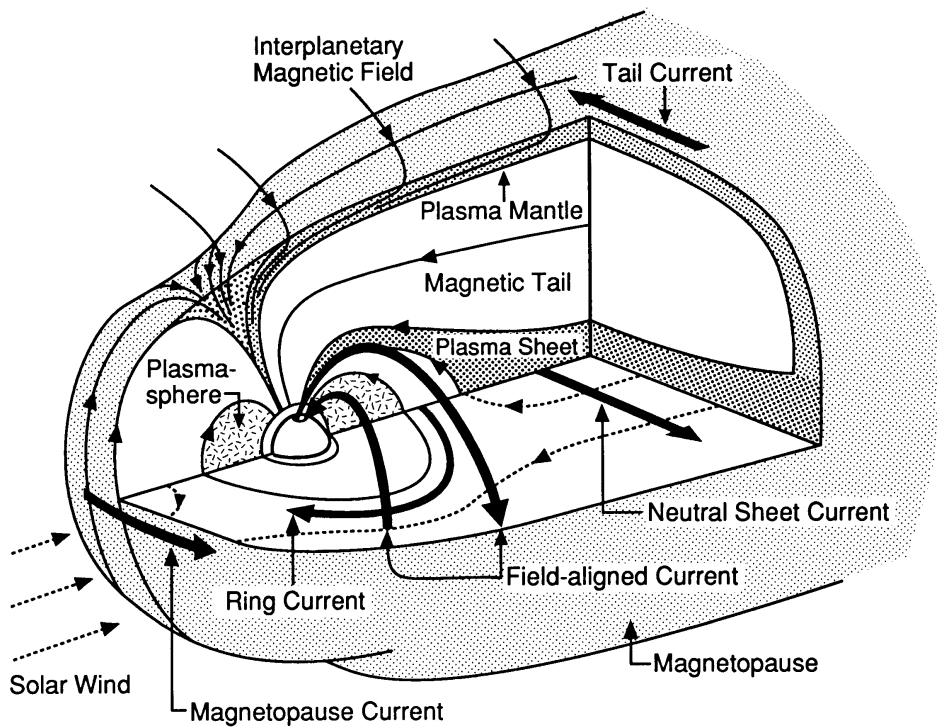
Figure 2.1 - Magnetosphere configuration.

SOURCE: Adopted from: Kivelson and Russell (1995).

2.6 Earth's Magnetosphere and Magnetic Reconnection

The first model for the magnetosphere was proposed by Chapman and Ferraro (1931), according to this model in which the Earth's magnetic field is always confined in a cavity, been reached by a cloud of plasma released on the Sun. In this model there are two magnetic null points in the cusps, and the transference of solar wind plasma is by viscous interaction generating a convection system in the magnetosphere and ionosphere. Later, Dungey (1961) proposed a new model for the interaction between Earth's magnetic field and interplanetary medium considering the plasma as magnetized fluid. In Dungey's model there are two magnetic null points also, but they are generated by the interconnection of the IMF and the geomagnetic field. These null points are located in the dayside magnetopause and the magnetotail.

Dungey's model predicts that, during southward IMF orientation, the magnetic reconnection should happen in the equatorial region and according to east-west component it will be tilted to the equator. On the other hand, equatorial reconnection is not favorable during northward IMF orientation. The region where the magnetic field points in opposite sense are located in the cusps. Therefore, the reconnection should happen in high latitudes during northward IMF. The importance of this model refers to the explanation of energy exchange between the solar wind and magnetosphere.

Since the IMF interacts with the Earth's magnetic field through reconnection, this process would disturb the equilibrium state of the magnetosphere. Following Gonzalez et al. (1994), the solar wind-magnetosphere coupling is responsible for disturbing the magnetospheric plasma convection and energy dissipation processes. Figure 2.2 shows a schematic of solar wind-magnetosphere coupling during the southward IMF orientation. Initially, the reconnection happens in the dayside magnetosphere, the field lines from the IMF connects with magnetospheric field lines in the subsolar region. Lorentz force acts over the reconnected field lines, pulling them up from the reconnection site. This "open" fields lines[1] (or flux tubes) contains a mixture of magnetosheath and magnetospheric plasmas, and they are dragged by the solar wind flow to anti-sunward direction. These field lines reach the Earth's magnetic tail, where energy and plasma flux are stored. The enhancement of solar wind/lobe magnetic pressure leads a second magnetic reconnection in the tail region. Then,

---

[1]The expression *open field lines* refers to magnetic line or flux tubes with one end at the Earth and the other end at the Sun.

part of the energy and plasma from the solar wind are released toward the Earth and the other part returns to the interplanetary medium. The part ejected into the magnetosphere reaches the inner magnetosphere like the ring current and modifies the natural plasma convection, causing disturbances as geomagnetic storms and substorms.

The magnetic field line convection from the dayside to the tail is also accompanied by the motion of the ionospheric footpoints of the magnetic field lines and the plasma tied to it across the polar cap. Likewise, the tail reconnection triggers the sunward convection of the footpoints in the dawn and duskside of low-latitude ionosphere, inside the auroral oval shown in Figure 2.3. These motions lead to a two-cell convection pattern in the polar ionosphere. Each pattern corresponds to an ionospheric electric field that is directed toward dusk in the northern polar cap, within the auroral oval is directed toward the pole on duskside and southward direction in the morning hours (BAUMJOHANN; TREUMANN, 1996).
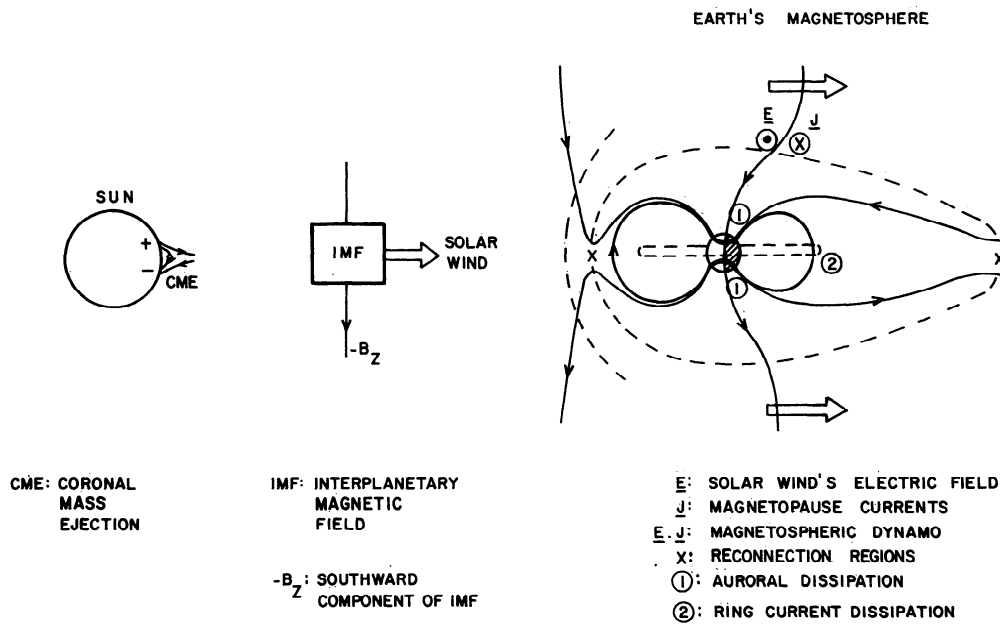
Figure 2.2 - Scheme of solar wind-magnetosphere coupling during a southward IMF orientation.

SOURCE: Adopted from: Gonzalez et al. (1994).
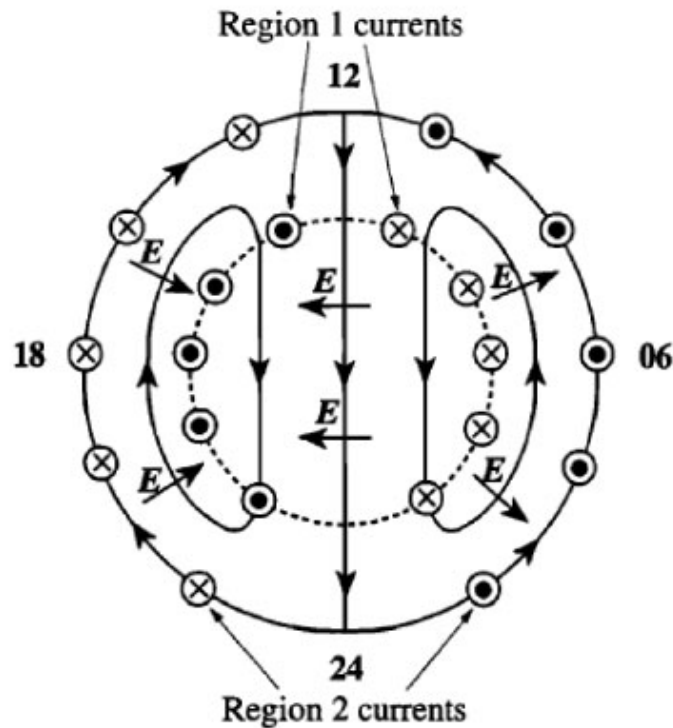
Figure 2.3 - Equipotential contours of the high-latitude electric field.

SOURCE: Adopted from: Cowley (2013).

As it was mentioned previously the magnetic reconnection can happen to both southward IMF and to northward IMF orientation. But, observations of an IMF purely northward or southward are rare and the most frequent situation are intermediate conditions due to a B_y component. There are two research schools with distinct hypotheses: One tells about the component reconnection model (GONZALEZ; MOZER, 1974) and (SONNERUP, 1974), which the reconnection line passes through the subsolar point and it is tilted according to relative values of B_y and B_z; The second school supports the hypotheses of the antiparallel reconnection, that is, magnetic reconnection happens only in the region where the shear angle of the magnetic fields is equal to 180°, or closer, which happens in high-latitude. Observations have been addressed to both kind of magnetic reconnection. In general the type of model adopted depend on the location where the reconnection is observed.

2.7 Flux Transfer Events

Although magnetic reconnection described by Dungey's model was confirmed directly by observations (PASCHMANN et al., 1979), the frequency of occurrence of global and steady reconnections to that of magnetopause crossings was much smaller than expected (PRIEST; FORBES, 2000). However, Haerendel et al. (1978) studying high-latitude magnetopause measurements from HEOS 2 suggested that reconnection could occur in a "burst" mode. Meanwhile, Russell and Elphic (1978) observed such structures in different latitudes, those are flux tube like structures interconnecting the magnetosphere and magnetosheath. Russell and Elphic dubbed these structures flux transfer events (FTE).

Russell and Elphic (1978) reported observations of FTEs using the initial results of ISEE 1 and 2 magnetometers. During two magnetopause crossings, interplanetary magnetic field was strongly southward and they observed a clear evidence for reconnection. Magnetic field data were projected in a local reference frame system (LMN system). The LMN boundary coordinate system has a component pointing outward to the nominal magnetopause $\mathbf{N}$, a component perpendicular to $\mathbf{N}$ and Z_{GSM} pointing dawnward $\mathbf{M}$ and the component $\mathbf{L}$ completes the right-handed set pointing northward. The LMN system will be discussed in Section 3.2.

Figure 2.4 shows an FTE example from ISEE 1 and 2 observations published by Russell and Elphic (1978). On November 8, 1977 the two spacecraft were in inbound orbit close to the magnetopause. The plots from top to bottom are magnetic field components (B_L, B_M, B_N), total magnetic field $|\mathbf{B}|$. The vertical dashed lines around 02:12 UT and 02:36 UT indicate the FTEs. One can see the variation in B_N component, which is almost zero outside the structure and oscillates from positive to negative values inside. At the same time $|\mathbf{B}|$ increases to magnetospheric levels. Other variations could be also observed in other components. After 02:54 UT the satellites encountered the boundary layer (BL) entering in the magnetosphere. The authors addressed the flux tubes arising from patchy reconnection upstream of the satellites.
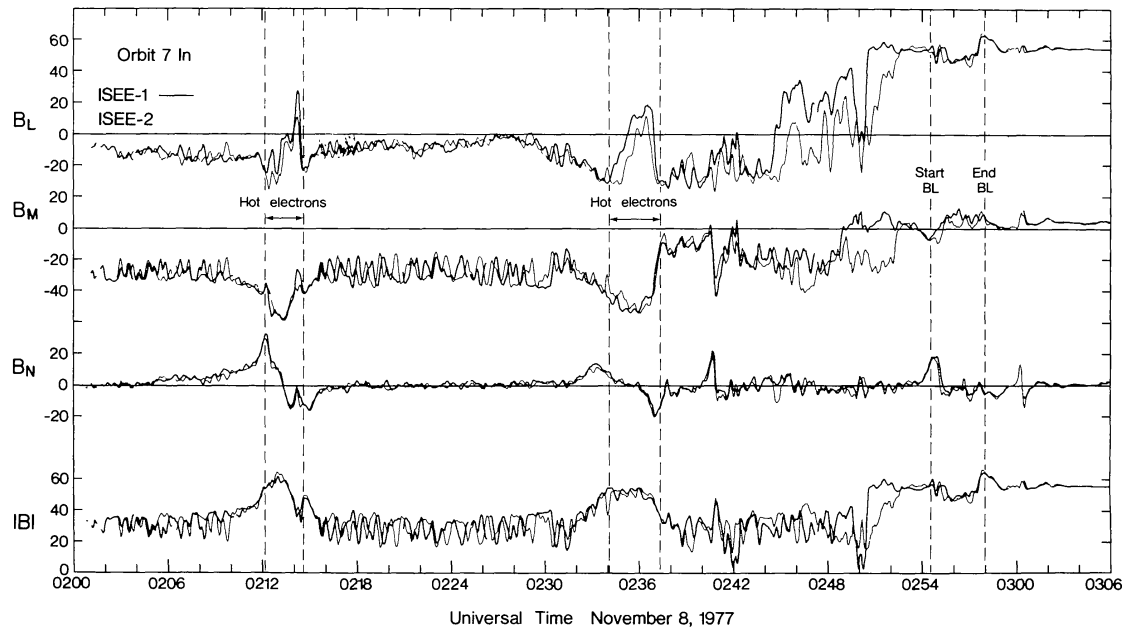
Figure 2.4 - Example of FTE observation by ISEE 1 (heavy line) and 2 (light line) measurements on inbound orbit. The data are in LMN system, from top to bottom are magnetic field components (B_L, B_M, B_N), total magnetic field $|\mathbf{B}|$.

SOURCE: Adapted from: Russell and Elphic (1978).

As results of these observations, the authors proposed the first generation model for FTEs, as illustrated in Figure 2.5. Magnetosheath field lines are depicted by oblique arrows (B_o) and the Earth's magnetic field lines vertical lines (B_i), as shown in Figure 2.5 (a). The magnetic reconnection may happen lower edge of the figure. After reconnection takes place, magnetic field lines from magnetosheath and magnetosphere are connected. The motion due to magnetic stress tension, $\mathbf{j} \times \mathbf{B}$, will pull the reconnected field lines out of the magnetosphere and sweep field lines up making bulge magnetic field shape. FTE's magnetic field orientation follows the Earth's magnetic field inside the magnetosphere and magnetosheath field in the magnetosheath. The structure presents a circular cross-section close to the magnetopause given a bipolar tangential magnetic field profile (RUSSELL; ELPHIC, 1978; RUSSELL; ELPHIC, 1979), as shown in the Figure 2.5 (b).

15
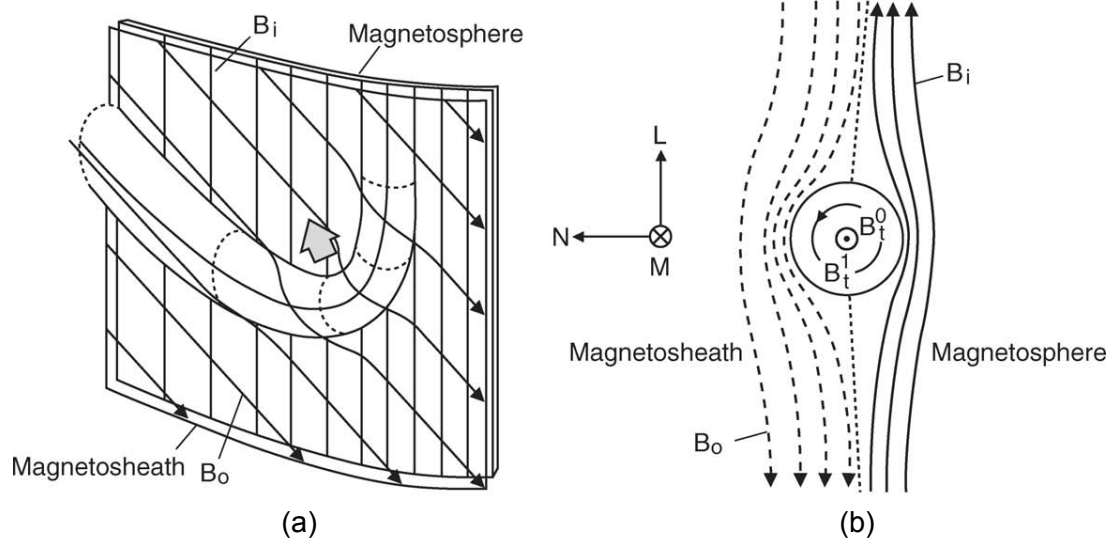
Figure 2.5 - Qualitative model of an FTE. Figure (a) shows magnetosheath field lines depicted by oblique arrows and the magnetospheric field lines depicted by vertical arrows. The magnetic reconnection may happens lower edge of the figure. After the reconnection cease, the flux tube is carried in the large arrow direction. Magnetosheath field lines not connected are dragged upward, wrapping the flux tube. Figure (b) shows the FTE's cross-section where the tangential magnetic field (B_t) gives the bipolar a bipolar magnetic field profile.

SOURCE: Adapted from: Russell and Elphic (1978) and Paschmann et al. (1982).

The polarity of B_N variation depends on relative motion between the FTE and the satellite which observed it. The FTEs observed by Russell and Elphic (1978) had a positive-negative B_N variation, termed "direct" or "standard" FTEs. This polarity is due to an FTE moving northward from the reconnection line. On the other hand, Rijnbeek et al. (1982) reported FTEs with opposite polarity, negative-positive, referred "reverse" FTEs. This polarity is consistent with an FTE moving southward from the reconnection line. These observations support the previous model that when magnetic reconnection occurs two FTEs are formed and they will move in opposite directions.

Paschmann et al. (1982) observed important characteristics about FTEs, such as an enhancement in magnetic field strength when compared to the ambient field; high energy particles from magnetospehere and low energy particle from magnetosheath are observed within FTEs; anti-correlation of density and temperature inside the structures. They noted also the violation of pressure balance across the FTEs, where

the total pressure inside the FTE is twice as large as outside. They addressed this effect by enhanced magnetic field tension of draped field lines.

Elphic (1995)' reviews suggest taxonomic classes for FTEs based on Paschmann et al. (1982) observations. Figure 2.6 shows idealized traces of magnetic field and plasma parameters to four FTE encounters in the magnetosheath (Figure (a)) and similar observation in the magnetospheric side (Figure (b)). From top to bottom are magentic field components (B_L, B_M, B_N), total magnetic field ($|\mathbf{B}|$), plasma density (N), bulk flow speed (V), temperature (T) and particle energy flux (EP). Bipolar variation in B_N component is a common feature among all observations, on the other hand, other parameters present big differences according to the observation location.
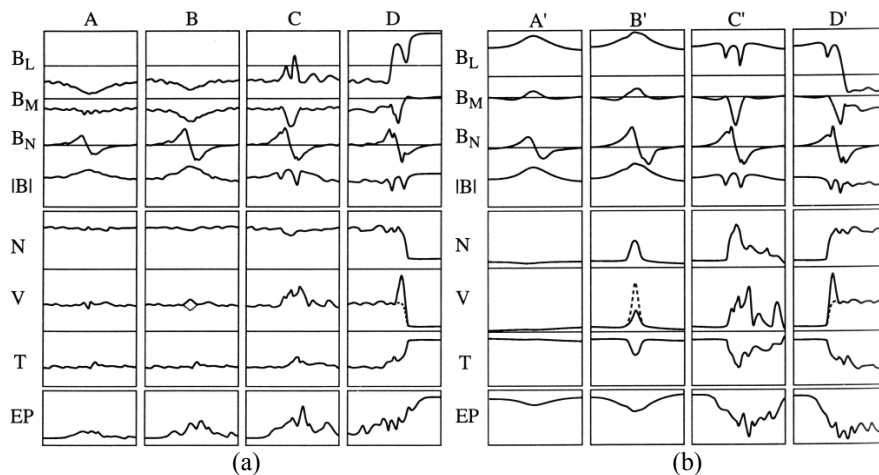
Figure 2.6 - Four taxonomic classes of FTEs by Paschmann et al. (1982) and Elphic (1995). From top to bottom are magentic field components (B_L, B_M, B_N), total magnetic field $|\mathbf{B}|$, plasma density N, bulk speed V, temperature T and energy particle flux EP.

SOURCE: Adopted from: Russell and Elphic (1978) and Paschmann et al. (1982).

According to Elphic (1995) and Fear (2006) the main characteristics to each class are described below.

- Class A (A') is characterized by a smooth enhancement of background B_L, it is possible to observe a weak tripolar B_M signature in the magnetospheric side. Variations in plasma parameters are almost null, except for energetic particle flux (EP) which increases in the magnetosheath side and decreases

in the magnetospheric side. These features indicate satellite trajectory just outside the FTE, and the signatures are due to the draped magnetic field.

- Class B (B') presents considerable excursion in B_M component besides B_L variation. Changes in plasma parameters are more considerable in the magnetospheric side. Bulk flow speed may or may not show accelerated flow. It is clearly seen the anti-correlation between density and temperature in the magnetospheric side. Class B (B') represents a crossing of the flux tube, but away from the point where the FTE touches the magnetopause.

- Class C (C') presents remarkable changes in magnetic field. In the magnetosheath side B_L has a northward excursion, while in the magnetospheric side there are minima values near the structure edges. B_M component has a large peak near the B_N inversion. Bulk flow speed is accelerated in both sides, the anti-correlation between density and temperature is present and energetic plasma flux increases (decreases) in the magnetosheath (magnetospheric) side. This class corresponds to a crossing near the region where FTE enters the magnetosphere. Magnetic field strength also presents minima values near the edges. Due to magnetic field peculiarity some authors termed this class as "crater" FTEs, e.g. Farrugia et al. (1988a) and Sibeck et al. (2008).

- Class D (D'), added by Elphic (1995), represents a magnetopause crossing during an FTE encounter. Basically, features of crossing from the magntosheath to magnetosphere (vice-versa) are superposition of FTE class C and magnetopause crossing signatures.

The increase of observational opportunity has allowed survey studies about FTE. Rijnbeek et al. (1984) and Berchem and Russell (1984) published survey studies of FTE location and occurrence. IMF observations showed that FTEs occurs almost exclusively during southward B_Z conditions. The north-south pattern and favorable IMF conditions were also reported in Rijnbeek et al. (1984). Using additional information about recurrence time approximately 8 minutes and FTE extension, the size of FTE was estimated as 1 R_E normal to and 2 R_E along the magnetopause (RIJNBEEK et al., 1984; SAUNDERS et al., 1984; LOCKWOOD; WILD, 1993). Daly et al. (1984) comparing the sign of B_N variation with energetic ion anisotropy along the magnetic field. Since direct FTEs are connecting and moving northward, they must present anti-parallel energetic ions escaping of the magnetosphere and opposite must

happen to reverse FTEs. However, they observed some cases in which the pitch angle observations indicated a connection with opposite hemisphere that indicated by B_N signature. They concluded that this can happen if the bulk speed, in opposite direction, exceed the Alfvén speed.

Dependence of occurrence of FTEs with IMF condition was studied by Kawano and Russell (1997b) and Kawano and Russell (1997a). They associated subsolar FTEs with southward IMF orientation and the influence of B_y affecting the motion of FTEs near noon. This component reconnection model was proposed by Gonzalez and Mozer (1974), it explains quite well the generation of equatorial FTEs. Kawano and Russell (1997a) extended the study to post-terminator FTEs during southward and northward IMF condition. They attributed the generation of the post-terminator FTEs during negative B_z to equatorial reconnection line, tilted according to IMF B_y. On the other hand, when IMF is northward, the cusp reconnection model can explain the observation. Other solar wind parameters like plasma beta, dynamic pressure, and Mach number did not affect strongly the rate of FTE occurrence (KUO et al., 1995).

With observational FTE studies, generation models have been proposed to explain the observation. First model was proposed by Russell and Elphic (1978) as explained earlier. Lee and Fu (1985) proposed a model which flux tubes are created by multiple reconnection lines at the dayside magnetopause. In this model the flux tube can be azimuthally extended along to the magnetopause plane, because there is no restriction to the x-lines' length, as shown in Figure 2.7.
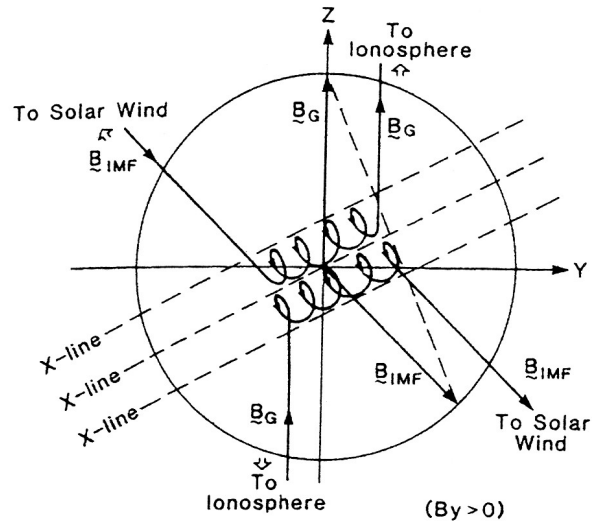
Figure 2.7 - Lee and Fu generation model of FTEs. Looking from the Sun, dashed lines represent the x-lines and the FTEs are represented by helical structures.

SOURCE: Adopted from: Lee and Fu (1985).

Different from Russell and Elphic's model, a single FTE can be generated by two reconnection lines in this model. The number of FTEs generated follows the relation $N_{FTE} = N_{x-line} - 1$, where N_{FTE} is the number of FTEs generated and N_{x-line} is the number of reconnection lines involved in the process.

Southwood et al. (1988) and Scholer (1988) independently proposed a model of FTE generation. In this model the reconnection on the magnetopause gives rise to bubble-like regions of plasma containing a twisted magnetic field with energetic particles in the outer layers. Figure 2.8 shows a sketch of steps for bubble formation. The field lines are antiparallel on both sides of the magnetopause (a). The onset of magnetic reconnection causes an plasma influx to the magnetopause near the reconnection site. Field lines will be bent due to localized flow (b). Panel (c) shows a high speed outflow region forming a bubble-like structure. This bubble is inflated by the plasma pressure around which the magnetic field was draped. The last stage is in (d), where the reconnection rate reduces to launch another outgoing front from the reconnection region which serves to slow down the inflow. After reconnection ceases the structures keep moving away from the reconnection site. This model is similar to Lee and Fu models in some aspects, however, the FTE happens from a single x-line.

As discussed previously, B_N polarity observed by a satellite passing through FTE gives some idea about the reconnection line location and to which hemisphere the FTE is connected. Kawano and Russell (1997b) have shown that the east-west motion of dayside FTEs is controlled by IMF B_y, corroborating with model of component reconnection, although this motion is affected as the plasma flow becomes super-Alfvénic. A more accurate work was done by Fear et al. (2005), which determined the FTE velocities using multi-spacecraft timing analysis and compared with predictions of Cooling et al. (2001) model. Their results show that observed FTE velocities were consistent with component reconnection on the lobe under strongly northward IMF.
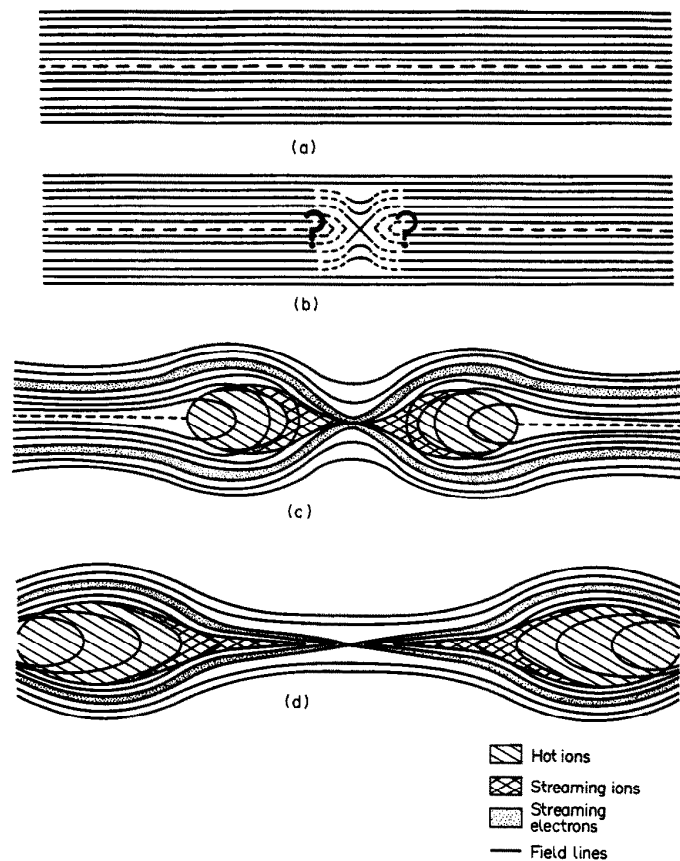
Figure 2.8 - Southwood et al. and Sholer generation model of FTEs. (a) A static neutral sheet (dashed line), where magnetic field (solid lines) are assume to be in opposite sense in both sides of the sheet. On (b) magnetic reconnection starts forming a single x-line. (c) Two bubbles arise from the x-line and (d) they move away from the reconnection region.

SOURCE: Adopted from: Southwood et al. (1988).

Sibeck and Lin (2011) also employed the Cooling et al. (2001) model to predict the location, motion and signatures of FTEs generated by component and high-latitude antiparallel reconnection for different IMF configurations and typical solar wind plasma parameters, as shown in Figure 2.9. Each row in the Figure shows the results obtained to FTEs generated by component reconnection (top line) and antiparellel reconnection (bottom line) under the IMF orientation indicated by bold arrows in the top panels. In the component reconnection cases (a - d), they assumed that reconnection occurs along a curve parallel to the current streamline initiated at the subsolar point (curves marked by crosses). For the antiparallel reconnection (e - h), the reconnection x-line starts along the point where the magnetosheath and magnetospheric magnetic fields are nearly antiparallel to each other (indicated by not connected crosses in the equator in Panel (e) and near the flanks in Panels (f - h)). The solid thin arrows represent the expected motion for direct FTEs and dashed arrows represent the expected motion for reverse FTEs. The magnetopause terminator is represented by the large circles and grey curves represent the draped magnetosheath field lines.
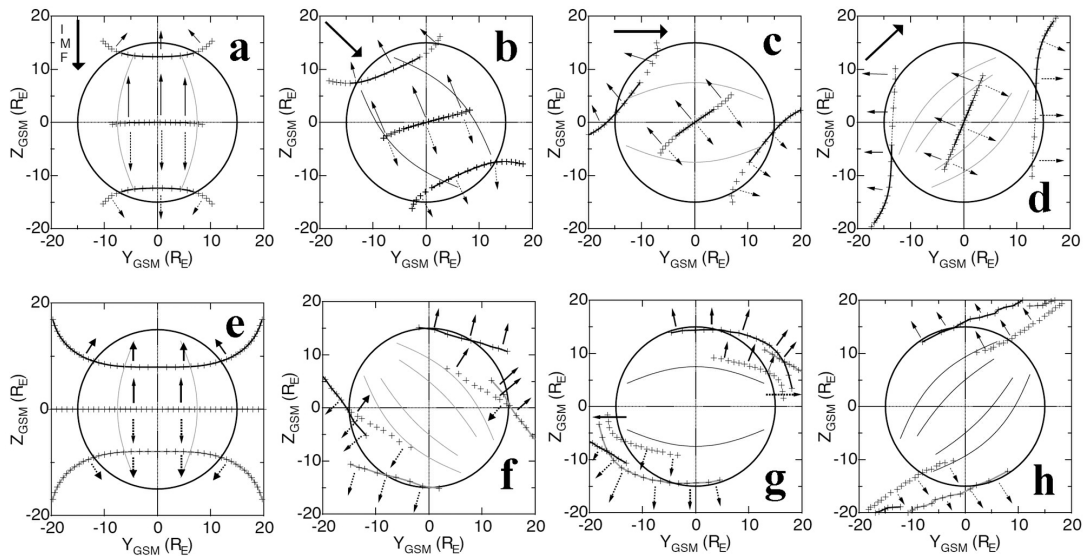
Figure 2.9 - FTE velocities predictions using Cooling model's by component reconnection (a - d) and by antiparallel reconnection (e - h). The circles shows the magnetopause terminator; the crosses indicate the initial reconnection line location; the bold arrows show the IMF orientation to each column; the gray lines indicate the magnetosheath magnetic field lines; the solid arrows show the motion of direct FTEs and the dashed arrows show motion of reverse FTEs.

SOURCE: Adopted from: Sibeck and Lin (2011).

In a general view, only for purely IMF southward there is a similarity (Panels a and e) but the FTEs motion predicted by two reconnection models are very different. For antiparallel reconnection it is very difficult to observe FTEs near the subsolar region because the high-latitude FTEs are blown away from the dayside to the magnetotail due to the magnetosheath flow. As a complement Collado-Vega (2013) used multi-spacecraft analysis to determine FTE velocities along the dayside and flank magnetopause and compared the observational results to the predictions presented by (SIBECK; LIN, 2011). Her results showed a good agreement with FTE velocities created by component reconnection model (COLLADO-VEGA, 2013).

3 INSTRUMENTATION AND DATA SET

3.1 The THEMIS Mission

The Time History of Events and Macroscale Interactions during Substorms (THEMIS) mission from NASA, was launched in 2007 to determine the trigger and large-scale evolution of substorms (ANGELOPOULOS, 2008). In the beginning, the mission was composed of five identically-instrumented satellites (probes) line up along the Earth's magnetotail. After 2009 two of them were migrated to the Moon's orbit to compose the ARTEMIS mission.

According to Angelopoulos (2008) the scientific objectives of THEMIS mission are divided in three priorities: the primary objective is to address the magnetotail science in order to establish the source and when the substorms begin; to determine how the individual components of the substorms interact; how they power the aurora; and to identify how local current disruption mechanisms couple to the geomagnetic storms. Secondary objectives include the Earth's radiation belts science, taken advantage of multi-point observations for tracking the motion of particle injection fronts through the magnetosphere; to determine radial gradients in phase space density to understand the variation in the electron flux variations; and to determine the extent of the wave fields that are proposed to accelerate the particles. And the tertiary objectives, where this work is included, address dayside interaction. From May to September 2007 the probes performed identical orbits with apogees in the dayside magnetosheath, as shown in Figure 3.1. The separation distances vary from 100's of km to one Earth radii, the probes provide observations to magnetic reconnection studies on micro- and meso-physics; magnetopause boundary layer structure and motion; and wave propagation in the magnetosheath.

The five THEMIS probes carry identical instruments to measure plasma and field parameters: Electric field instruments (EFI) which consist of four spherical sensors mounted on two pairs of 20 m and 25 m long Spin-plane Booms and provide measures of electric field in three dimensions. Fluxgate Magnetometer (FGM) measures the background magnetic field and its fluctuations (up to 64 Hz) in the near-Earth space (AUSTER et al., 2008). Search Coil Magnetometer (SCM) measures low-frequency magnetic field fluctuations and waves, its antennas cover the frequency bandwidth from 0.1 to 4 kHz. Ion and Electron electrostatic analyzers (ESA) measure plasma over the energy range from a few eV up to 30 keV for electrons and 25 keV for ions. Solid State Telescope (SST) measures superthermal particle distribution functions, namely the number of ions and electrons coming towards the spacecraft from speci-

fied directions with specified energies within the energy range from 25 keV to 6 MeV. Besides, THEMIS mission has ground based instruments such as all-sky imagers and ground magnetometers cover North America from Eastern Canada to Alaska.
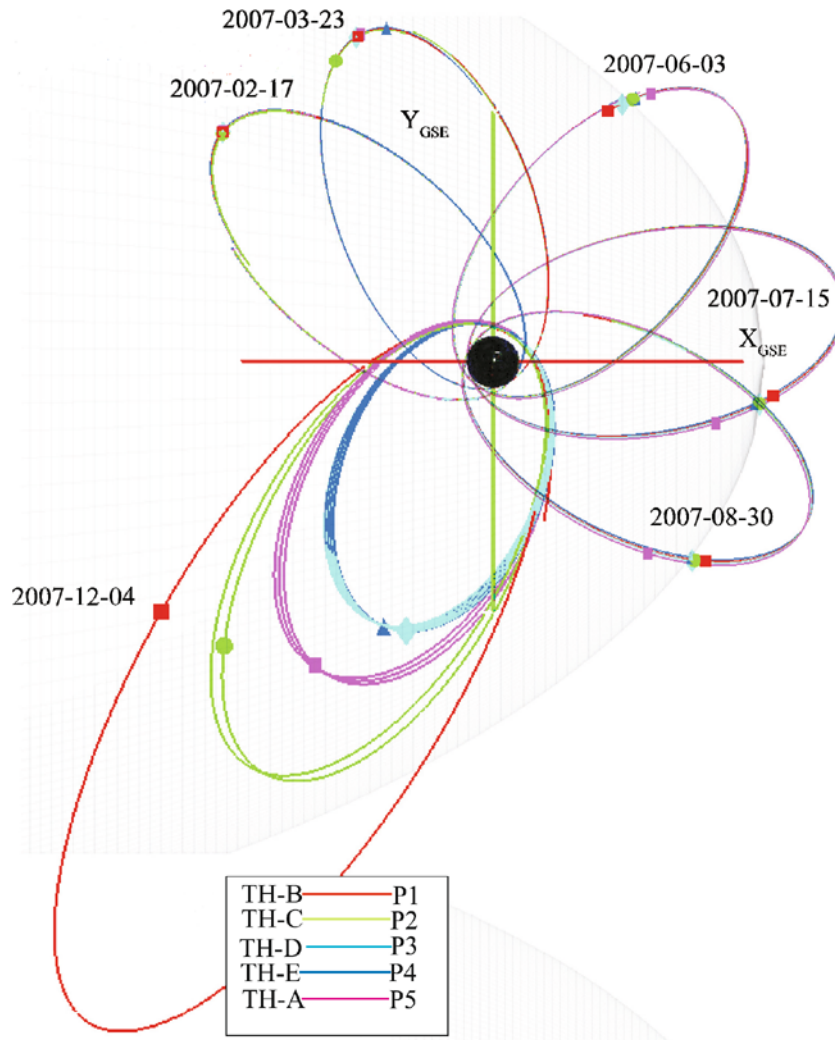
Figure 3.1 - Equatorial projection of TEHMIS orbits in 2007.

SOURCE: Adopted from: Angelopoulos (2008).

FGM instrument has two levels of data L1 (un-calibrated) and L2 (calibrated) in four resolution modes, low resolution (FGL), FGH (high-resolution), FGE (engineering data), and FGS (spin-resolution). ESA instrument also has two levels of data L0 and L2 three resolution modes, full mode with a high angular resolution and low time resolution; reduced mode with degraded angular resolution, high time resolution;

and burst mode with high angular resolution and high time resolution. In this work it was used calibrated data with FGS and FGL resolution for FGM instrument and reduced mode for ESA instrument. The data provide by the satellites are in Geocentric solar magnetospheric (GSM) coordinate system, which is based on Sun-Earth line. The X_{GSM} axis is toward the Sun and the Y_{GSM} axis pointing duskward, and the Z_{GSM} axis is the projection of the Earth's magnetic dipole axis (positive northward).

THEMIS data can be accessed directly through Space Physics Data Facilitie (SPDF) website or using THEMIS Science Data Analysis Software (TDAS, more recently SPEDAS). The TDAS software platform is a library of IDL routines which read data in CDF format (Common Data Format), as well as other data sets. TDAS is used to download, open, analyze and plot THEMIS data.

3.2 Boundary Coordinate System

To analyze magnetopause dynamics it is convenient to project the magnetic field vector and bulk flow velocity to boundary coordinate system (LMN), as shown in Figure 3.2. The advantage to use the local system instead of a global system like GSM is to reduce the field variations to two dimensions and simplifies their understanding. In this way, similar magnetic field features can be observed independently of the FTE location. In this work the LMN coordinate system was employed as Russell and Elphic (1978) did, where **N** is determined through the gradient of modeled magnetopause surface calculated to each probe location by

$$\mathbf{N} = \frac{\nabla r}{|\nabla r|} \tag{3.1}$$

where r is a function which describes the magnetopause. After **N** is determined, it is possible to obtain the other components, **M** is defined as

$$\mathbf{M} = \frac{\mathbf{N} \times \mathbf{Z}_{GSM}}{|\mathbf{N} \times \mathbf{Z}_{GSM}|}, \tag{3.2}$$

where $\mathbf{Z}_{GSM}$ is the north-south component in the GSM system. North-south component, **L**, is defined as

$$\mathbf{L} = \mathbf{M} \times \mathbf{N}. \tag{3.3}$$
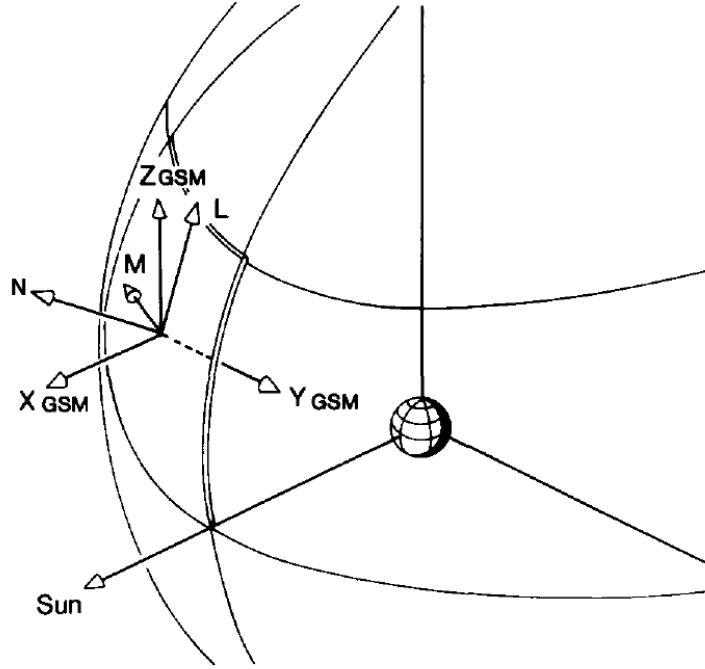
Figure 3.2 - Boundary coordinate system, where **N** component points outward to the local magnetopause, **L** component is the projection of the Earth's magnetic dipole field and the **M** component completes the right-handed set, pointing dawnward (**M** = **N** × **L**).

SOURCE: Farrugia et al. (1988b).

The magnetopause surface r is estimated by Shue et al. (1997) and Shue et al. (1998) model, which is empirical model to fit the shape and size of the magnetopause based on interplanetary parameters. The r function is determined by:

$$r = r_0 \left(\frac{2}{1 + \cos\theta} \right)^\alpha \tag{3.4}$$

where r_0 and α are the standoff distance and the level of tail flaring, respectively. The parameter r_0 is the distance whose the solar wind dynamic pressure and Earth's magnetic pressure are balanced at the subsolar point, and θ is the angle between the Earth-Sun line and the probe position. The values for r_0 and α can be obtained by:

$$r_0 = 10.22 + 1.29 \tanh[0.184(B_z + 8.14)](P_{dyn})^{-\frac{1}{6.6}}, \tag{3.5}$$

$$\alpha = (0.58 - 0.007B_z)[1 + 0.024]ln(P_{dyn})], \tag{3.6}$$

where B_z and P_{dyn} are the north-south magnetic field component and the solar wind dynamic pressure (ρv^2). This model assumes a symmetric magnetopause in YZ plane, so, r can be projected in $X = r\cos\theta$ and $R = r\sin\theta$, whit $R = \sqrt{Y^2 + Z^2}$. The numerical terms in the equations are empirical coefficients which better adjust the model's solution to the Shue et al. (1998) observations. So, it was used solar wind parameters obtained by OMNI data (it will be discussed in the next chapter) as input to Shue model. Using TDAS routine it is possible to determine the magnetopause position to each THEMIS probe location at the observation time and rotates the GSM magnetic field to boundary normal system. When the probe position did not coincide with the magneopause, it was assumed the expansion of it in the radial direction in order to estimate the normal direction.

3.3 FTE Selection Criteria

It was chosen the period from May to September 2007 to look for FTEs in THEMIS data. As discussed before, the probes performed identical orbits with apogees in the dayside of the magnetosheath and its separation was nearly the size of the FTE cross section in this period. Thus, the magnetic field vector and ion velocity were projected in the LMN system for all probes of each THEMIS magnetopause crossing. The criteria below were used to select the FTEs used in this thesis.

1 - Bipolar variation in B_N component around the variation of the total magnetic field;

2 - The amplitude of the bipolar signature must be larger than 10 nT;

3 - Ion velocity, density and temperature must be available;

4 - Criteria 1, 2, and 3 must be satisfied by at least two probes;

5 - The behavior of the magnetic field components must be one of those illustrated in Figure 2.6;

6 - Do not select other types of FTE like variability, i.e., a periodical variation

with more than one cycle in B_N. The bipolar signature of the normal component must have only one cycle.

These criteria restricted the number of events, on the other hand they can avoid the possibility of magnetopause oscillations or Kelvin-Helmholtz wave-like. The data set used has 63 FTEs observed close to the Earth's magnetopause. The FTEs' list is presented in Table 3.1, where are indicated the event number of the FTE, the ΔB_N polarity, the starting and ending time of the FTE events.

Table 3.1 - FTEs' list.

FTE	Polarity	Start Date	End Date
1	Direct	2007-05-01/05:56:00	2007-05-01/06:04:00
2	Direct	2007-05-06/11:30:00	2007-05-06/11:36:00
3	Reverse	2007-05-13/01:14:00	2007-05-13/01:20:00
4	Reverse	2007-05-17/00:58:00	2007-05-17/01:04:00
5	Reverse	2007-05-19/15:31:00	2007-05-19/15:35:00
6	Reverse	2007-05-19/16:31:00	2007-05-19/16:35:00
7	Reverse	2007-05-20/22:00:00	2007-05-20/22:04:00
8	Reverse	2007-05-20/22:20:00	2007-05-20/22:24:00
9	Reverse	2007-05-20/22:24:00	2007-05-20/22:28:00
10	Reverse	2007-05-20/22:25:00	2007-05-20/22:29:00
11	Reverse	2007-05-20/22:47:00	2007-05-20/22:52:00
12	Reverse	2007-05-21/15:48:00	2007-05-21/15:53:00
13	Reverse	2007-05-27/12:44:00	2007-05-27/12:49:00
14	Direct	2007-05-31/09:40:00	2007-05-31/09:45:00
15	Reverse	2007-06-05/02:37:00	2007-06-05/02:40:00
16	Reverse	2007-06-10/22:26:00	2007-06-10/22:31:00
17	Reverse	2007-06-10/22:31:00	2007-06-10/22:36:00
18	Reverse	2007-06-16/03:09:00	2007-06-16/03:13:00
19	Reverse	2007-06-16/03:29:00	2007-06-16/03:33:00
20	Reverse	2007-06-16/03:52:00	2007-06-16/03:57:00
21	Reverse	2007-06-16/04:00:00	2007-06-16/04:05:00
22	Reverse	2007-06-16/19:44:00	2007-06-16/19:48:00
23	Reverse	2007-06-17/10:20:00	2007-06-17/10:25:00
24	Reverse	2007-06-17/10:40:00	2007-06-17/10:46:00
25	Reverse	2007-06-17/10:40:00	2007-06-17/10:46:00
26	Reverse	2007-06-17/10:46:00	2007-06-17/10:50:00

Table 3.1 - FTEs' list: continuation.

FTE	Probes	Start Date	End Date
27	Direct	2007-06-26/14:30:00	2007-06-26/14:35:00
28	Direct	2007-07-07/01:50:00	2007-07-07/01:55:00
29	Direct	2007-07-07/16:20:00	2007-07-07/16:25:00
30	Direct	2007-07-10/06:55:00	2007-07-10/07:00:00
31	Reverse	2007-07-12/07:02:00	2007-07-12/07:06:00
32	Reverse	2007-07-12/07:07:00	2007-07-12/07:11:00
33	Direct	2007-07-20/16:11:00	2007-07-20/16:16:00
34	Direct	2007-07-28/13:00:00	2007-07-28/13:06:00
35	Reverse	2007-07-28/13:25:00	2007-07-28/13:30:00
36	Reverse	2007-07-30/14:22:00	2007-07-30/14:27:00
37	Reverse	2007-08-03/11:42:00	2007-08-03/11:50:00
38	Reverse	2007-08-03/12:19:00	2007-08-03/12:26:00
39	Reverse	2007-08-05/09:29:00	2007-08-05/09:34:00
40	Direct	2007-08-14/13:32:00	2007-08-14/13:38:00
41	Reverse	2007-08-17/03:10:00	2007-08-17/03:17:00
42	Reverse	2007-08-17/03:26:00	2007-08-17/03:29:00
43	Reverse	2007-08-17/03:30:00	2007-08-17/03:34:00
44	Reverse	2007-08-22/08:21:00	2007-08-22/08:27:00
45	Direct	2007-08-24/08:00:00	2007-08-24/08:04:00
46	Reverse	2007-08-26/07:48:00	2007-08-26/07:54:00
47	Reverse	2007-08-28/07:48:00	2007-08-28/07:54:00
48	Reverse	2007-08-28/07:58:00	2007-08-28/08:04:00
49	Reverse	2007-08-29/15:02:00	2007-08-29/15:08:00
50	Reverse	2007-08-30/04:47:00	2007-08-30/04:50:00
51	Reverse	2007-08-30/04:51:00	2007-08-30/04:54:00
52	Reverse	2007-08-30/04:59:00	2007-08-30/05:03:00
53	Reverse	2007-08-30/05:01:00	2007-08-30/05:06:00
54	Direct	2007-09-06/10:22:00	2007-09-06/10:25:00
55	Reverse	2007-09-06/10:37:00	2007-09-06/10:42:00
56	Direct	2007-05-01/06:22:00	2007-05-01/06:30:00
57	Direct	2007-06-08/22:15:00	2007-06-08/22:23:00
58	Reverse	2007-07-23/08:45:00	2007-07-23/08:56:00
59	Direct	2007-08-17/20:58:00	2007-08-17/21:08:00
60	Reverse	2007-06-14/03:58:00	2007-06-14/04:03:00
61	Reverse	2007-09-05/01:33:00	2007-09-05/01:38:00
62	Direct	2007-09-06/08:57:00	2007-09-06/09:02:00
63	Direct	2007-09-06/09:34:00	2007-09-06/09:38:00

4 FTEs OBSERVED BY THEMIS MISSION: GENERAL ASPECTS

4.1 Introduction

This chapter presents the results of the survey about FTEs' features and the ambient conditions in which they are observed. The solar wind condition during the observations are shown in Section 4.2. Then, in Section 4.3, the FTE events are investigated according to their spatial distribution associated with their magnetic structure and external parameters. In Section 4.4 a comparative study between the FTEs' motions and predictions from an empirical model is done. Finally in section 4.5, those FTEs which occurred during northward IMF are analyzed qualitatively.

The objective in this chapter is to present a scenario where the FTEs used in this research occur and when it is possible to compare such scenario with previous studies. Also, it is tried to understand their relation with IMF conditions and their subsequent dynamics.

4.2 Solar Wind Conditions

OMNI data were used in order to determine the solar wind conditions during FTE observations. It can be obtained from the GSFC/SPDF OMNIWeb interface at http://omniweb.gsfc.nasa.gov. The data source consists of measurements from two satellites located at the interplanetary medium, ACE and WIND. OMNI data set consists of 1-min and 5-min resolution, solar wind magnetic field and plasma data time-shifted to the Earth's bow shock nose. Time shifting analysis is based on the assumption that IMF data measured by a satellite at a given time and a place lie on a planar surface convecting with the solar wind, and it is assumed that the same values will be observed at a different place when the phase front sweeps over such location (KING; PAPITASHVILI, 2005). In this work, OMNI average data over 5 minutes to various plasma and IMF parameters, using 1-min data resolution, to each FTE observation were used.

Figure 4.1 shows histograms of IMF values during the FTEs' occurrence (color bars) and the IMF distribution during the whole period of observation (black line), that is, from May to September 2007. Figure 4.1 (a) shows the IMF strength $|\mathbf{B}|$ and (b), (c) and (d) show its GSM components B_{x-GSM}, B_{y-GSM} and B_{z-GSM}, respectively. For 60 of 63 FTEs observed, OMNI data are available. In general view, most of the events happen during typical IMF values. Histogram (a) shows that the majority of the events ($> 95\%$) occurs to $|\mathbf{B}| < 6nT$, while other three events are observed with

intense magnetic field magnitude ($|\mathbf{B}| > 7nT$). Analyzing histogram (b), one can see that a large number of events ($> 53\%$) occur for a weak B_{x-GSM} between $-1nT$ and $2nT$, and there is one case where B_{x-GSM} is intense ($\sim -8nT$). In B_{y-GSM} and B_{z-GSM} components, which are considered as most important parameters to magnetic reconnection, it is possible to observe two peaks in FTE occurrence in $B_{y-GSM} \sim -2nT$ and $\sim 3nT$, and a few events for small values. As for B_{z-GSM} which is considered as most important parameters to magnetic reconnection, more than 68% of events occur during negative B_{z-GSM}, and all of them are small negative values ($B_{z-GSM} > -4nT$). Whilst, a considerable number of FTEs occur during northward IMF, which will be discussed further in Section 4.5. One can clearly see the influence of B_y component on occurrence of FTEs, i.e. $B_{y-GSM} \neq 0$. These observations were reported by Russell et al. (1985) and Kawano and Russell (1997b), and they are considered as evidences for component reconnection model in low-latitude region (GONZALEZ; MOZER, 1974; TRATTNER et al., 2007).
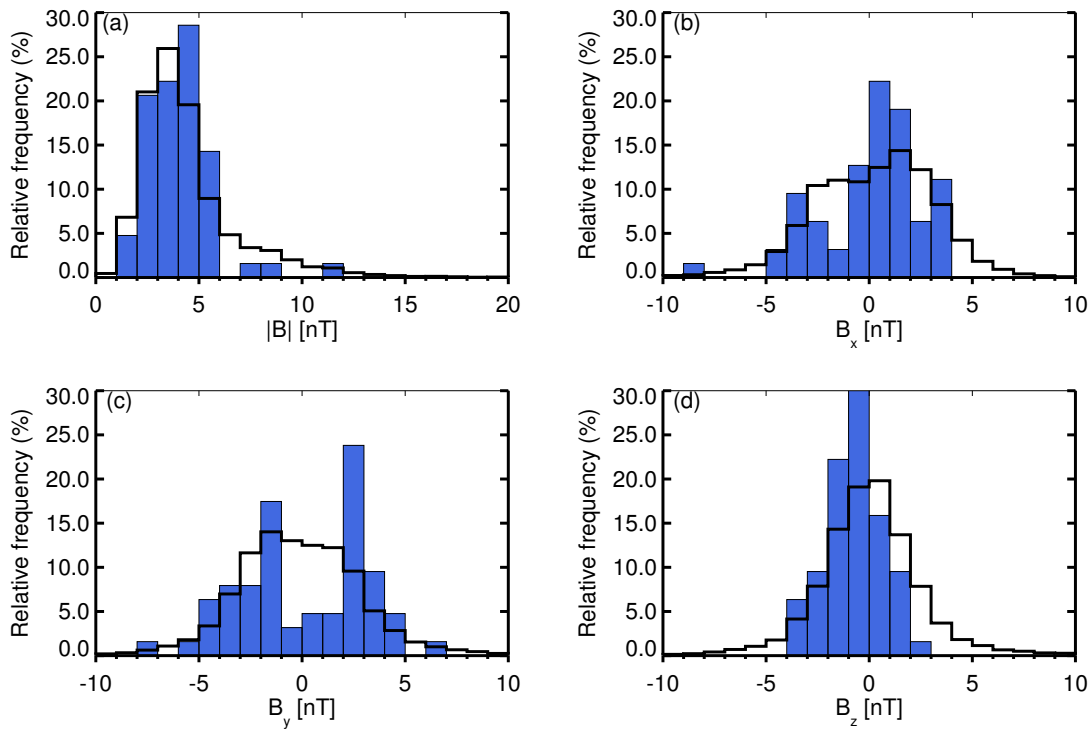

Figure 4.1 - Histogram of FTEs occurrence according to interplanetary magnetic field. (a) total magnetic field strength $|\mathbf{B}|$, (b) B_{x-GSM} component, (c) B_{y-GSM} component, and (d) B_{z-GSM} component.

Complementary plasma and magnetic field parameters are shown in Figure 4.2. His-

togram (a) shows plasma flow speed, where the FTEs are observed during typical values of solar wind speed, lower than $700km/s$. Histogram (b) presents solar wind dynamic pressure ($\rho_p V_p^2$, where p means proton), where the distribution is concentrated around $1nPa$.

IMF orientations are presented in the last two histograms. Histogram (c) shows the IMF cone angle, that is the angle between the IMF direction and the Earth-Sun line, calculated by $\arccos(B_{x-GSM}/|\mathbf{B}|)$. That cone angle equals to 0° means IMF pointing sunward, while 90° cone angle means an IMF completely perpendicular to the ecliptic plane, and obviously a cone angle of 180° means anti-sunward. Each bin corresponds to 20° wide and most of FTEs are observed for cone angles between 45° and 135°. The information if IMF points northward or southward is in histogram (d), IMF clock angle. It is defined as the angle between the magnetosheath and magnetospheric magnetic fields in the YZ_{GSM} plane. Clock angle is often used to indicate the importance of B_{y-GSM} component, which implies if anti-parallel or coponent reconnection. In this analysis each bin corresponds to 20° wide. There is a concentration of events around $80^o - 120^o$ and $240^o - 280^o$, indicating a large FTE occurrence for B_{y-GSM}-dominant intervals. On the other hand, a few FTEs are observed for strongly southward IMF ($\sim 180^o$) as previous studies showed, e.g. Fear (2006).

4.3 Spatial Distribution of FTEs

With the purpose to analyze the spatial distribution of the FTEs observed, the events were separated in direct and reverse FTEs according to B_N polarity. As it has been discussed before, several studies show that direct FTEs are generally found in northern hemisphere while reverse FTEs are found in southern hemisphere. That is related to the relative FTE motion to the x-line and to which hemisphere it is connected. In this database each event is observed by at least two probes. But, it will be shown the locations of one probe which detected each FTE to not overlie in the Figure 4.3.

Figure 4.3 shows the FTE distribution in the equatorial cut. Direct FTEs are represented by black triangles and reverse FTEs by red circles. The axes are the distance in GSM coordinate system normalized by terrestrial radius (R_E)[1]. The solid black line represents the nominal magnetopause position determined by Shue et al. (1997) model. The period of observation used in this study covers the low-latitude region

---

[1]One terrestrial radius (R_E) is approximately 6,370 km.
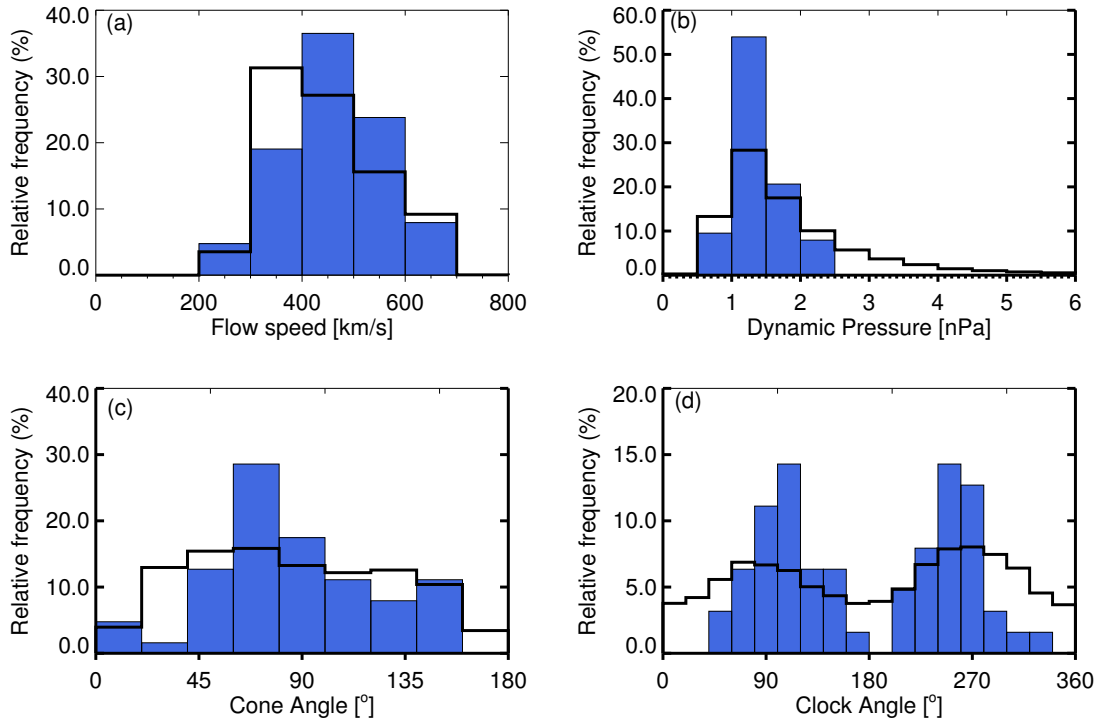
Figure 4.2 - Histogram of FTEs occurrence according to interplanetary medium parameters. (a) plasma flow speed, (b) dynamic pressure, (c) IMF cone angle, and (d) IMF clock angle.

on the dayside of the magnetopause. The distribution of the FTEs' location is the result of the probes' orbit.

Complementarily, Figure 4.4 shows a meridional distribution of FTE events. The distribution shows that the FTEs are located between $Y_{GSM} = -10R_E$ to $15R_E$ in east-west direction and between $Z_{GSM} = -5R_E$ to $5R_E$ in north-south direction. The majority of the 63 FTEs analyzed has reverse B_N polarity 44 (70%), whilst 19 (30%) of them are direct FTEs. The small number of direct FTEs observed is probably due to THEMIS orbit phase, which was more concentrated in southern hemisphere.
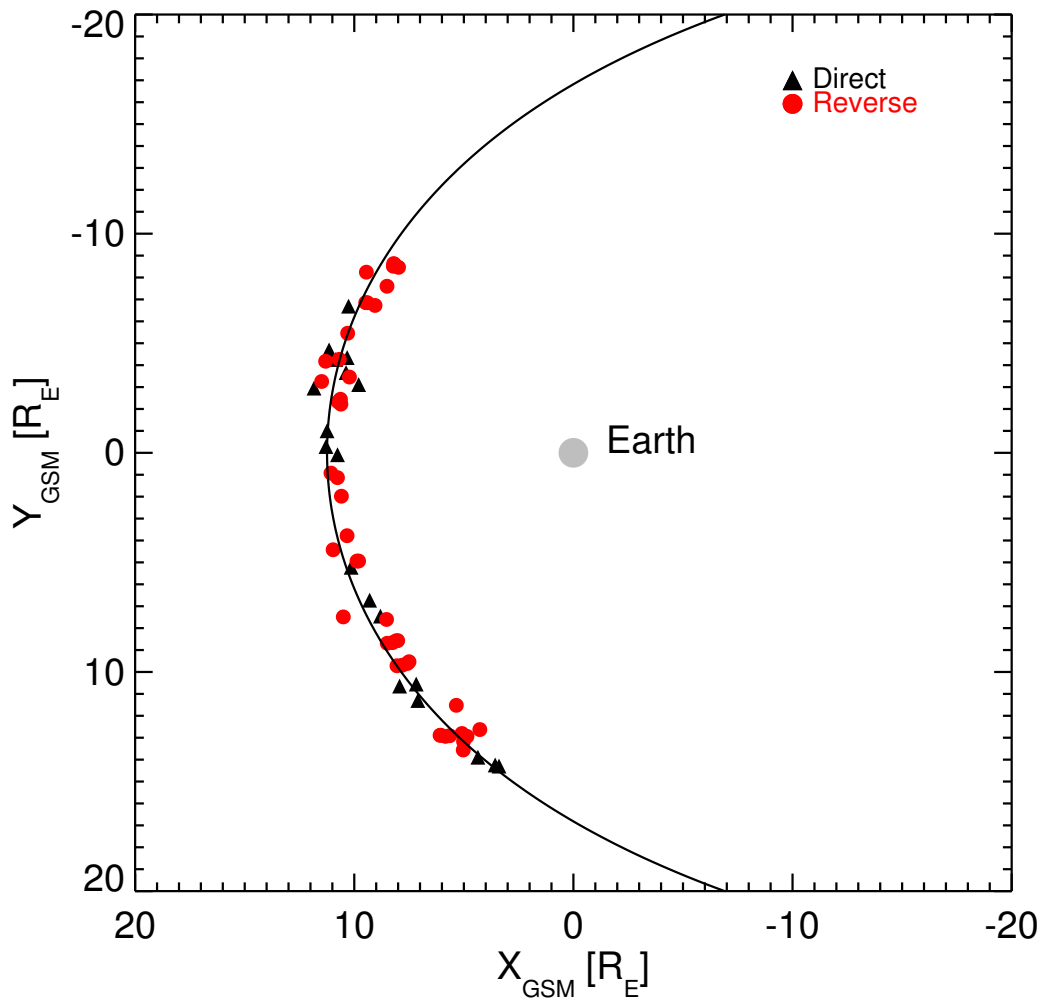
Figure 4.3 - Spatial distribution of FTEs observed by THEMIS in XY_{GSM} plane. Direct FTEs are represented by black triangles and reverse FTEs by red circles. The Earth is the grey circle and the solid line indicates the nominal magnetopause.
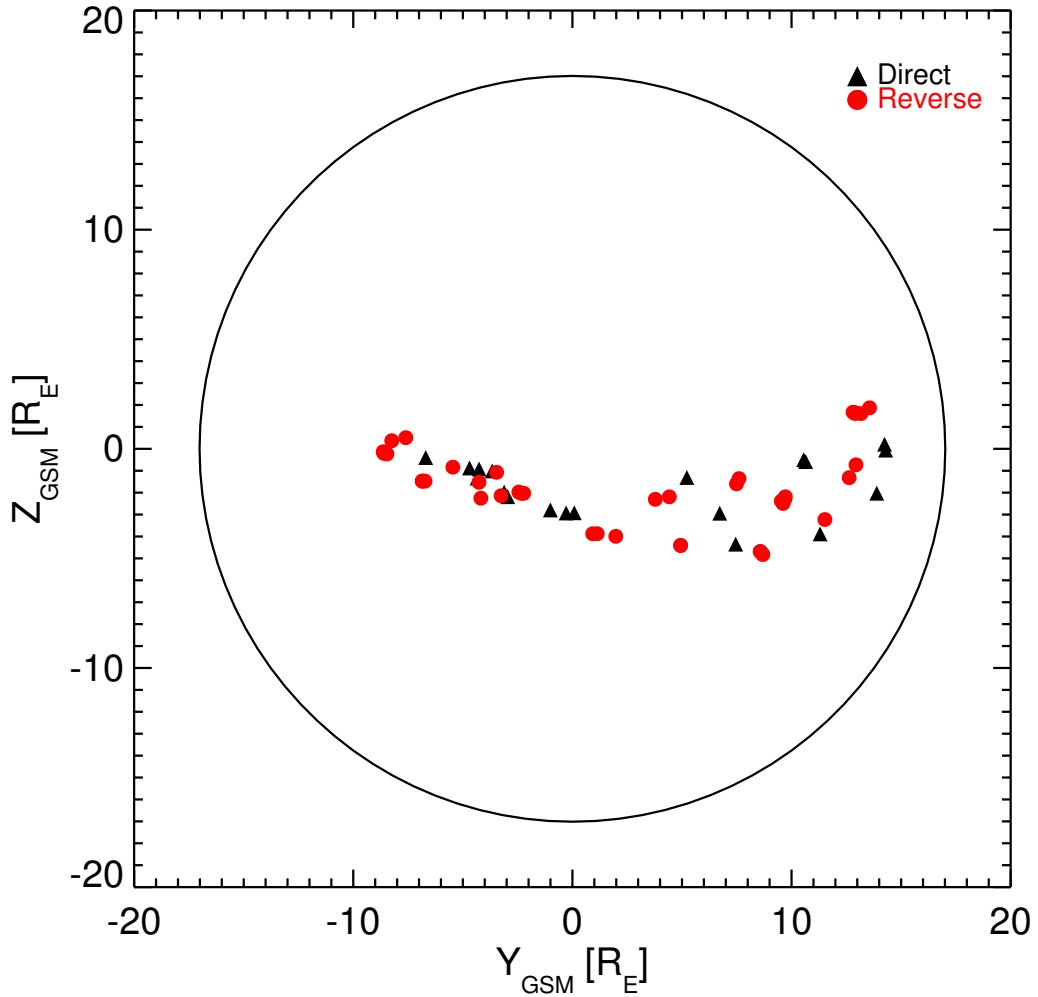
Figure 4.4 - Spatial distribution of FTEs observed by THEMIS probes in YZ_{GSM} plane.

It is interesting to analyze the FTE locations according to IMF orientation, since the reconnection line tilt depends strongly on IMF orientation. Figure 4.5 shows the FTE locations according to IMF clock angle (θ_{CA}). A long reconnection line (black dashed line) based on Gonzalez and Mozer (1974) model was considered to each clock angle interval. The reconnection line tilt was calculated in the central clock angle for each interval, wich are indicated by the green sectors. A complementary table shows the number of events for each clock angle bin (Table 4.1). Bins of 45° wide were considered for the first five plots and 55° wide for the last one. The reason why a bin 55° wide was chosen for the last case was to include one case where the

FTE was observed for a clock angle of 323°.

Analyzing individually each plot it is possible to point out:

- Figure (a): Only reverse FTEs are observed and most of them are located in the south/dusk quadrant. There are two FTEs observed slightly above the equator.

- Figure (b): Both direct and reverse FTEs are present, most of them are located in the south/dusk quadrant and have reverse polarity.

- Figure (c): This θ_{CA} range shows the lowest number of FTEs, 4 reverse and 1 direct. They are located at the equator.

- Figure (d): Similar to Figure (c). Equal number of reverse and direct FTEs are observed. They are concentrated on the dusk side of the magnetosphere.

- Figure (e): In this θ_{CA} range both types of FTEs are observed again, and they are spread along a large extension of Y_{GSM}. Reverse FTEs are concentrated in the dawn side, while direct FTEs are concentrated in the dusk side.

- Figure (f): Most of FTEs observed for this range are reverse, and are located in the dawn side close to the equator.

From this Figure, it is possible to note a pattern in spatial distribution of the FTEs related to IMF clock angle, i.e., the changes in the FTE polarities tend to follow the clock angle rotation. The Gonzalez and Mozer (1974) subsolar reconnection line model can explain most of this polarity distribution for the present observations. For plots (a) and (b), it is possible to apply the concept of component reconnection line. Such line is expected to be tilted over the dusk/northern and dawn/southern quadrants. Thus, for this reconnection line-tilt it is reasonable to observe reverse FTEs on the south of the reconnection line and direct ones for north of it. For clock angles close to 180°, Figures (c) and (d), would be more convenient to consider antiparallel subsolar reconnection which could explain the events near the equator. Figures (a) and (f) are mirrored in relation to Y-axis, which also happens with (b) and (e). Another feature is the higher occurrence of FTEs whenever B_{y-GSM} is dominant. On the other hand, when the clock angle is between 135° to 225°, i.e., IMF is mostly southward, only a few FTEs are observed. This result is consistent

with Kuo et al. (1995) and Fear (2006) showing that the highest probability of FTE occurrence is during IMF southward with a strong dawn/dusk component.
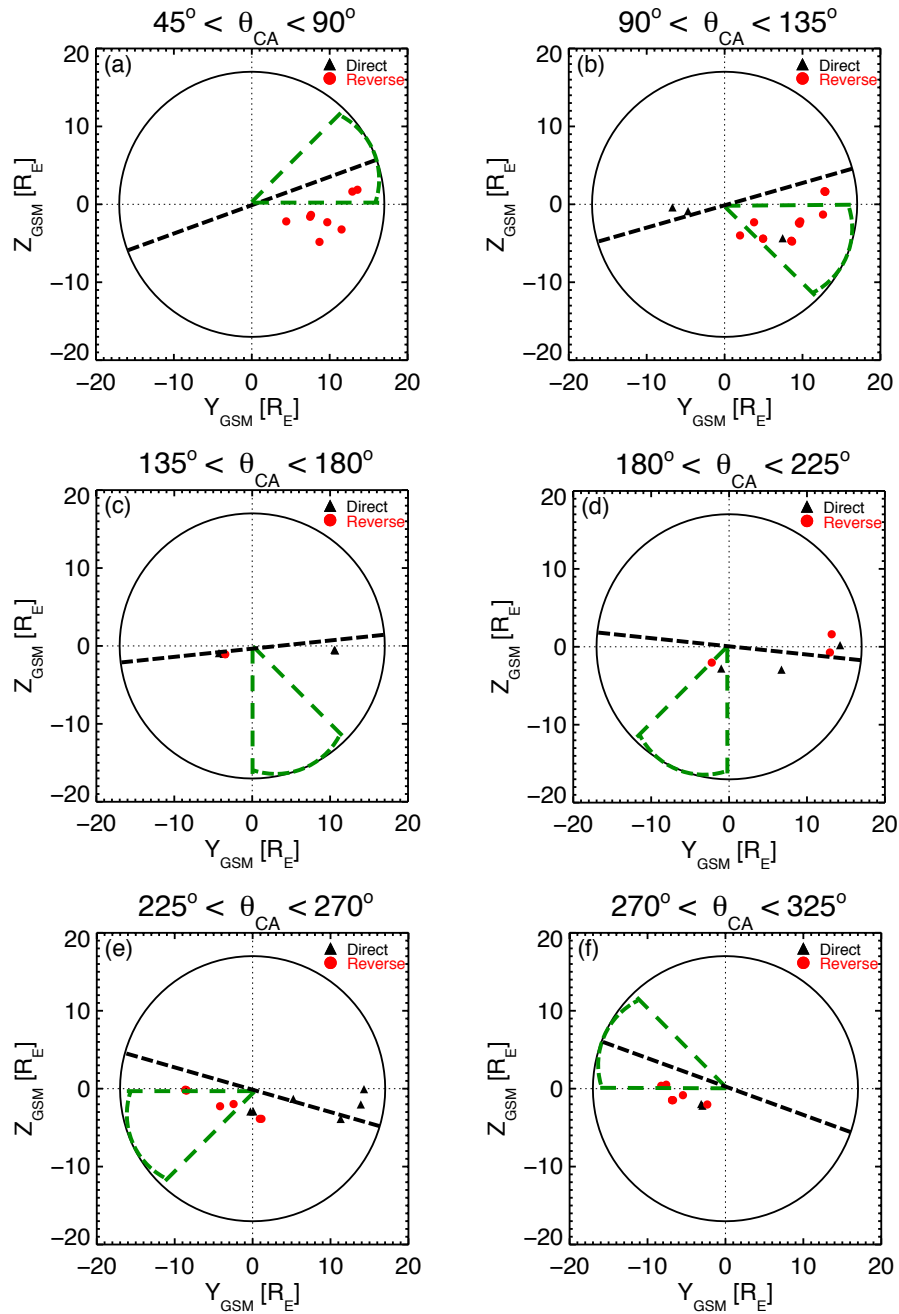
Figure 4.5 - Spatial distribution of FTEs according to IMF θ_{CA}. Direct FTEs are represented by black triangles and reverse FTEs by red circles. The θ_{CA} range considered in each plot is shown of the top.

Table 4.1 - Number of FTEs observed according to IMF θ_{CA}, as illustrated in Figure 4.5.

θ_{CA} bin	Direct FTEs	Reverse FTEs	Total FTEs
$[45^o - 90^o]$	0	8	8
$[90^o - 135^o]$	3	15	18
$[135^o - 180^o]$	4	1	5
$[180^o - 225^o]$	3	3	6
$[225^o - 270^o]$	6	8	14
$[270^o - 325^o]$	2	7	9

4.4 Motion of Flux Transfer Events

Since FTEs are formed by magnetic reconnection (RUSSELL; ELPHIC, 1978), which occurs somewhere on the magnetopause, it is interesting to investigate the subsequent motion of them. It is known that the reconnection outflow is initially generated by the tension force stored in the highly bent reconnected field lines. According to FTE generation models (RUSSELL; ELPHIC, 1978; LEE; FU, 1985; SCHOLER, 1988), a perpendicular motion to the reconnection line is considered in this work. Thus, in this Section, the deHoffmann-Teller reference frame is used to estimate the FTE velocities (PAPAMASTORAKIS et al., 1989; WALTHOUR et al., 1993), with the aim of comparing the observed FTE velocities with those predicted by the Cooling et al. (2001) model.

4.4.1 FTEs' Velocities in the deHoffmann-Telller Frame

The deHoffmann-Teller reference frame (DEHOFFMANN; TELLER, 1950) technique has been largely employed to analyze jump conditions across space plasma discontinuities, such as shock wave, boundary layer, and FTEs observed at the magnetopause (WALTHOUR; SONNERUP, 1995; SONNERUP; GUO, 1996). The existence of such a reference frame indicates that a coherent quasi-stationary pattern of a magnetic field and plasma velocity is present (KHRABROV; SONNERUP, 1998). This assumption comes from Faraday's law, where $\nabla \times \mathbf{E}' = -(\partial \mathbf{B}/\partial t)' = 0$. If the electric field measured in the laboratory frame is $\mathbf{E}$, then, the deHoffmann-Teller frame satisfies the relation,

$$\mathbf{E}' = \mathbf{E} + \mathbf{V}_{HT} \times \mathbf{B} = 0, \qquad (4.1)$$

were $\mathbf{V}_{HT}$ is the velocity in the deHoffmann-Teller reference frame. For real plasma

measurements it is unlikely to satisfy this relation precisely. When the analysis is done over the structure or a region where ideal MHD is approximately valid, the convective electric field, $\mathbf{E} = -\mathbf{v} \times \mathbf{B}$, can be used as a proxy for the eletric field $\mathbf{E}$, where $\mathbf{v}$ is the local plasma velocity and $\mathbf{B}$ is the magnetic field. In practical data sets, there are several values of $\mathbf{B}^{(m)}$ and $\mathbf{v}^{(m)}$, where $m = 1, 2...M$ are the number of measurements. For an FTE or a magnetopause crossing, the residual electric field $\mathbf{E'}$ can be used to obtain an approximation for $\mathbf{V}_{HT}$. The minimization of this electric field is determined by the minimization of a function $D(\mathbf{V})$ given by,

$$D(\mathbf{V}) = \frac{1}{M} \sum_{m=1}^{M} |\mathbf{E'}^{(m)}|^2 = \frac{1}{M} \sum_{m=1}^{M} |(\mathbf{v}^{(m)} - \mathbf{V}) \times \mathbf{B}^{(m)}|^2, \tag{4.2}$$

where $\mathbf{V}_{HT}$ is the value of the frame velocity, so that $\mathbf{V}$ minimizes D. Two parameters can be used to test the quality of the deHoffmann-Teller frame: one is the linear correlation (c) between the convection electric electric field ($\mathbf{E}_c^{(m)} = -\mathbf{v}^{(m)} \times \mathbf{B}^{(m)}$) and the electric field in the deHoffmann-Teller frame ($\mathbf{E}_{HT}^{(m)} = -\mathbf{V}_{HT} \times \mathbf{B}^{(m)}$); the second parameter is the ratio $D(\mathbf{V}_{HT})/D(\mathbf{V} = 0) \ll 1$.

The deHoffmann-Teller velocity was determined for each FTE. The time interval chosen to evaluate $\mathbf{V}_{HT}$ is between B_N peaks to avoid the influence of an external structure and to guarantee the frame quality. Figure 4.6 shows an example of the deHoffamnn-Teller frame determination for an FTE observed by four of five THEMIS probes. Only two of them had plasma data available. Therefore it was possible to apply the technique only for these two probes. The probe chosen in Figure 4.6 is the one with a clear magnetic field signature and with a well determined deHoffmann-Teller frame.

Figure 4.6 shows the magnetic field on the top and the plasma bulk velocity on the bottom, as observed by one of THEMIS probe (THEMIS-E). Both magnetic field and plasma velocity are projected in the LMN system, discussed in Chapter 3. The FTE is characterized by a bipolar variation in the B_N component (red line) simultaneously with the total magnetic field peak (black line). Dashed lines indicate the period of time when the frame was evaluated, from 06:00:11 to 06:00:38 UT. Figure 4.7 shows a scatter plot of all $\mathbf{E}_{HT}$ and $\mathbf{E}_c$ components obtained from the THEMIS data for the period between the dashed lines. In this example it was found a good deHoffmann frame, based on the test of quality described previously, where the correlation coefficient is $c = 0.984$ and $D(\mathbf{V}_{HT})/D(\mathbf{V} = 0) = 0.030$. The deHoffmann-Teller velocity found for this FTE in GSM is $\mathbf{V}_{HT} = -244.9\hat{e}_x + 137.32\hat{e}_y + 0.8948\hat{e}_z$ km/s.

This velocity is consistent with the FTE position near the dusk flank shown by the green arrow in Figure 4.8. It is applied the same analysis to all FTE observations individually. There are only six events with correlation coefficient c lower than 0.9 and five with $D(\mathbf{V}_{HT})/D(\mathbf{V} = 0)$ higher than 0.2. Thus, the deHoffmann-Teller method was used to estimate the FTE velocity locally.
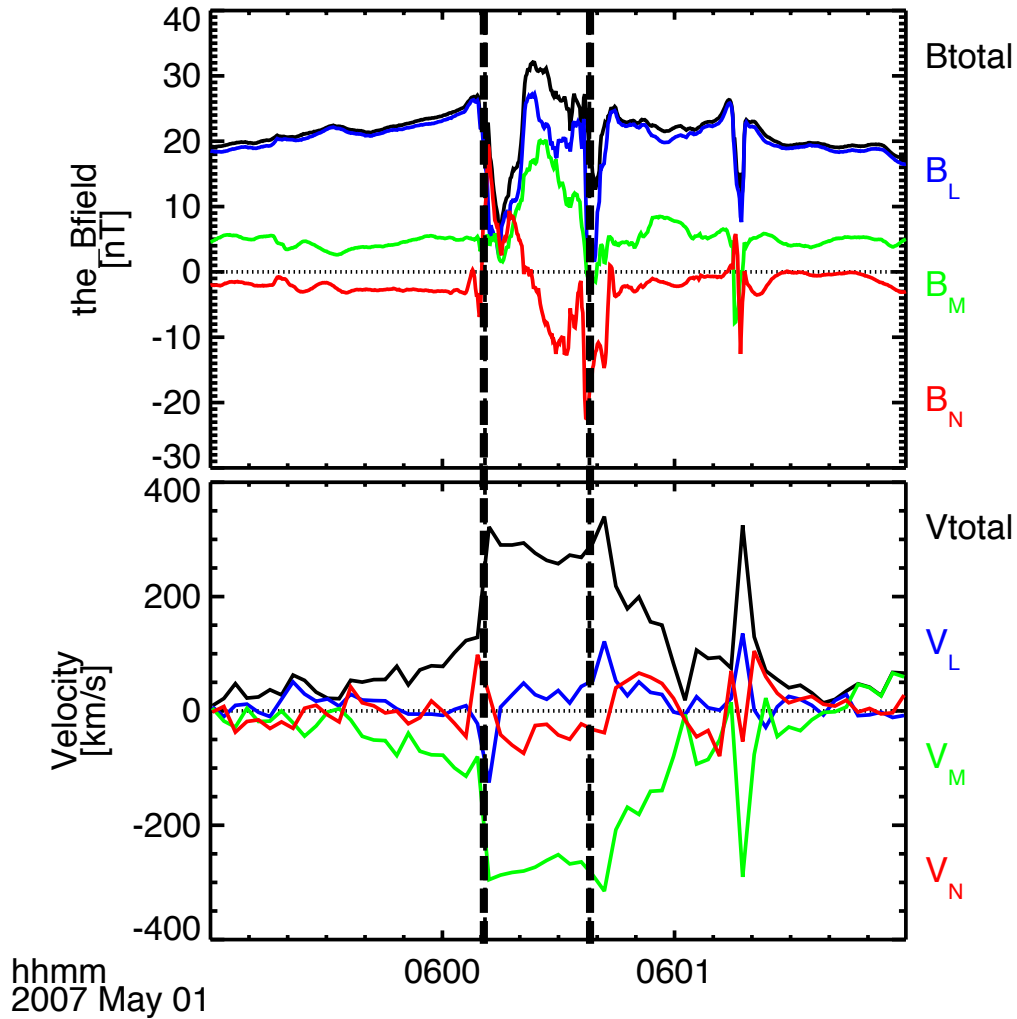
Figure 4.6 - Magnetic field on the top and plasma bulk velocity on the bottom, both in the LMN system. The vertical dashed lines indicate the period of time when the deHofmann-Teller reference frame was evaluated.
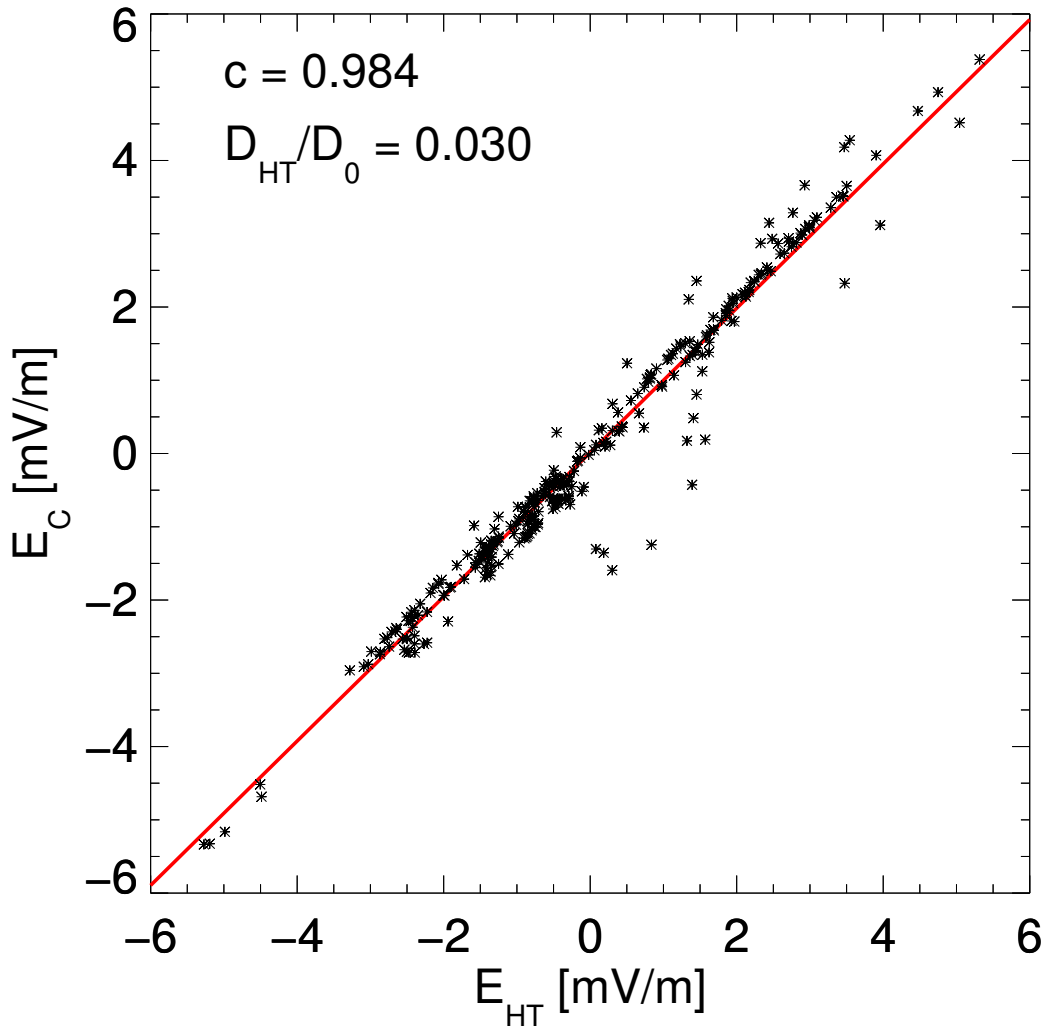
Figure 4.7 - Scatter plot of the $\mathbf{E}_{HT}$ and $\mathbf{E}_c$ components obtained from THEMIS data for the period indicated in Figure 4.6 between the dashed lines.

Figure 4.8 shows the deHofmann-Teller velocities in YZ_{GSM} plane for all FTEs observed. Again one probe to illustrate the FTE positions and velocity orientation was chosen. Black arrows represent the velocities of direct FTEs and red arrows represent the velocities of reverse FTEs. The vector magnitudes are normalized by 200km/s. In a general view, it is clear that FTE velocities point toward the flanks for structures located at the flanks ($|Y_{GSM}| \geq 10R_E$), whereas both velocity components are important for FTEs at intermediate longitudes ($-10R_E < Y_{GSM} < 10R_E$), with the FTE motions duskward/dawnward and southward. The velocities turn southward when the FTEs observed are close to the subsolar region. Although it was expected a higher contribution of positive V_{HTz} for direct FTEs, most of them

present small northward component contributions for the FTEs in the duskside and negative ones in the dawnside. One possible explanation for the low northward FTEs velocities is the opposite magnatosheath plasma flow, which points southward in southern hemisphere and would be near Alfvénic or super-Alfvénic flow. There is one FTE with a strong northward velocity located close to the subsolar region.
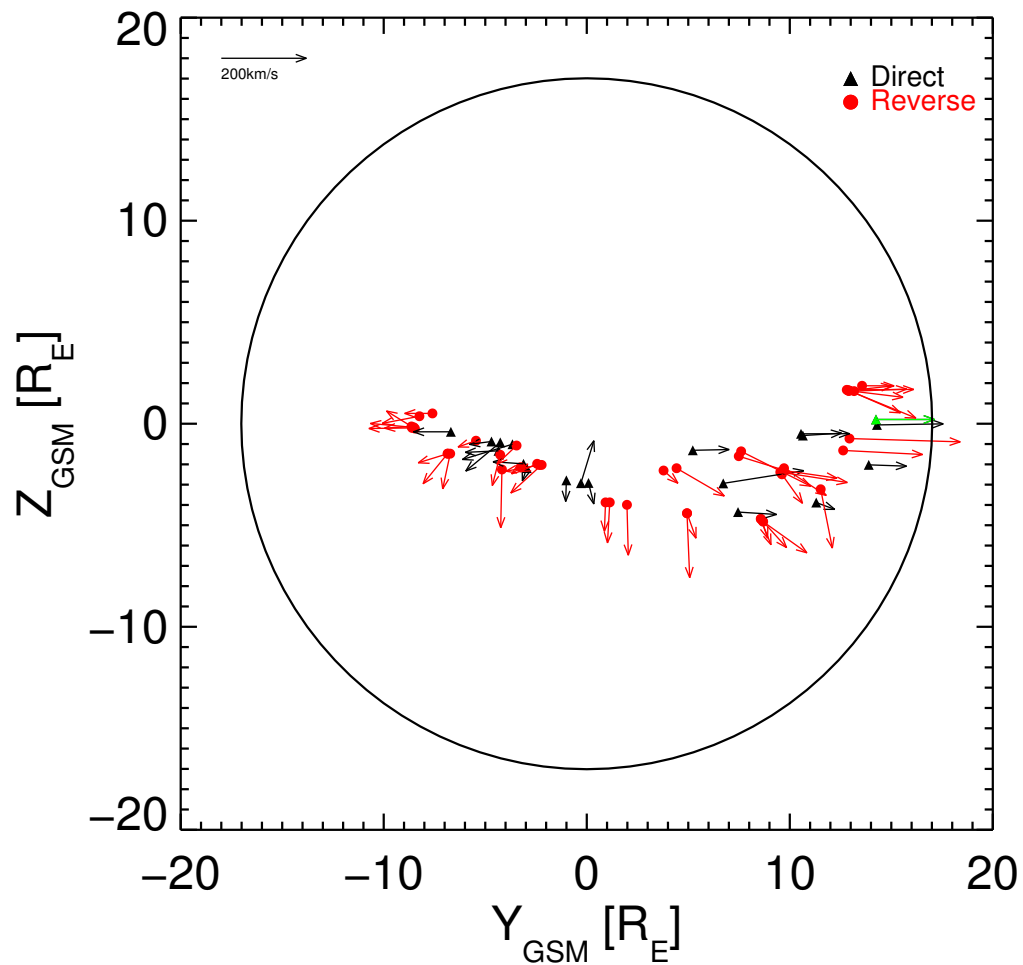
Figure 4.8 - deHoffmann-Teller velocities and FTE positions projected in YZ_{GSM} plane. Direct FTEs are represented by black arrows and reverse FTEs are represented by red arrows. The FTE showed in Figure 4.6 is represented by the green arrow.

4.4.2 Flux Tube Velocity predicted by the Cooling Model

Cooling et al. (2001) presented a model to examine the motion of flux tubes generated by magnetic reconnection along the magnetopause surface. Cooling's model is based in the Cowley and Owen (1989) model, in which they assume uniform fields on either side of the magnetopause, but with arbitrary relative orientation, and a stagnation-point flow in the magnetosheath. The open flux tube motion is determined by applying the equilibrium condition for the one-dimensional current sheet.

As presented in Chapter 2, Cooling's model has been employed to understand the motion of FTEs and their relation with antiparallel and component nature of magnetic reconnection. Fear et al. (2007) employed the Cooling model to an extensive number of FTEs observed by Cluster spacecraft under a variety of IMF conditions. They pointed out that 78% of these events were consistent in both, direction of motion and speed, with Cooling's model predictions. Such results differ up to 30° in their motion direction and a factor of two in their speed values. Sibeck and Lin (2010) also employed the Cooling model to generate FTEs for various IMF orientations and using the subsolar magnetic reconnection by component model. Tracking the FTEs motion and estimating their perturbation in the ambient magnetosheath and magnetosphere. They showed that during southward IMF orientation, the FTEs tend to move rapidly over the polar caps. On the other hand, those generated during northward IMF orientation slip slowly around the magnetospheric flanks. Events formed during periods of duskward IMF orientation have a north-dawnward or south-duskward motion. They investigated also FTEs generated by the IMF with large B_{x-GSM} and B_{y-GSM} components, (i.e. Parker spiral orientation) and observed that the events moved antisunward more slowly prior to the local noon than after local noon.

In this work it was employed the same version of Cooling's model as that used by Sibeck and Lin (2010). The FTEs' prediction used in this thesis were generated by component reconnection line. The reconnection line starts in the subsolar point on the magnetopause and its tilt depend on the IMF orientation. The assumptions adopted in this work are the same as Sibeck and Lin (2010), and references therein, which considered that FTEs are generated by burst reconnection along single or multiple reconnection lines.

The reconnection line extends up to $19R_E$, which is consistent with observations of steady reconnection (PHAN et al., 2006). Parameters of the magnetosheath for this

model are those determined by the Kobel and Fluckiger (1994) model, which defines the magnetosheath as a function of the IMF components, the distance to the subsolar magnetopause and the distance to the subsolar bow shock. The magnetospheric field was determined by the Alexeev et al. (2003) model, which provides magnetic field strength and directions within a paraboloid magnetopause as a function of dipole tilt, solar wind plasma density and bulk velocity, IMF components and geomagnetic indices D_{st} and AL. As in Sibeck and Lin (2010) the D_{st} and AL indices were set to zero, corresponding to quiet times. However, the model considers contributions from Earth's dipole, superposed IMF, Ring, Cross-tail, Region 1, and Chapman-Ferraro currents to determine the total magnetic field and direction as a function of location within the dayside magnetosphere.

These models provide the flow speed, density, and magnetic field on either side of the magnetopause. The reconnection line begins at the subsolar point, which is determined by Shue et al. (1997), and extends along curves that maximize the shear between the magnetosheath and magnetospheric magnetic fields parallel to the magnetopause current vector (SONNERUP, 1974; GONZALEZ; MOZER, 1974). Another important assumption is that the point where the reconnected field line intersects the magnetopause surface moves with the deHoffmann-Teller velocity.

Thus, the initial velocities of the reconnected field lines in the deHoffmann-Teller frame were obtained by magnetic field and plasma pressure balance (COWLEY; OWEN, 1989). The relationship between the velocity in the deHoffamnn-Teller frame, the velocity of the plasma in the magnetosheath and Alfvén speed is:

$$\mathbf{V}_{HTN} = \mathbf{V}_{sh} - V_A\widehat{\mathbf{b}}_{sh} \tag{4.3}$$

$$\mathbf{V}_{HTS} = \mathbf{V}_{sh} + V_A\widehat{\mathbf{b}}_{sh}, \tag{4.4}$$

where $\mathbf{V}_{HTN}$ and $\mathbf{V}_{HTS}$ are the deHoffmann-Teller velocities of the flux tubes connected to the northern and southern hemispheres, $\mathbf{V}_{sh}$ is the magnetosheath plasma velocity, V_A is the Alfvén speed, and $\widehat{\mathbf{b}}_{sh}$ is the sheath magnetic field unit vector. First step for the model is to track individual points of the flux tube from the initial point to the new point, with a speed V_{HT} over a short time interval. The new point is fed back in the model where all parameters are calculated again. This process is repeated as required in order to determine the trajectory of each flux tube along the magnetopause.

47

Figure 4.9 shows a flux tube velocity predicted by the Cooling model and projected in YZ_{GSM} plane. A complementary projection in ZX_{GSM} plane is shown in Figure 4.10. In this case, it was used the interplanetary conditions observed during an FTE encounter on May 1, 2007 at 06:00 UT, shown in Figure 4.6. The input parameters are obtained taking the average over 5 minutes from OMNI data, which are: $\mathbf{B}_{GSM} = [-0.45, -1.71, -2.14]$ nT; $V_{sw} = 511.4$ km/s; $n = 1.97 cm^{-3}$. The IMF orientation is indicated in the right-upper corner of figures by black arrow. Here the clock angle is 210°, pointing southward and dawnward. According to the component reconnection concept, it is expected that the reconnection line extends from north-dawn to south-dusk quadrant, as shown by the dashed line. Analyzing Figure 4.6 (a) again, one can conclude that the direct polarity of B_N is consistent with an FTE observed on the north of the reconnection line. Thus, it is convenient to employ the Cooling's model considering a flux tube connected to the northern hemisphere, that is, using Equation 4.3. As discussed before, each individual point of the flux tube has its new position calculated using V_{HT} over a short time interval. The subsequent positions of each parcel or point of the flux tube is tracked and they are shown by the solid lines. The predicted velocity by Cooling's model was evaluated approximately in the point where the FTE was observed by THEMIS probes. Thus, it is possible to compare the predicted velocity ($\mathbf{V}_{Cool}$) with the velocity calculated by the observation $\mathbf{V}_{HT}$.
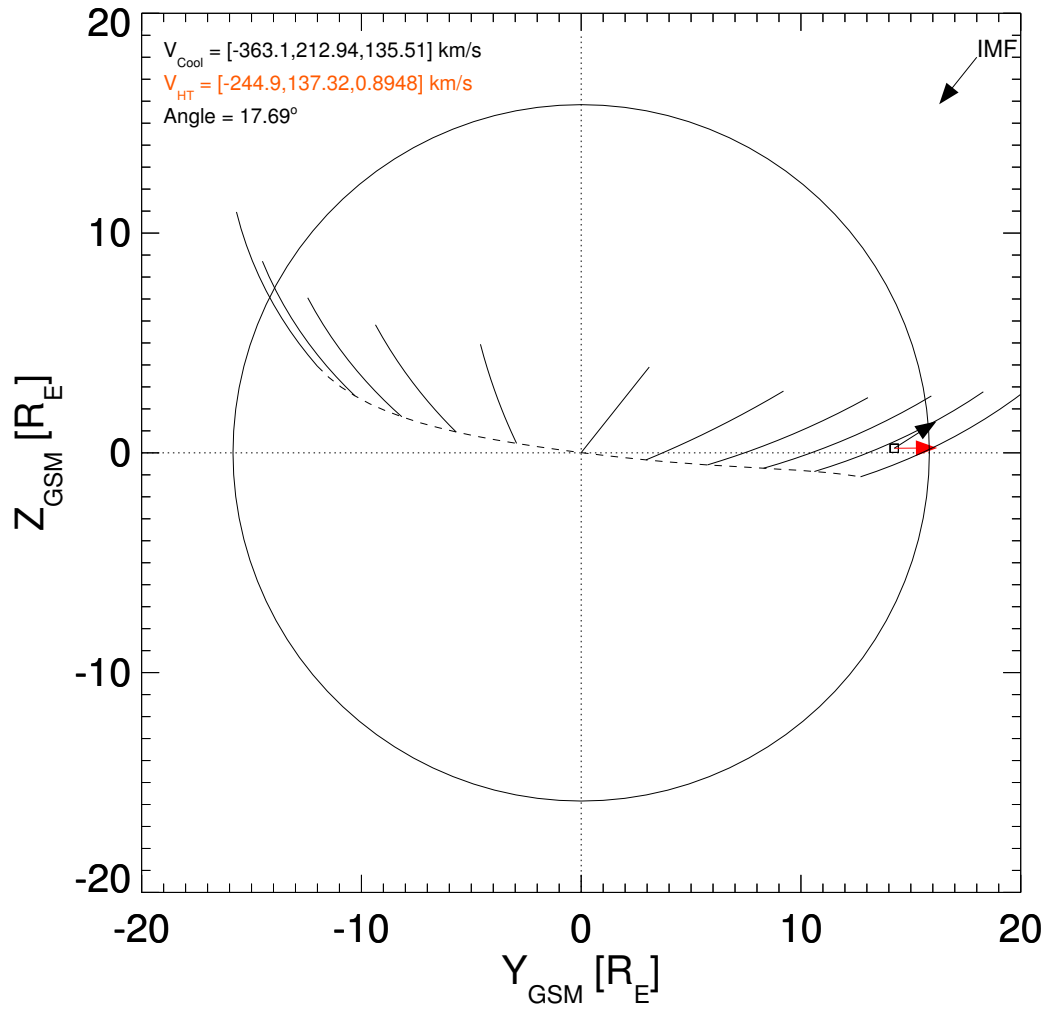
Figure 4.9 - Flux tube motion predicted by the Cooling model in the YZ_{GSM} plane. The solid lines are the paths followed by individual points generated on the reconnection line (dashed). The black and red arrows are the velocities predicted by the Cooling model and by the deHoffmann-Teller technique, respectively. The IMF clock angle was 210° and the angle between the two velocities is $= 17.69^o$.
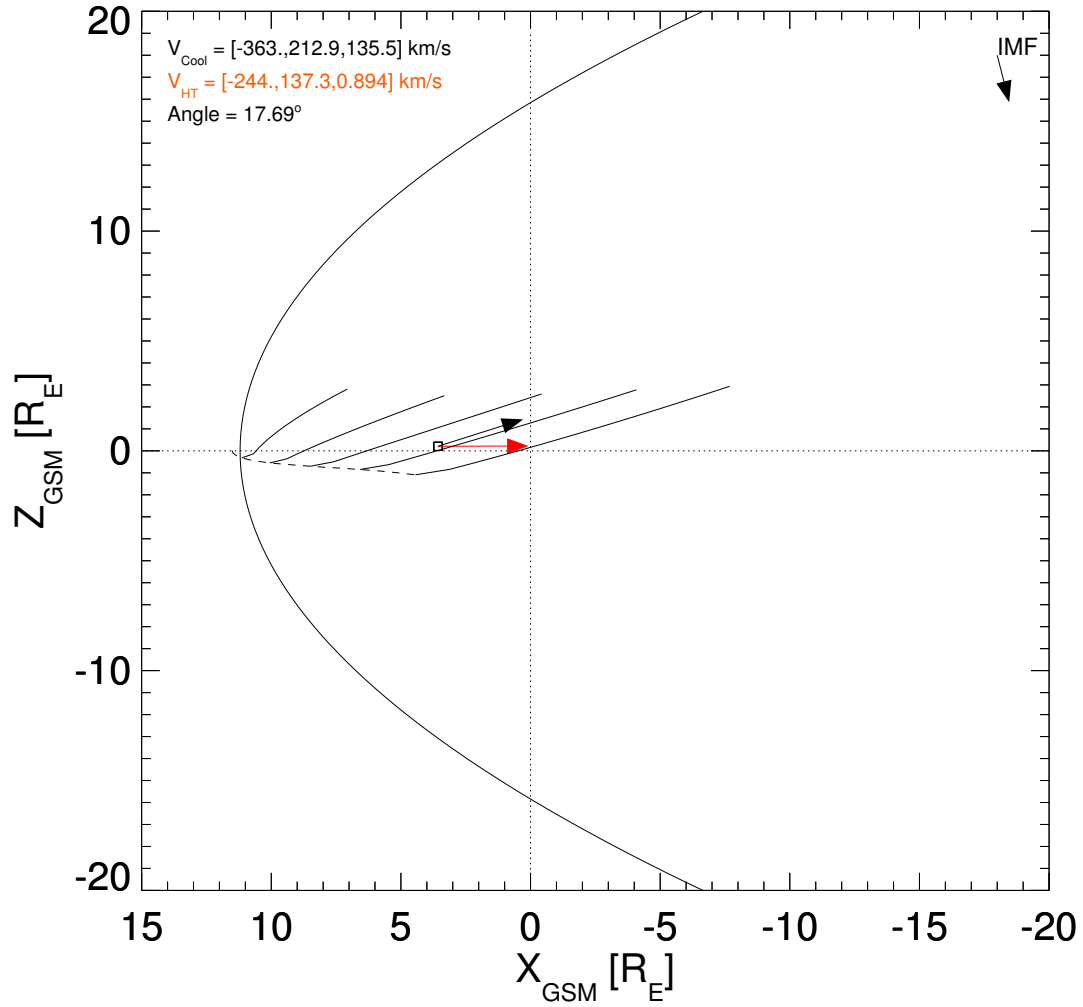
Figure 4.10 - Flux tube motion predicted by the Cooling model in the XZ_{GSM} plane. The solid lines are the paths followed by individual points generated on the reconnection line (dashed). The black and red arrows are the velocities predicted by the Cooling model and by the deHoffmann-Teller technique, respectively. The IMF clock angle was 210° and the angle between the two velocities is $= 17.69^o$.

Analyzing the flux tube at the probe position it is possible to make a comparison between Cooling's model and deHoffmann-Teller velocity. At the top left, Figure 4.10 shows the velocity predicted by Cooling's model (V_{Cool}), the velocity determined in the deHoffmann-Teller frame (V_{HT}), and the angle between these velocities. The high velocity in $-x$ direction is due the fact that the FTE was observed at the flank ($Y_{GSM} = 14R_E$), which is clearly seen in Figure 4.10. The comparison of speed and

direction between values predicted by Cooling's model with those calculated by data shows a difference in the angle of 17° and a speed ratio of 1.57.

The Cooling model was applied for 58 FTEs in which all input parameters were available. The FTE polarity and the relative probe location to the reconnection line are used to determine which Cooling branch to consider, that is, to choose either Equations 4.3 or 4.4. Since, the information about the hemisphere where the FTE is connected is directly related to its ΔB_N polarity (RUSSELL; ELPHIC, 1978; RIJNBEEK et al., 1982). Therefore, in some cases, the FTE polarity had a better agreement with a flux tube predicted by Cooling's model connected to the opposite hemisphere, as shown in Figure 4.11. In this case the reverse FTE was located in the Southern hemisphere and according to the polarity, it is expected by the Cooling prediction to be linked to the south flux tube. But, FTE motion predicted by the model which passes by the probe location was good agreement with observation using V_{HTN} instead of V_{HTS}. Thus, the choice of modeled flow velocity should be made to adjust the model to observations. Figure 4.12 shows the magnetic field, ion energy distribution, and ion pitch angle for the FTE observed on August 05, 2007. It is clear the reverse polarity of ΔB_N and the mixture of plasma from magnetosphere (high-energy) and from the magnetosheath (low-energy). The pitch angle distribution shows a stream in the anti-parallel direction ($\sim 180^o$), which confirms the FTE connection to the southern hemisphere.
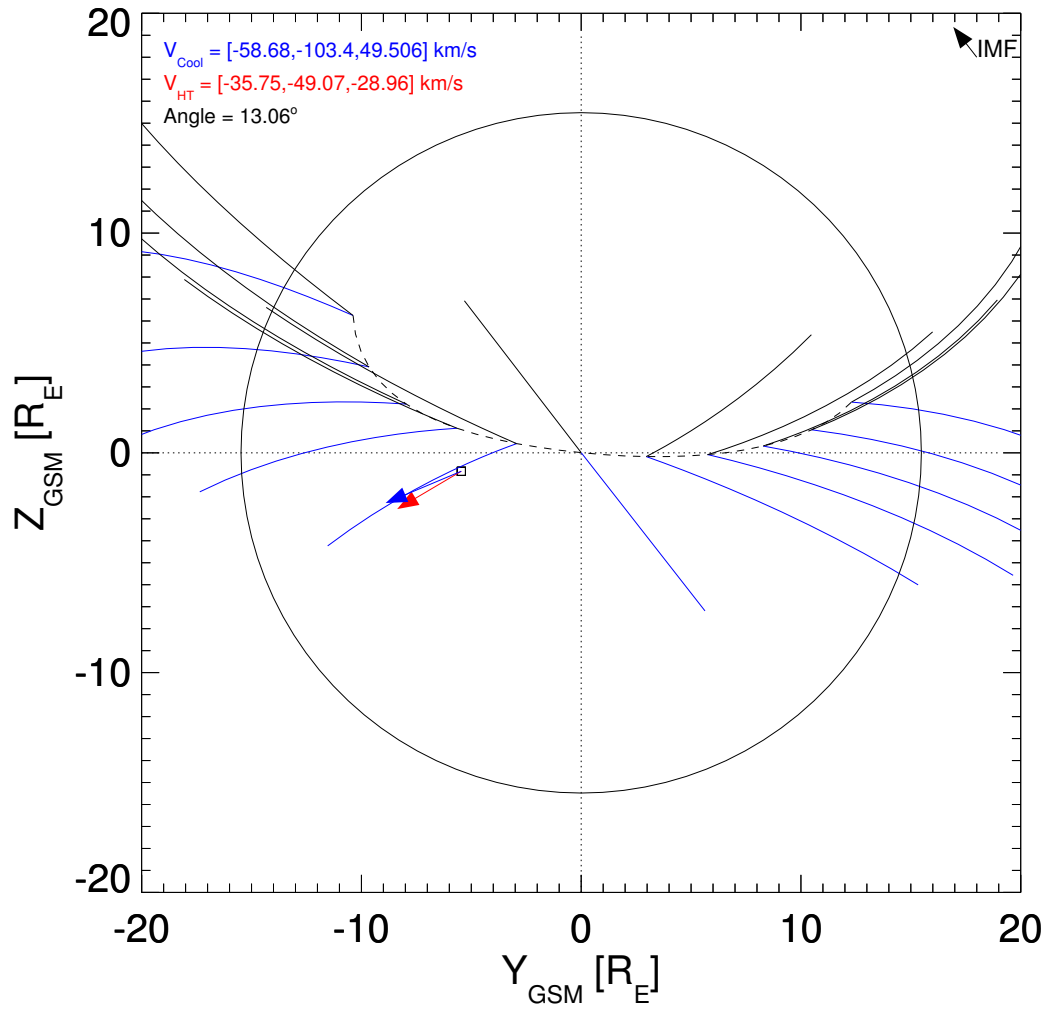
Figure 4.11 - Example of the Cooling model adjust and FTE polarity. The solid blue lines are resulted from V_{HTN} (Eq. 4.3) and the solid black lines are resulted from V_{HTS} (Eq. 4.4). The red arrow represents the FTE velocity in deHoffamnn-Teller frame and the blue arrow represents the velocity predicted by Cooling's model.
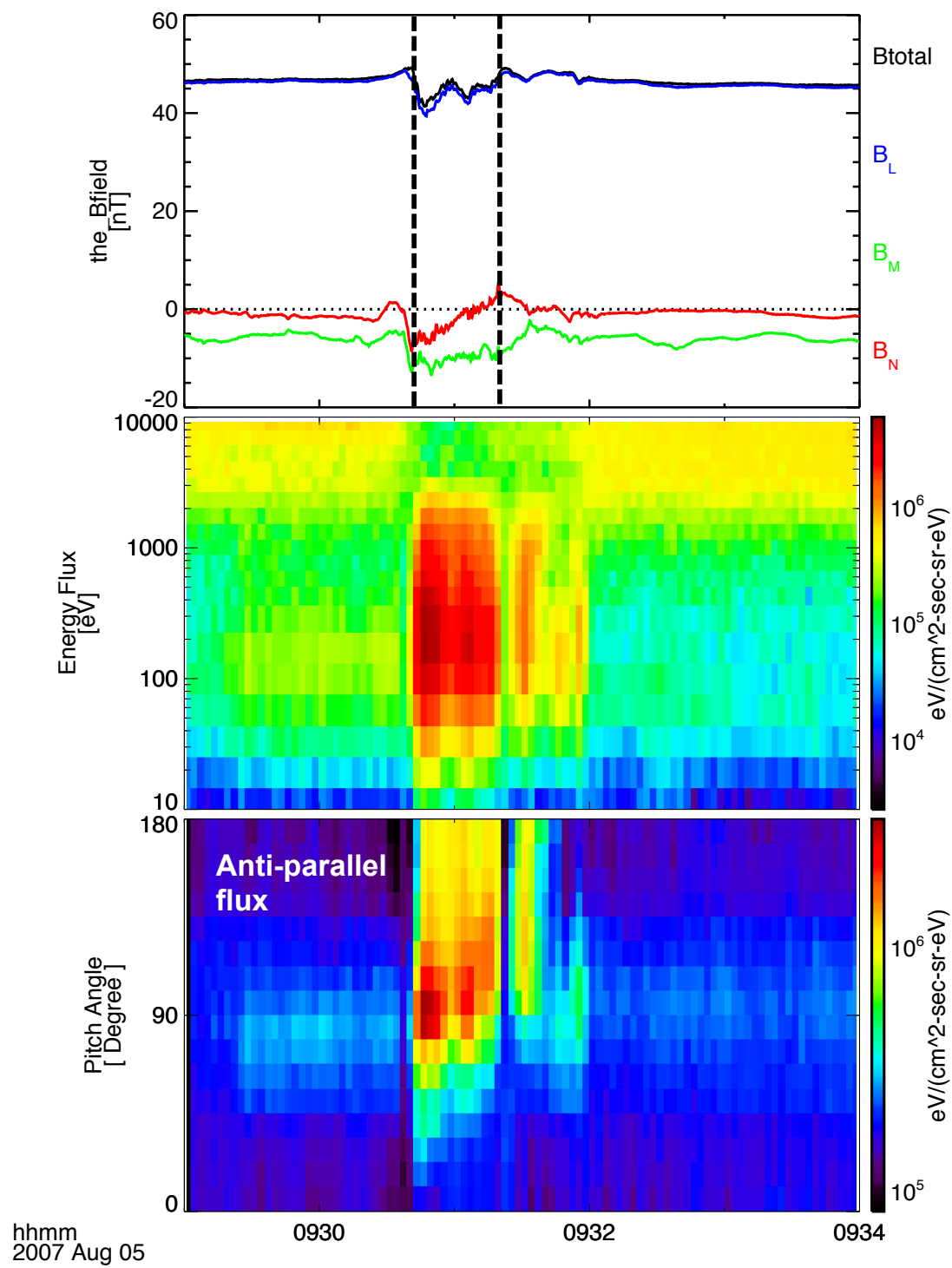
Figure 4.12 - FTE parameters related to Figure 4.11. From top to bottom is the magnetic field, ion energy flux, and pitch angle distribution. The magnetic filed is in LMN coordinate system.

Figure 4.13 shows the velocity predicted by the Cooling's model in the YZ_{GSM} plane for each flux tube analyzed in those points where THEMIS observed FTEs. As in the observational analysis presented before, the black arrows represent velocities of direct FTEs and red arrows represent velocities of reverse FTEs, normalized by $200km/s$. In general, the flux tubes obtained with the Cooling model present the tendency to move toward the flanks for those observations obtained in the dawn and dusk regions. Also, it is possible to observed some flux tubes in the dawn-side presenting a strong southward motion, due to their southern location. Other flux tubes located close to $Y_{GSM} = 0$ present a motion toward the flanks. Unlike the deHoffmann-Teller analysis, the model predicts small or negative southward velocities for direct FTEs.
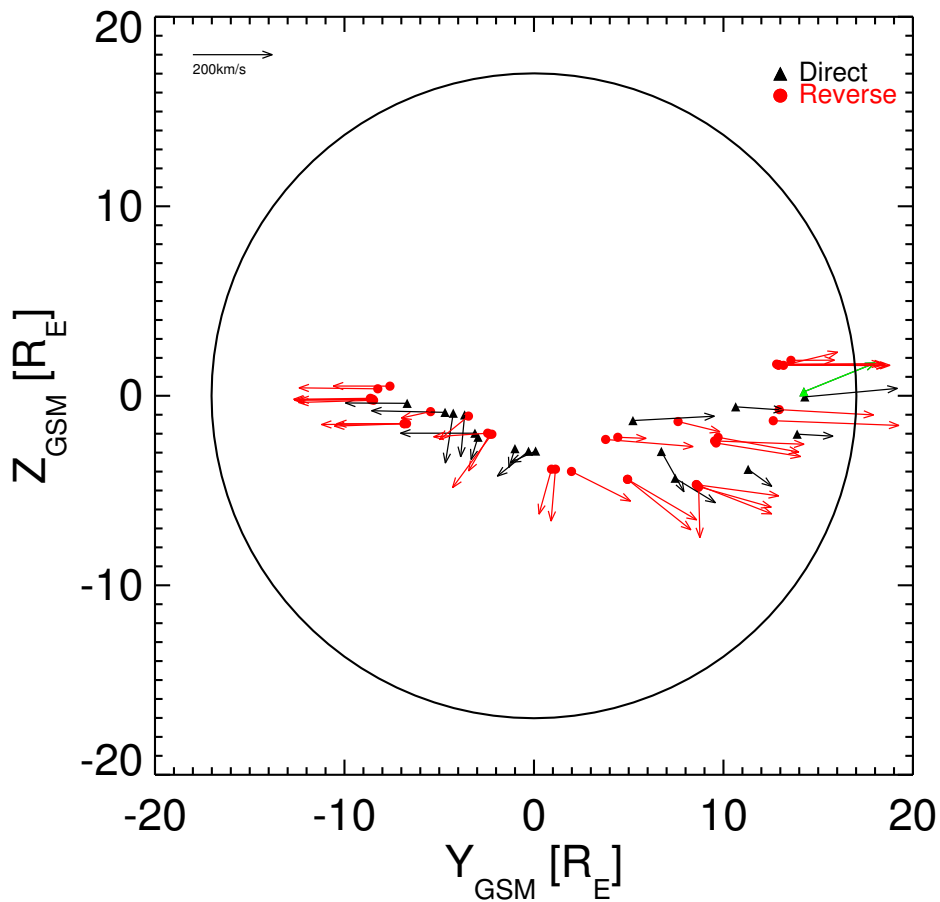
Figure 4.13 - Flux tubes velocities predicted by Cooling's model in the YZ_{GSM} plane. Directe FTEs are represented by black arrows and reverse FTEs are represented by red arrows. The FTE showed in Figure 4.6 is represented by the green arrow.

Of 58 events analyzed 38 (65%) are consistent with the polarity of B_N observed by THEMIS, that is, direct (reverse) FTEs agree with flux tubes connected in the Northern (Southern) hemisphere. There are three events which do not agree with either southern or northern flux tube predictions. Thus, it is possible to compare 55 flux tubes velocities with the observed FTE velocities. Considering the same criteria adopted by Fear et al. (2007), a maximum angular deviation of 30° for velocity vector and a factor of 2 for speed, it was found that 29 (52%) of the flux tubes were consistent with observations. When each condition is analyzed separately, velocity vector and speed, 41 (74%) of cases were consistent with the velocity direction (Figure 4.14) and also 41 (74%) were consistent with speed observations (Figure 4.15).
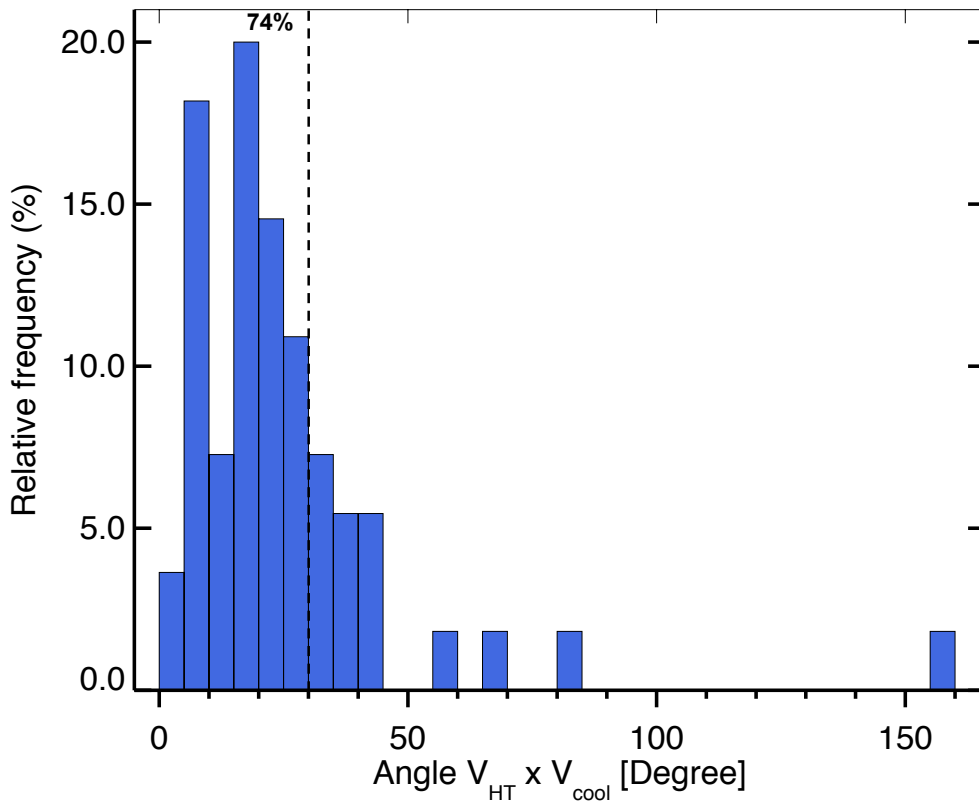
Figure 4.14 - Histogram of the angle between the deHoffmann-Teller velocity calculated by THEMIS observation and predicted by Cooling's model. The dashed line indicates the threshold of 30°, which represents 74% of the observations.
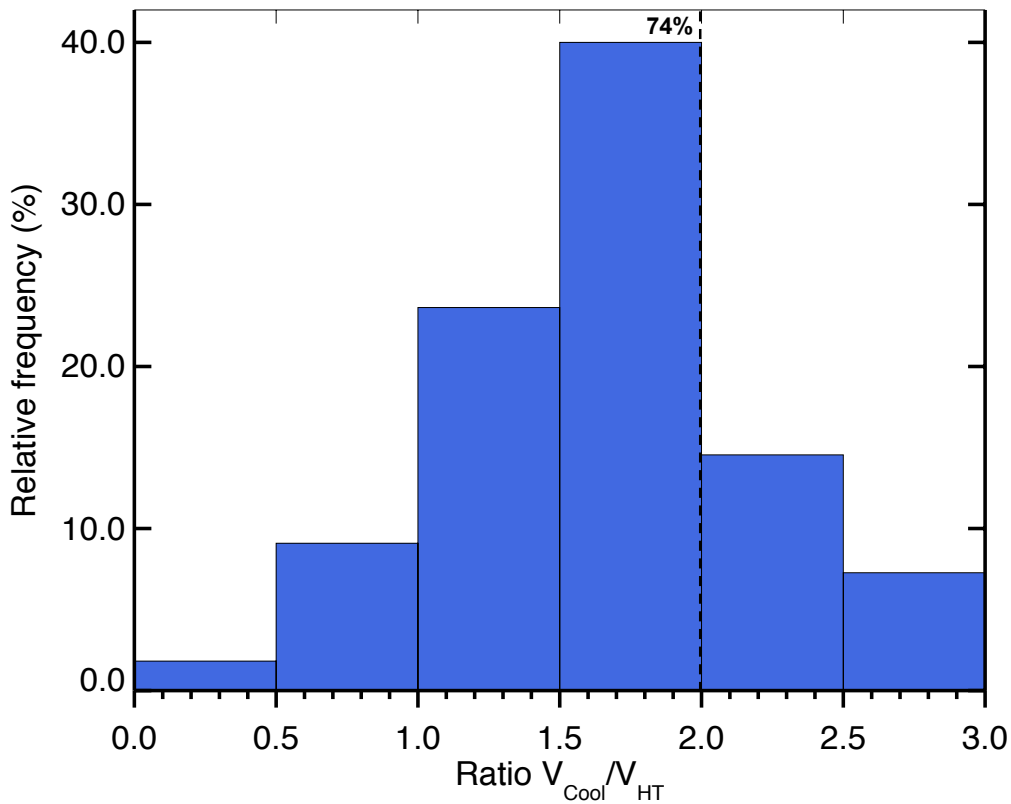
Figure 4.15 - Histogram of the ratio between the deHoffmann-Teller velocity calculated by THEMIS observation and predicted by Cooling's model. The dashed line represent the threshold of 2 factor, which represents 74% of the observations.

4.5 FTEs During Northward IMF

Dayside magnetic reconnection is in general associated to intervals of southward IMF. However, Dungey (1963) model also indicates the possibility of an antiparallel reconnection at high latitudes during northward IMF. Kawano and Russell (1997a) investigated the causes of post-terminator FTEs, located in $X_{GSM} < 0$, with a considerable number of events occurring during northward IMF. They attribute these FTEs to two possible sources, as is illustrated by Figure 4.16. For strongly northward IMF, the FTEs are explained by antiparallel reconnection near the polar cusp region shown in Figures 4.16 (a) and (c). In Figure 4.16 (b), the grey arrow represents the IMF and the black arrow represents the Earth's magnetic field lines. The thick white arrows show the expected direction of the FTE motion observed. Fear et al. (2005) also investigated FTEs during strongly northward IMF, with absolute

clock angle $< 70^o$, at high-latitude and flanks' locations. They concluded that FTE signatures were consistent with a long, component reconnection line originating from high magnetic shear in the lobe.
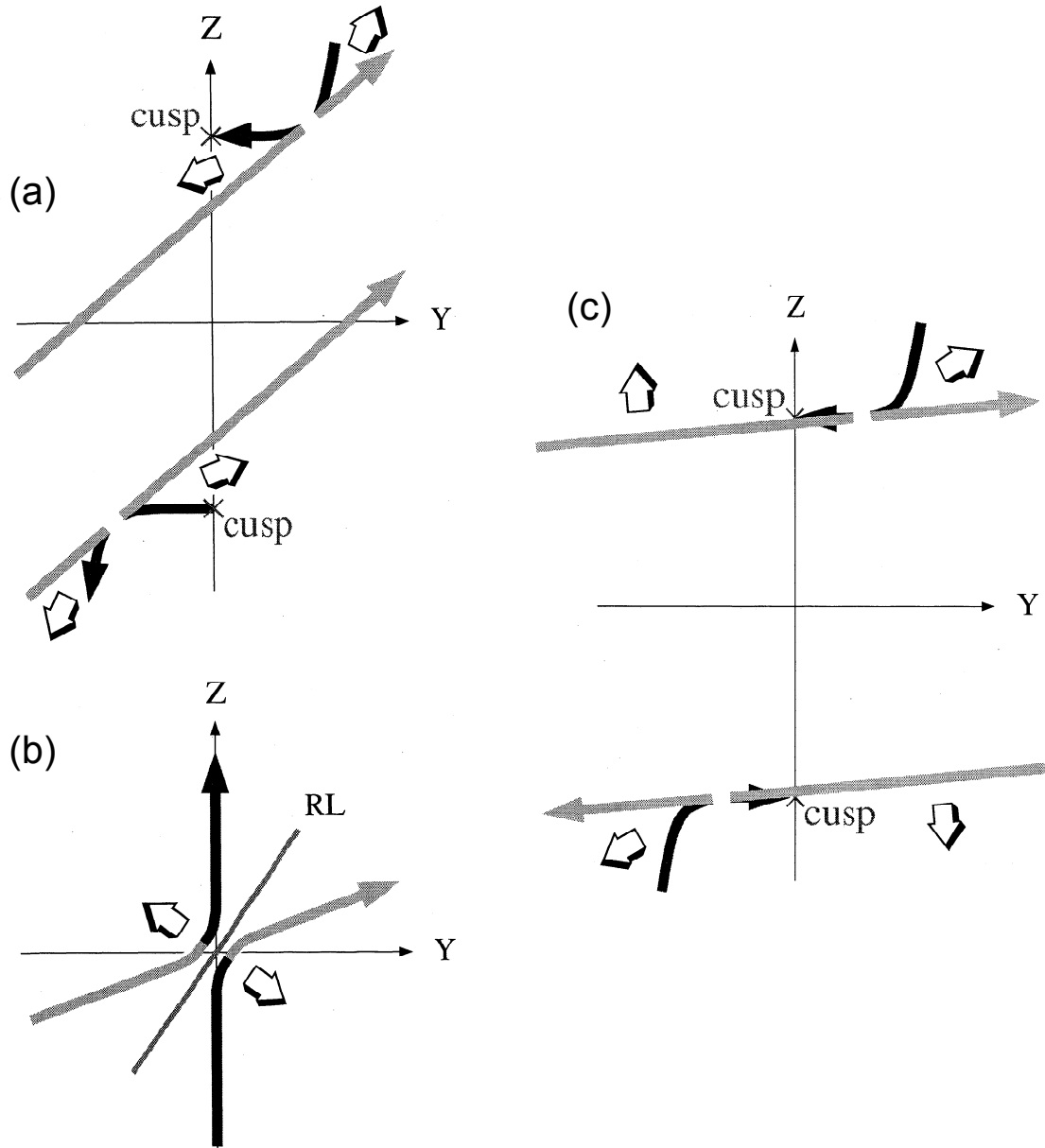
Figure 4.16 - Sketch of magnetic field line and outflow motion during northward and duskward IMF. Panel (a) shows reconnection at the cusps for strongly north-ward reconnection, panel (b) shows equatorial reconnection, and (c) shows cusp reconnection for slightly northward IMF.

SOURCE: Adapted from: Kawano and Russell (1997a).

In section 4.3 it has been presented FTE locations for several clock angle bins. There are a considerable number of events during northward IMF. This section will describe some of these events according to the available data. Figure 4.17 shows a scatter plot of B_{y-GSM} versus B_{z-GSM} IMF components in GSM coordinate system. As discussed previously, since an average value of the interplanetary parameters was taken, the error bars in the figure indicate the deviation of the measurements. In order to be confident about the IMF northward orientation during the FTE observation, it is used in this study those events which the IMF B_{z-GSM} does not change the sign to negative when the deviation is subtracted from the average, as shown by red color in Figure 4.17. More details about the FTEs are shown in Table 4.2, where one can find the event number of the FTE in the list, observation date and time, polarity of ΔB_N, IMF B_{y-GSM} and B_{z-GSM} components, and θ_{CA}.
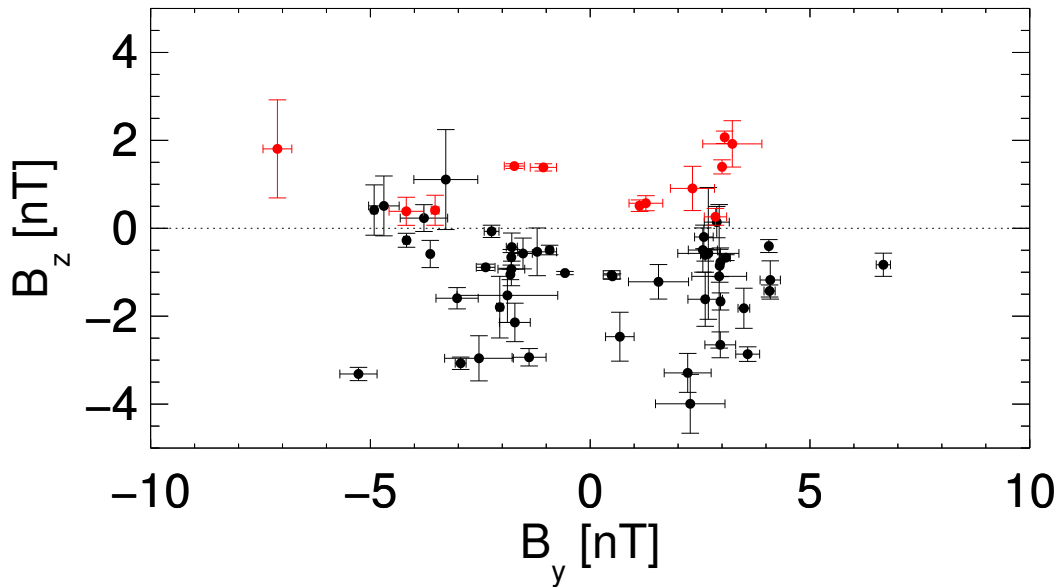
Figure 4.17 - IMF $B_{y-GSM}B_{z-GSM}$ relation with their respective pattern deviation. Red points represent those positive IMF B_{z-GSM} values that do not turn negative when the pattern deviation is subtracted from the average.

Table 4.2 - FTEs during northward IMF.

FTE	date (UT) [mm-dd-yy]	ΔB_N	B_{y-GSM} [nT]	B_{z-GSM} [nT]	θ_{CA} [^{o}]
3	05-13-07/01:16	Reverse	1.12	0.51	65.5
12	05-21-07/15:50	Reverse	3.06	2.07	55.9
13	05-27-07/12:46	Reverse	2.32	0.90	67.9
15	06-05-07/02:38	Reverse	3.00	1.39	65.0
19	06-16-07/03:30	Reverse	2.85	0.26	84.8
22	06-16-07/19:46	Reverse	1.26	0.57	64.2
23	06-17-07/10:22	Reverse	3.23	1.92	58.6
33	07-20-07/16:12	Direct	-7.11	1.80	284
39	08-05-07/09:30	Reverse	-1.06	1.38	323
42	08-17-07/03:27	Reverse	-4.18	0.38	275
44	08-22-07/08:24	Reverse	-3.52	0.41	276
45	08-24-07/08:02	Direct	-1.72	1.41	309

Figure 4.18 shows the locations of the FTEs shown in Table 4.2 and Figure 4.17. The direct FTEs are indicated by triangles and the reverse by circles. Arrow shows velocities in the deHoffmann-Teler frame. Blue arrows are the events that occurred during duskward IMF ($B_{y-GSM} > 0$) while in green are the events that occurred during dawnward IMF ($B_{y-GSM} < 0$). It is difficult to draw any conclusion about the FTEs' polarity during northward IMF because of small number of the events, i.e., only two direct FTEs and ten reverse FTEs. It is clear the separation due to B_{y-GSM} sign: for $B_{y-GSM} > 0$ the FTEs are located duskward and for $B_{y-GSM} < 0$ the FTEs are located dawnward. Many FTEs presented in this work have $|\theta_{CA}| < 70^o$, as also presented by Fear et al. (2005), but unlike their observations the FTEs are located at low latitudes of the dayside magnetopause ($X_{GSM} > 0$). Most of the velocities are toward the flanks, which is consistent with low-latitude reconnection, as described in Figure 4.16 (b). Analyzing the polarity of B_N, only direct FTEs do not agree with a magnetic reconnection at low latitudes.
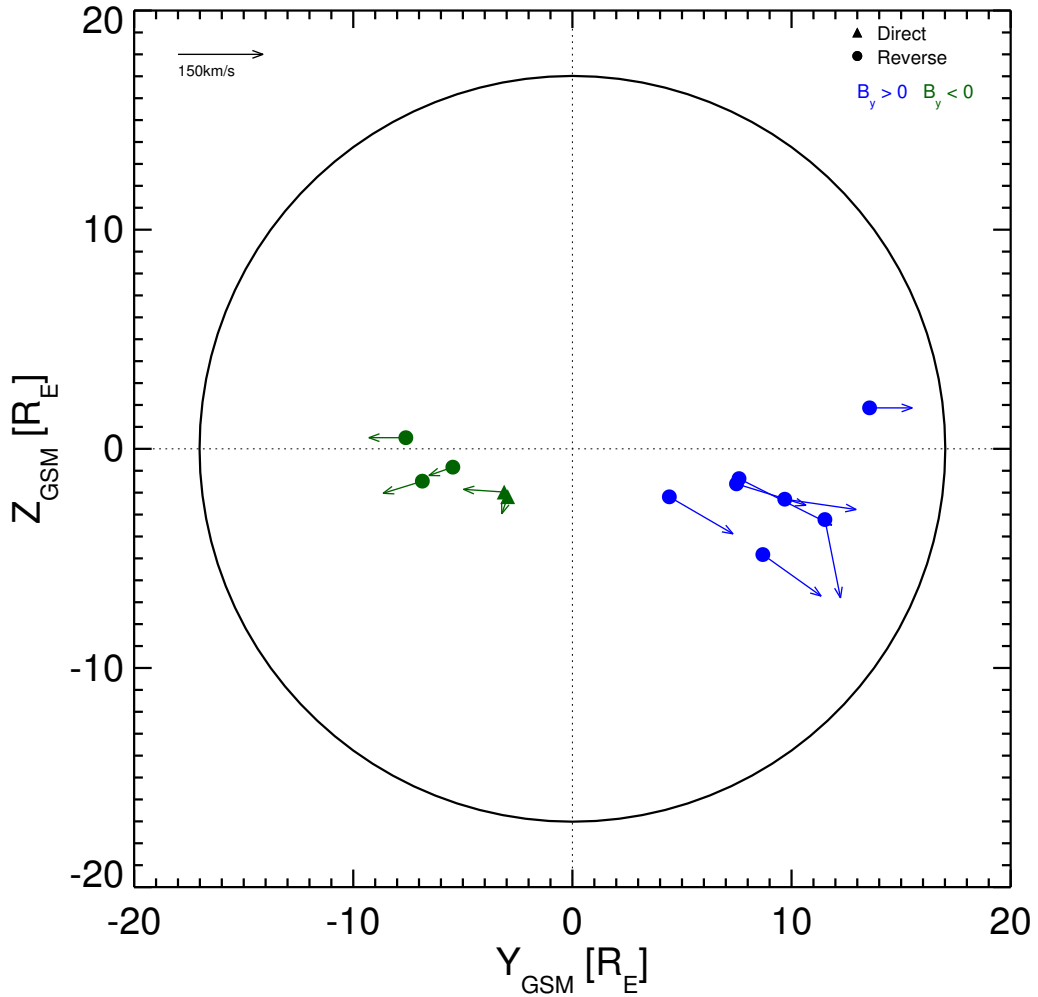
Figure 4.18 - FTE locations for northward IMF projected in the YZ_{GSM} plane. Direct FTEs are shown by triangles, reverse FTEs are show by circles. The color indicate the B_{y-GSM} orientation, in blue are the events with B_{y-GSM} positive (duskward), whilst in green are the events with B_{y-GSM} negative (dawnward). The arrows represent the deHoffmann-Teller FTE velocities in the YZ_{GSM} plane.

4.6 Summary and Discussion

In this Chapter several features about FTEs were presented using a statistical approach. Initially, OMNI data were used to do an inspection of interplanetary condition during the FTEs ocurrence. It was found that FTEs can occur during typical conditions, as shown Figures 4.1 and 4.2, including northward IMF orientation.

A fact that deserves to be emphasized is the frequent occurrence of FTEs for a B_{y-GSM}-dominant IMF condition, as shown in Figure 4.1 (c).

For the spatial distribution analysis, showed in Figure 4.3, it was observed that the FTEs spread along a large extension of Y_{GSM}. Previous works, e.g., Berchem and Russell (1984), Rijnbeek et al. (1984), showed that FTEs can be observed along the whole magnetopause. The Figure 4.5 shows again a larger occurrence during a B_{y-GSM}-dominant IMF, and a clockwise rotation of the event position can be observed as θ_{CA} increases, which is consistent with the observations by Fear (2006).

Two techniques were employed to analyze the FTE motion, in Section 4.4. The deHoffmann-Teller velocity, calculated from THEMIS data, indicates that FTEs located at the flanks of magnetosphere move antisunward and dawn/duskward. For intermediate longitudes, there is a combination of dusk/dawnward and southward motions, the latter becoming dominant at the subsolar region. Some direct FTEs have small positive V_{z-GSM} component.

The restriction that a reconnection line passes through the subsolar point can contribute to a high discrepancy of the Cooling model comparison with observational data. Trattner et al. (2007) suggest the effect of the IMF B_{x-GSM} component on the location of reconnection at the magnetopause. Recently, Hoilijoki et al. (2014) also found an effect of a superposition of B_{x-GSM} with the Earth's dipole tilt angle effects. An IMF with positive B_{x-GSM} component contributes to a reconnection line formation at the northward of the equator, whilst an IMF with negative B_{x-GSM} component contributes to a reconnection line formation at the southward of the equator. This effect is superposed to the magnetic dipole tilt and can create a considerable shift in the reconnection line location. The Earth's dipole tilt angle for the presented events (not shown) varies from -1° to 30°, and most of the events occurred for larger tilt angles. This is favorable to a reconnection line shifted southward, since B_{x-GSM} does not reach large values.

Fear et al. (2005) show that FTEs observed at the flanks are consistent with antiparallel reconnection in the lobe region. In this work 12 FTEs were observed at the equatorial region during northward IMF, but the direction of motion and bipolar signature were not consistent with high-latitude reconnection. They agree well with equatorial reconnection, since their velocities point antisunward.

5 PLASMA FLOWS ASSOCIATED WITH FTES

5.1 Introduction

In Section 4.4 it was investigated the motion of FTEs based on their location relative to the probable reconnection line position. However, it is equally important to also consider the disturbance in the ambient plasma and magnetic field caused by this motion. Russell and Elphic (1978) suggested that after a reconnection process the flux tube moves away from the reconnection site and sweeps up unreconnected field lines, generating a perturbation in the magnetic field and plasma media. Southwood (1985) also investigated the hydromagnetic aspects of perturbations inside and outside the flux tube. He noticed that the forces acting on the flux tube are different from those on the sheath and magnetosphere environment. Consequently, the flux tube and the surrounding plasma could move with different velocities. Since the FTE has rigid structure, their motion move out the external plasma way from the tube.

Farrugia et al. (1987) developed a model of field draping in FTEs to investigate the effects in the magnetic field and plasma flow outside the tube. They observed that in the FTE rest frame the flow perturbations present a bipolar form. Korotova et al. (2009) pointed out that flow perturbations in the ambient plasma depend on the relative FTE velocity to the ambient plasma. Thus, FTEs moving faster than or opposite to the ambient media must generate bipolar inward/outward flow perturbation normal to the nominal magnetopause in the magnetosphere, and outward/inward in the magnetosheath. FTEs moving with the ambient flow velocity generate no perturbation in the surrounding plasma.

The fact that the THEMIS mission is constituted of five probes allows to do multipoint observations of an FTE and of its surrounding ambient. Using THEMIS data Zhang et al. (2011) analyzed background perturbations in the magnetosphere and magnetosheath associated with FTE observations. They observed a flow vortex inside the magnetopause associated with an FTE moving antisunward.

In this chapter, multi-point observations provided by the THEMIS mission were used to investigate perturbations in the plasma parameter, outside FTEs. The objective of this chapter is to understand how the FTEs' motion disturbs the environment and how further it can be observed. In Section 5.2 it is presented an FTE moving with magnetosheath plasma velocity, in Section 5.3 bipolar variations in V_N component of ambient plasma velocity are investigated. In the Section 5.4 is presented an FTE

with rotational plasma flow in the core.

5.2 FTE Moving with Magnetosheath Plasma Velocity

On May 06, 2007 around 11:30 UT, THEMIS was in an inbound orbit in the duskside of the magnetosphere, slightly below the equator. The probes compose a line-up orbit configuration, and the largest separation among the probes was approximately 2.5 R_E in the X_{GSM} direction. In this analysis the THEMIS probes will be referenced by th+letter, from 'a' (*tha*) to 'e' (*the*), to distinguish one among the others. Figure 5.1 (a) shows the probes' locations in the XY_{GSM} plane. The nominal magnetopause is represented by the black line and is determined by the Shue et al. (1997) model. Figure (b) shows a zoom of the duskside in the same plane where it is possible to distinguish the probes' locations.
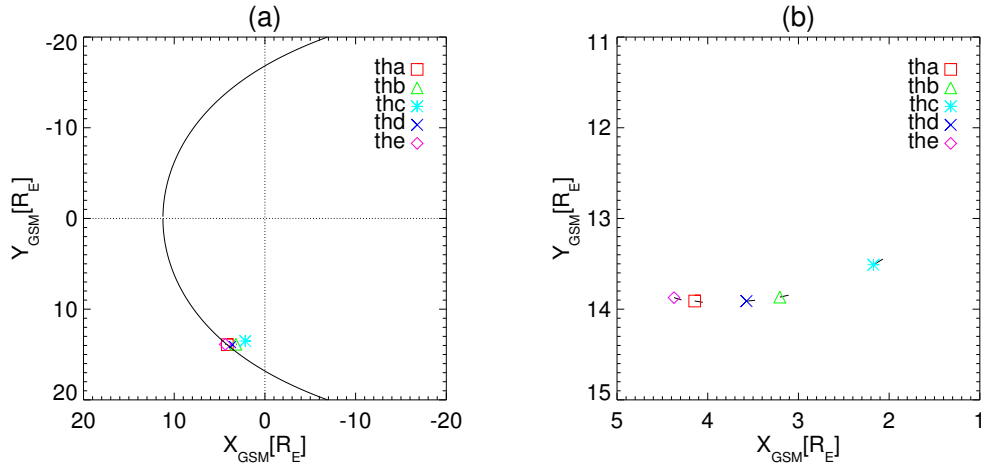
Figure 5.1 - THEMIS probes' locations for the FTE of May 06th, 2007. Panel (a) shows the location of the probes in a global view in plane XY_{GSM} and panel (b) shows a zoom for the separation among the probes.

Figure 5.2 shows the THEMIS magnetic field and plasma observations from 11:28 UT to 11:40 UT, when the FTE was observed. The IMF orientation is southward and dawnward, B_{x-GSM} is the strongest component of the field. The direct FTE in the dusk is consistent with a reconnection line by component reconnection model (GONZALEZ; MOZER, 1974), which lies in the northern-dawn to southern-dusk quadrants. Four of five probes observed FTE signatures in the magnetic field, but *tha* and *thb* did not have plasma data available. The farthest probe, *thc*, observed just plasma perturbations.
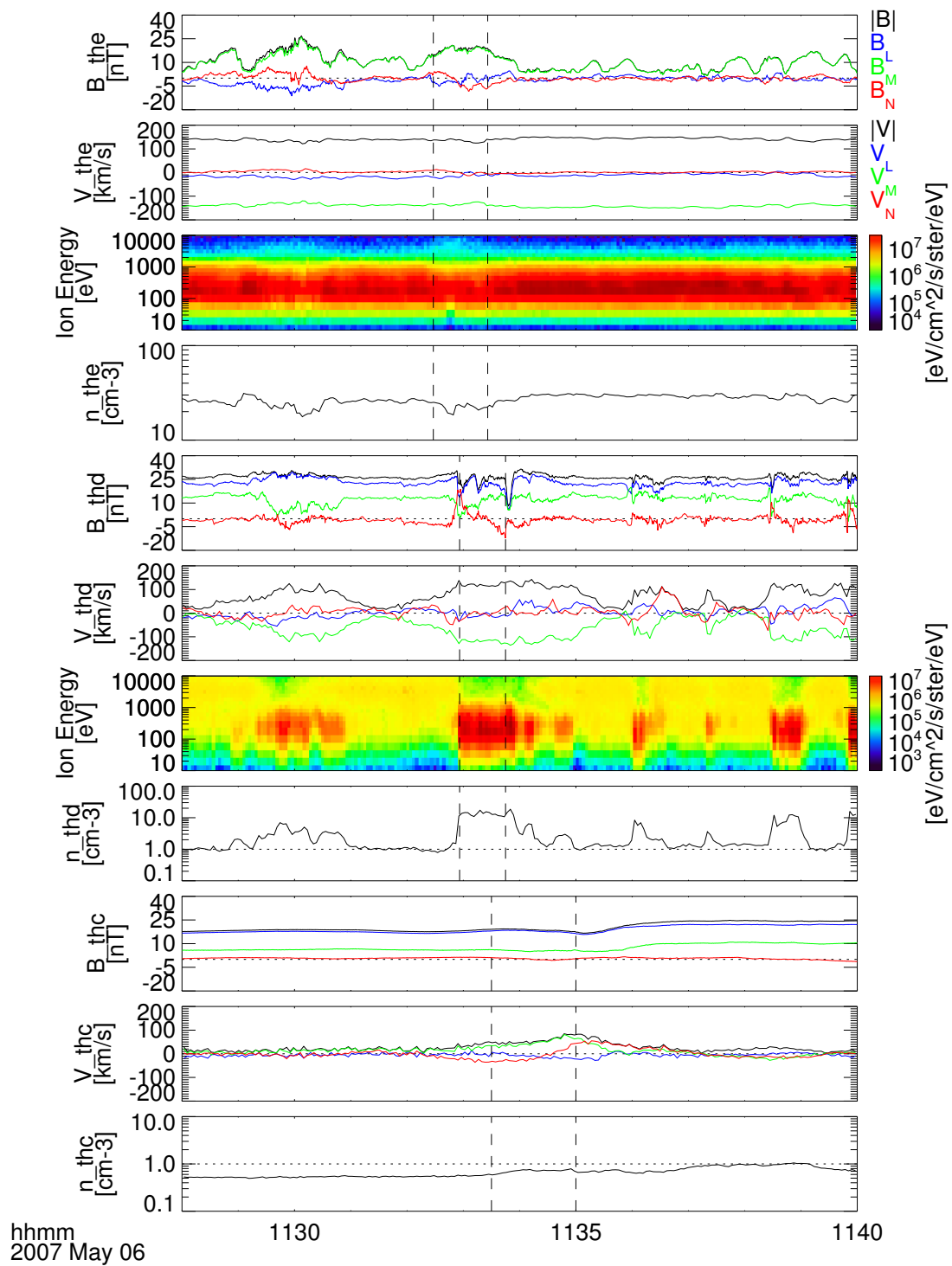
Figure 5.2 - FTE observed by the THEMIS probes on May 06th, 2007. The plots show magnetic field, ion flow velocity, ion energy distribution, and numerical ion density observed by probes *the*, *thd*, and *thc* (energy distribution was not available for *thc*). The dashed lines delimit the FTE structure.

The plots in Figure 5.2 are sorted following the FTE timing observations, where the FTE is seen by the probes *the*, *thd* and *thc*. The dashed lines delimit the FTE structure and they are defined as peak-to-peak of B_N for each probe observation. For each probe the magnetic field and flow velocity are shown in the magnetopause boundary coordinate system together with the ion energy flux distribution and ion density. Unfortunately, *thc* did not have ion energy data available for this period.

The focus of present study is on the FTE observed between 11:32 UT and 11:35 UT, marked by dashed lines. The first probe which observed the FTE was *the*. The concentration of low-energy particles (0.1 - 1 keV) and a high density of ions indicate ($> 10cm^{-3}$) that it was located in the magnetosheath. The magnetic field was predominant in the positive B_M component (green line). The B_L component (blue line) did not oscillate significantly except during the structure encounter. The same happens to the B_N component (red line), but there is a period of positive and negative deflections due to FTEs passages. It is assumed that the FTE edges are defined by maximum and minimum values of B_N. One can see the positive-negative bipolar signature in B_N centered in an $|\mathbf{B}|$ enhancement. At this time there is a slight increase in the energetic ion flux (> 1 keV) showing the presence of magnetospheric ions inside the structure. The flow velocity (V_the) does not change, as discussed by Korotova et al. (2009), and it is an evidence of the FTE flows moving with magnetosheat flow velocity.

More internal, probe *thd* was located at the boundary layer in the magnetospheric side. The magnetic field was orientated northward (see B_L component) with a considerable contribution in the positive B_M direction. During the period of interest, between dashed lines, the B_N component suffers a large variation with an amplitude of $\sim 25nT$. The most notable variations in the other components (B_L and B_M) were depletion at the FTE edges, which produced the same behavior in $|\mathbf{B}|$. The depletion layer was reported by Zhang et al. (2010) as a layer between the FTE and the magnetosphere region. The flow velocity had large variations, and sometimes the values were comparable to sheath levels ($> 100km/s$). At the FTE's core the velocity was predominant in the $-V_M$ component and almost zero in the other components, while outside the FTE there was a negative (inward) V_N before the structure encounter and a positive (outward) V_N after the structure observation. The ion distribution had an increase of the low-energy particle flux (0.1 - 1 keV) when the FTE was observed. One can notice the presence of particles from the magnetosheath after the FTE passed, but not before it. Another clear feature was the ion density remains higher after the FTE passed.

Probe *thc* was the farthest from the magnetopause and inside the magnetosphere. The magnetic field was almost in the positive B_L direction, the plasma flow was very slow, and the ion density was lower than $1cm^{-3}$. There was no significant change in the magnetic field. However, it is possible to note a variation in the flow velocity. V_N experienced a smooth rotation from negative (inward) to positive (outward) values, while V_M increased to positive values, that is in the sunward direction, since the probes are located at the duskside of the magnetosphere. Probably *thc* observed only the plasma perturbation generated by the FTE motion. The inward-outward V_N and sunward V_M indicated a plasma flowing in an opposite direction to the FTE motion, as discussed by Korotova et al. (2009) and Zhang et al. (2011).

Figure 5.3 shows a cartoon summarizing the observation of the Figure 5.2. The real scales of the structures were not considered to let the figure easily understandable. The sketch shows the FTE cross section projected in the **NM** plane. The FTE is represented by the ellipsoid surrounded by disturbed magnetic field (thin black lines) and the magnetopause, that is represented by the thick black line. The most external trajectory, magnetosheath-FTE-magnetosheath, is associated to *the*. This probe observed no variation in the flow velocity suggesting that the FTE moves with the same magnetosheath flow velocity (blue arrows). Probe *thd* in the boundary layer (delimited by grey line), passed by boundary layer-FTE-boundary layer and observed an inward flow and the disturbed magnetic field outside the FTE. Zhang et al. (2011) suggested the existence of a transition region between the FTE and the magnetopause. This region was observed by *thd* as a depletion in the magnetic field, ahead and behind the FTE. Probe *thc* observed only the disturbed magnetospheric flow in opposite sense of the FTE motion (dashed arrows), and no changes in the magnetic field.
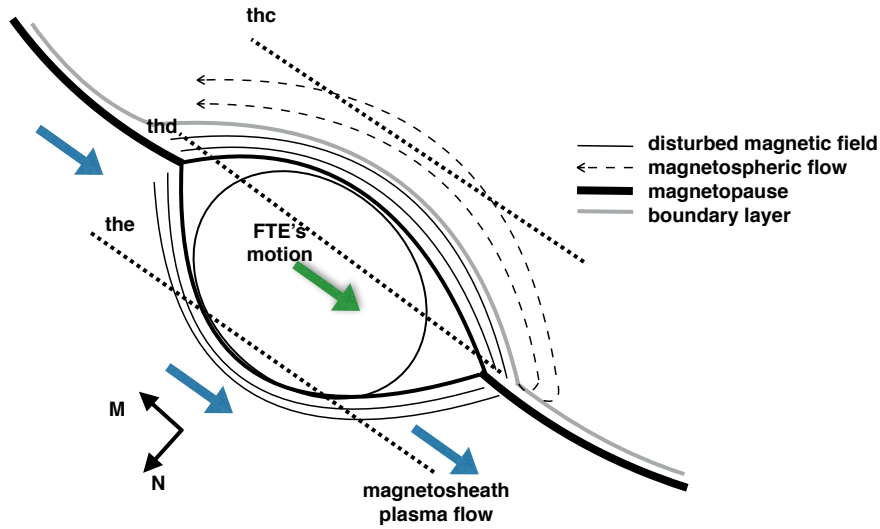
Figure 5.3 - Plasma disturbance associated to FTE motion with $V_{FTE} = V_{sh}$ related to observation showed in Figure 5.2. The FTE is represented by the ellipsoid surrounded by disturbed magnetic field (thin black lines). The FTE moves (green arrow), along the magnetopause (thick black line), with the same velocity of the magnetosheath flow (blue arrows). The probes' trajectory are indicated by dotted lines.

5.3 Magnetospheric Bipolar Flows Associated with an FTE Motion

On June 10, 2007 the THEMIS was in an inbound orbit in the dusk side of the equatorial magnetosphere. The probes were line-up into the magnetosphere and the maximum separation among them was approximately 2 R_E in the X_{GSM} direction. Figure 5.4 (a) shows a global view in the XY plane of probes' locations and (b) shows a zoom of the duskside where it is possible to see more details about their locations. Probe *tha* was the outermost and located at the magnetospheric boundary layer, while *thb* was the farthest from the magnetopause, located inside the magnetosphere.
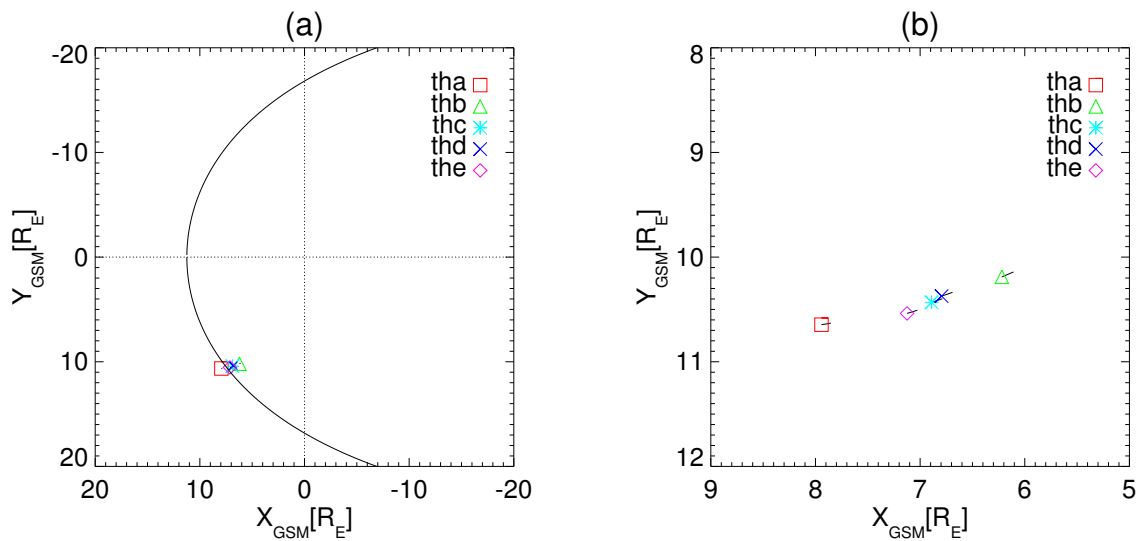
Figure 5.4 - THEMIS probes locations for the FTE of June 10th, 2007. Panel (a) shows the locations of the probes in a global view and panel (b) shows a zoom for the separation among the probes.

Figure 5.5 shows the magnetic field and plasma flow velocity in the magnetopause boundary coordinate system recorded by the THEMIS when the FTE was observed. The sequence of plots follows the probes' locations shown in Figure 5.4, where the sequence of probes which observe the FTE is *tha, the, thc, thd* and *thb*. For this event it was plotted the ion density and the ion energy flux separately from the magnetic field, in Figure 5.6. In this period the IMF orientation was southward and duskward, but B_{x-GSM} was the strongest component of the field (not shown). The equatorial and duskward FTE location at $Z_{GSM} = -0.5R_E$ was not consistent with the model of component reconnection line, which lies in northern-dusk to southern-dawn quadrants. However the direct signature of B_N component suggests that the reconnection occurred southward of satellite position.
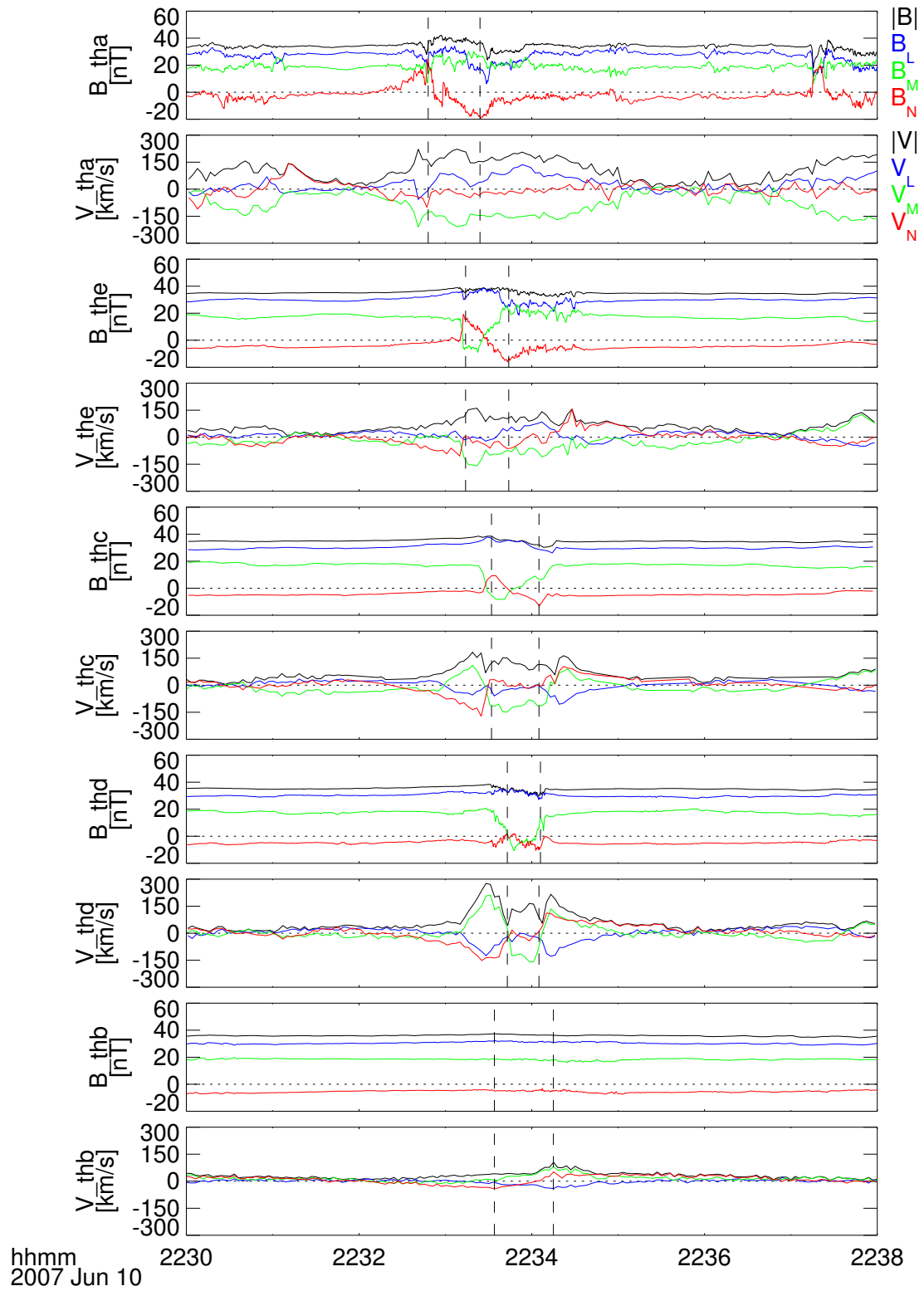
Figure 5.5 - FTE observed by the THEMIS probes on June 10th, 2007. The plots show magnetic field and ion flow velocity observed by the probes *tha*, *the*, *thc*, *thd* and *thb*, respectively. Dashed lines delimit the FTE's structure.

Figure 5.6 - Ion density and energy flux observed by the THEMIS probes on June 10th, 2007. The plots show numerical ion density and ion energy distribution observed by the probes *tha*, *the*, *thc*, *thd* and *thb*, respectively. Dashed lines delimit the FTE's structure.

The outermost probe, *tha*, was located at the magnetospheric boundary layer, which is characterized by ion density, between 1 and 10 cm^{-3}, and mixture of particles from both magnetosheath and magnetosphere regions during whole interval. The magnetic field observed by *tha* 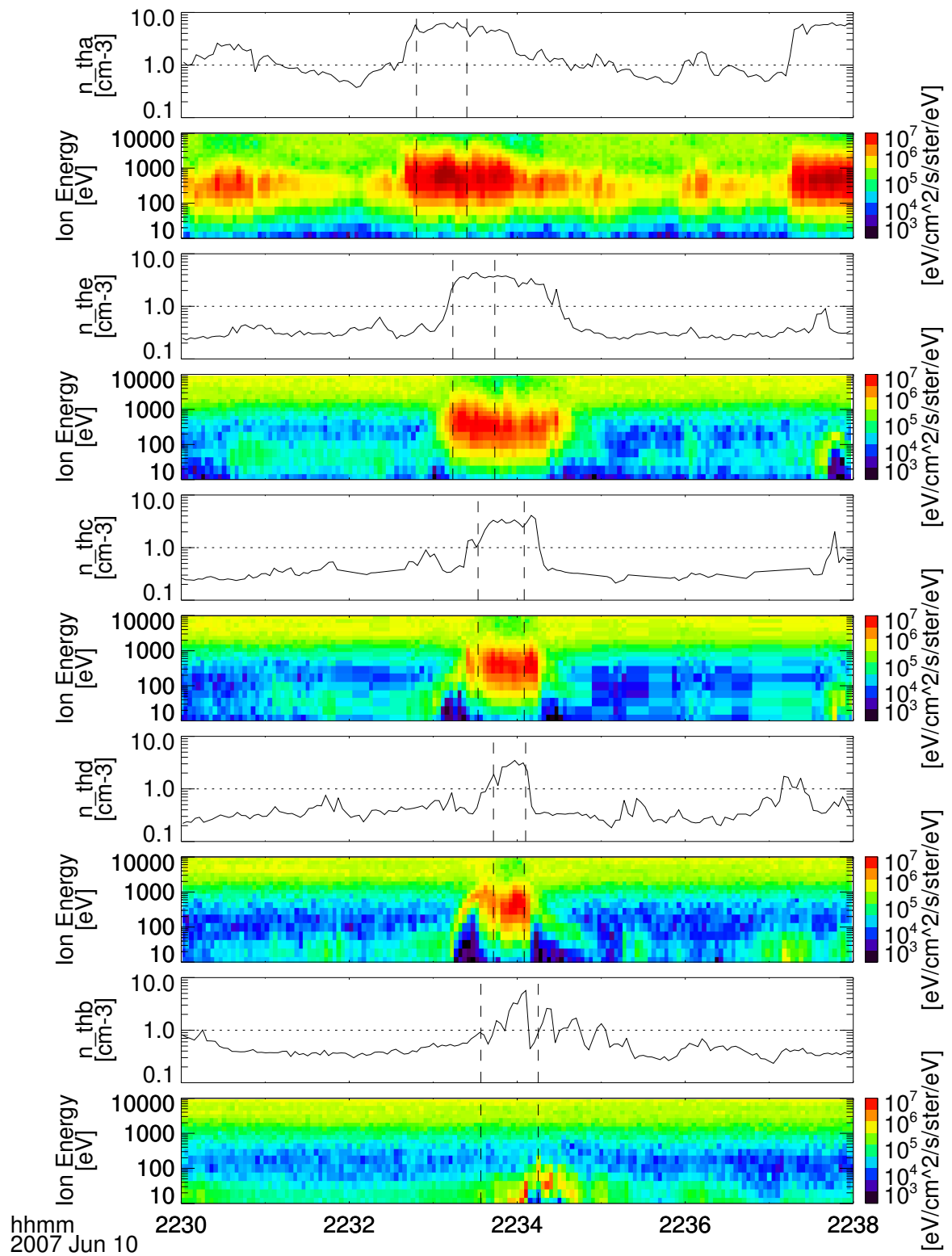had a northward (positive B_L) component and a positive B_M, which points dawn-sunward at the probe location simultaneously to almost zero B_N component. At 22:33 UT the magnetic field presented a direct bipolar variation in B_N (with $\Delta B_N \sim 40$ nT) centered in the increased of magnetic field strength. A large variation was observed in the other components as well. B_M component had a decrease at the FTE's core at the same time when B_L increased. Besides both B_M and B_L components presented depletion close to the FTE edges (indicated by dashed lines). Analyzing flow velocity it is possible to note the inward component $(-V_N)$ before the FTE observation. Within the FTE structure (indicated by dashed lines), plasma flow was more intense to anti-sunward direction $(-V_M)$, there was also a positive V_L contribution. The flow velocity remained intense behind the FTE, probably because the probe was observing the magnetosheath flow velocity.

The second probe which observed the FTE was *the*. It was located at the magnetosphere, where the ion density was lower than 1 cm^{-3} and the flux of energetic particles was higher than 1 keV. The bipolar variation of the observed ΔB_N was lower than for *tha*, ~ 30 nT, and the total magnetic field did not increase significantly at the FTE's core, as seen in the B_L component. The variation in B_M was dramatic, it turned to negative values in the beginning of the structure and returned to high positive values at the trailing edge. The depletion close to the FTE edges is not clear. There were small fluctuations in all components after the FTE observation. Flow velocity showed an inward flow before the FTE, and the flow inside the FTE was mainly in the $-V_M$ direction. The expected outward flow after the structure did not appear just after the structure passed, it was observed a few seconds after the probe left the FTE where the other components remained disturbed.

During the magnetosphere entrance the probes *thc* and *thd* were close to each other and observed similar features in magnetic field and flow velocity. Both observed a bipolar variation in the B_N and dramatically decrease in the B_M component, which changed its orientation. B_L had a smooth decrease as seen in the magnetic field strength and there was no signature of the transition region. Most remarkable signatures were observed in the velocity data. In the beginning of the observation the velocities were typical in the magnetosphere without large perturbations. Just before the structure encounter there was a jump in all velocity components, V_N inward, V_L southward and V_M sunward. The speed at the same time reached 150 km/s in

thd and approximately 300 km/s in *thd*. Inside the FTE both probes observed flow in only $-V_M$ direction with speeds lower than the outside. Behind the FTE both probes observed an outward V_N flow, a sunward V_M, and southward V_L. The speeds also were higher than those inside the FTE.

Probe *thb*, the farthest from the magnetopause, observed no magnetic field variation. However velocity variations were observed in the same period which the FTE was observed by the other probes. The inward/outward V_N, southward V_L and positive V_M flow were consistent with plasma displacement in opposite sense of the FTE's motion. An increase in ion density was observed at the same period of the velocity variation and it stayed longer.

Figure 5.7 shows the sketch to illustrate the probes' trajectories through the FTE for the present event. As seen in Figure 5.3, the FTE cross section is represented by the ellipsoid surrounded by the disturbed magnetic field and the magnetospheric plasma flow. It is assumed that FTE's motion is in **NM** plane. Using information provided by all the THEMIS, it is possible to observe different layers in the structure. The observations of *tha* are consistent with a trajectory passing through the FTE's core and in the magnetospheric side of the magnetopause. Similar observations are found by *the*, however the inward/outward flow is more clear, suggesting a trajectory more distant from the magnetopause than *tha*.

Well defined inward/outward flow variation was observed by *thc* and *thd*. They showed the three regions with different plasma flow regimes. The first one is before the structure where the plasma is pushed by FTE motion inward the magnetosphere and in opposite direction of the structure motion. Inside the FTE the flow is predominately in the $-V_M$ direction, which it is expected to an FTE observed in the equatorial dusk flank.

Just after the structure the V_N points outward the magnetosphere, V_L points again to southward and V_M sunward, in opposite sense of the an FTE's motion. These observation can be interpreted as a plasma vortex due to FTE motion, discussed by Zhang et al. (2011). *thd* observed speeds outside the FTE higher than the inside, this is probably because the probe passed by the FTE's "flank" where the flows must be higher. The deepest probe, *thb*, only observed variations in velocity and ion density. These observations are consistent with an FTE moving duskward and displacing the ambient plasma in an opposite direction.
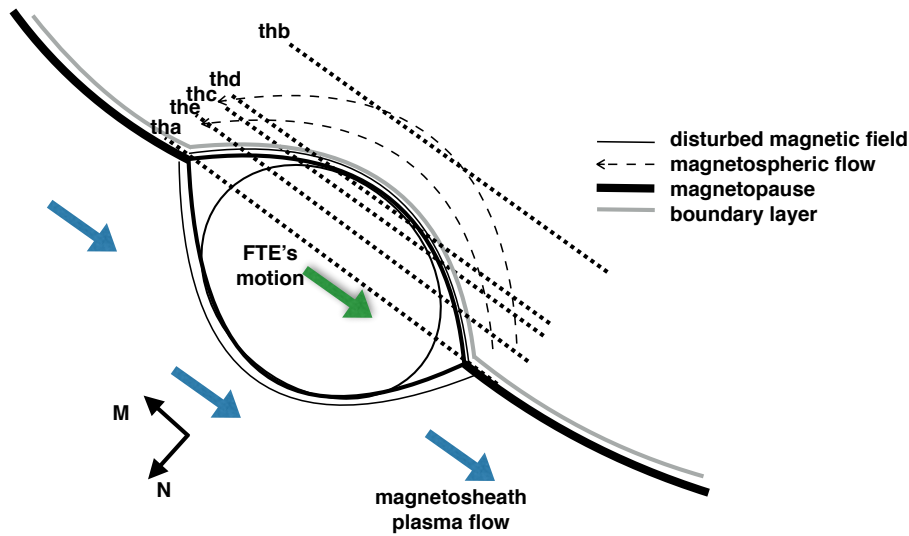
Figure 5.7 - Magnetospheric flows associated to an FTE. The sketch is similar to previous Figure 5.3. In this case four probes crossed the FTE showed in Figure 5.5 and its effects in the ambient plasma.

5.4 Rotational Flow in an FTE's Core

On May 13, 2007 the THEMIS was in an inbound orbit in the duskside of the magnetosphere, in the Northern hemisphere. Figure 5.8 (a) shows a global picture of the probes' locations in the XY_{GSM} plane of the magnetosphere and (b) shows a zoom in the dusk region, where it is possible to observe the separation among the probes. The maximum separation among the probes was about 2 R_E in the X_{GSM} direction.

Figure 5.9 shows magnetic field and plasma data recorded by three of five THEMIS probes. All probes were in the dusk side of magnetosphere, slightly above of the equator, between 01:12 UT and 01:20 UT. The lagged IMF (not shown) indicates a constant positive B_{z-GSM} and a duskward B_{y-GSM}. The observation of a reverse FTE moving toward the flank is consistent with the IMF orientation. The outer probe, *tha*, was close to the magnetopause boundary layer followed by probe *the*. The deepest probes *thc* and *thd* did not have ion velocity data available, so they will not used in this analysis. Sorted by probes location in Figure 5.8 the plots from top to the bottom show the magnetic field and ion velocity in magnetopause boundary coordinate system, ion energy flux distribution, and number density to each probe.
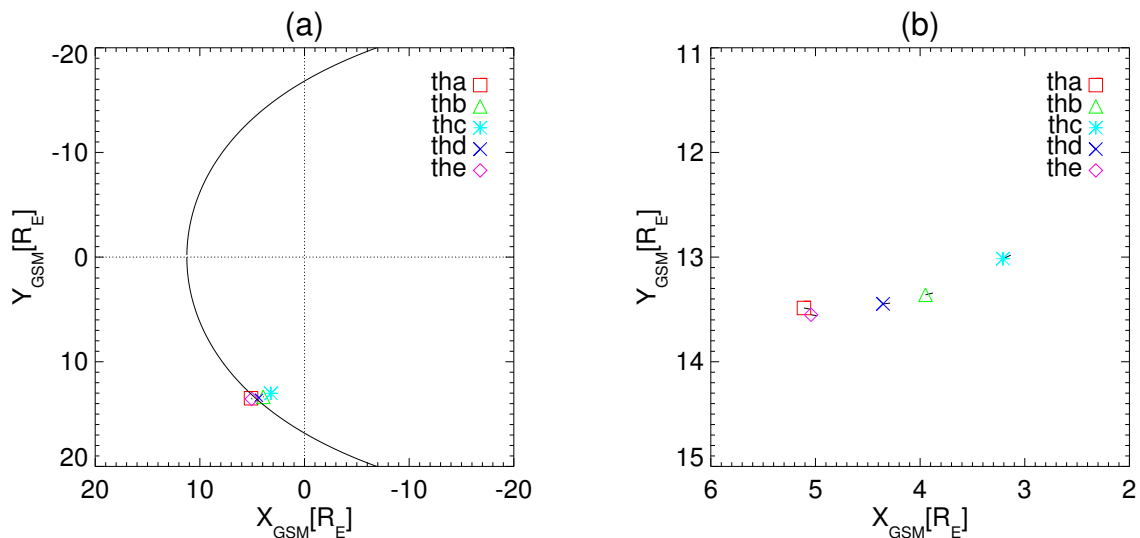
Figure 5.8 - THEMIS probes' locations for FTE on May 13th, 2007. Panel (a) shows the locations in a global view and panel (b) shows a zoom in where it is possible to see the separation among the probes.

Probes *tha* and *the* were located close to the other in the internal boundary layer of the magnetosphere. The magnetic field had a strong B_L pointing northward and a dawn-sunward B_M component during the whole period observed. Total magnetic field was almost constant (~ 25 nT) and B_N component was around zero for most of the observation time. In a short time before 01:16 UT *tha* and *the* observed a large bipolar variation ($|\Delta B_N| \sim 22$ nT) indicating the presence of an FTE, marked by dashed lines. In both probes' observations, B_M had an enhancement in the beginning of the structure followed by a negative excursion, reaching a minimum value at the end of the structure. The total magnetic field $|\mathbf{B}|$ and B_L component had a similar behavior, there was a significant depletion just before the FTE and a small one after the FTE. These observations are consistent with FTE class C' suggested by Paschmann et al. (1982) discussed in Chapter 2. Ion energy flux shows the coexistence of energetic ions (> 1keV) from the magnetosphere and the magnetosheath (< 1 keV), with a little high magnetospheric ion flux. But, inside the FTE the flux of low-energy ions increased considerably and remained a few seconds, which indicates the entry of plasma from the magnetosheath.

Figure 5.9 - FTE observed by the THEMIS probes on May 13th, 2007. The plots show
magnetic field, ion flow velocity, ion energy distribution, and numerical ion
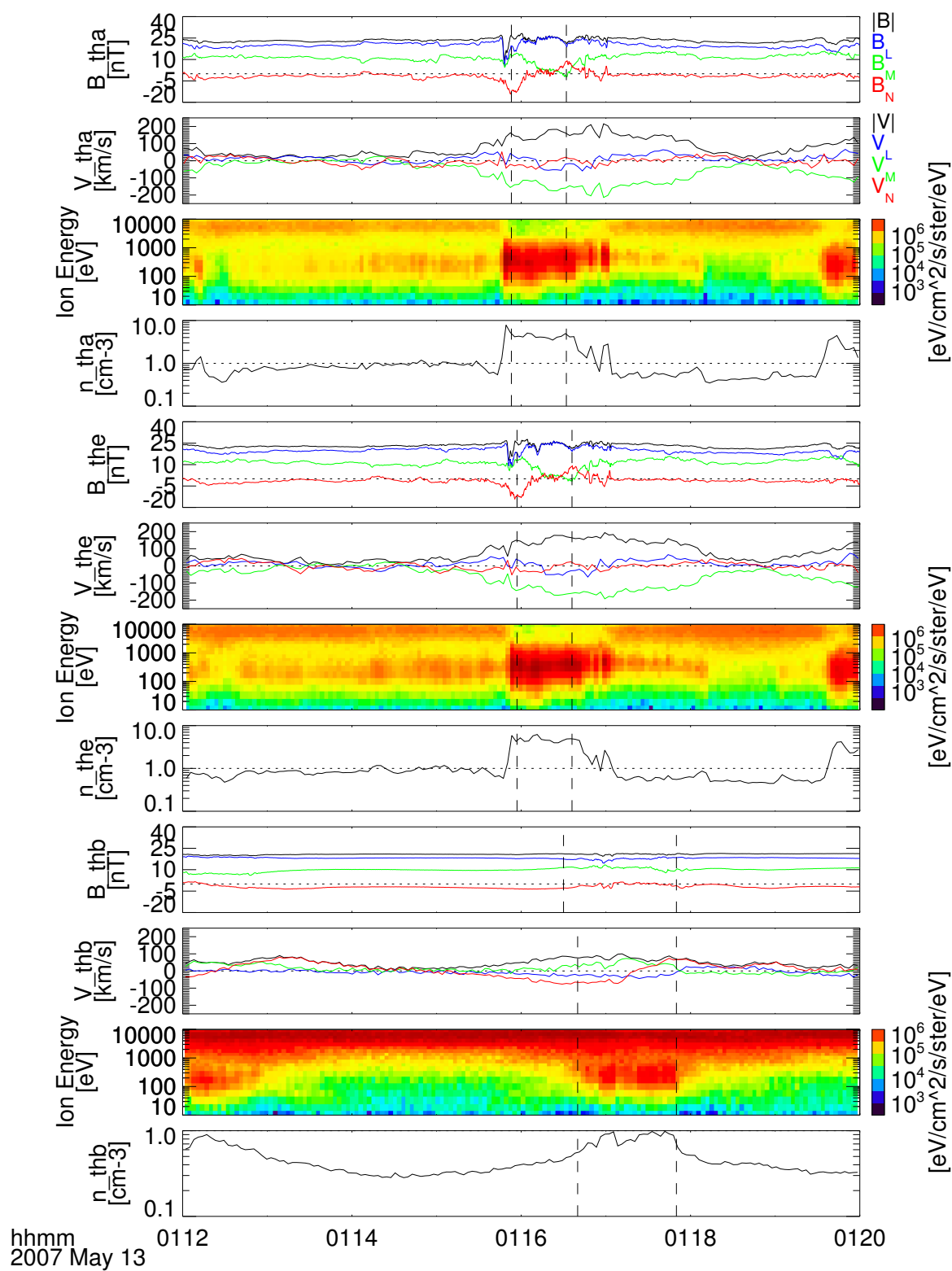density observed by probes *tha*, *the*, and *thb*, respectively. Dashed lines delimit
the FTE's structure.

Analyzing the ion velocity far from the event the plasma flow was typically from the magnetosphere and almost steady. Around the encounter with the FTE the flow speed increased. The V_M component pointed in the anti-sunward direction which is consistent with the magneosheath flow. The V_N component presented a very quick bipolar variation (outward-inward) in front of the FTE, this feature is more clear in *the* observation. Inside the FTE the velocity was dominant in the $-V_M$ direction and rotation in V_N and V_L was observed. V_N rotated from inward to outward and V_L rotated from northward to southward. Korotova et al. (2009) suggested a rotation in FTE core associated with Alfvén waves propagating parallel or anti-parallel to the magnetic field. A positive correlation between V_N and B_N indicates an opposite propagation to local magnetic field lines. After the FTE passed the velocities remained in the magnetosheath levels.

Perturbations due to the FTE motion were observed by *thb*, which was distant from *tha* by 1.16 R_E in X_{GSM} and 0.14 R_E in Y_{GSM} further in the magnetosphere. A bipolar variation was observed in the V_N component around a few seconds after the two previous probes observed the structure. As discussed in previous case, V_M increases in opposite sense of the FTE flow. These indicate that, again, the FTE motion generates a displacement in the ambient plasma. Plasma density and the flux of particle energy observed by *thb* also were disturbed by FTE's motion. The flux of particle energy with low-energy, probably from the magnetosheath, was enhanced at the same time that disturbed velocity was observed. Also, it was shown an increase in the number density of ions for the same period.

Figure 5.10 shows a sketch to explain the observations of the FTE showed in Figure 5.9 moving duskward with rotating plasma in the core. Considering the location of the reconnection line the reverse FTE must have a southward component in the velocity. But taking into account the location where the FTE was observed, it is assumed that its motion is mainly in the **NM** plane. The FTE is represented by an ellipsoid surrounded by a disturbed magnetic field. The dashed arrows indicate the magnetospheric plasma flowing in opposite sense of the FTE's motion. Probes *tha* and *the* were close to each other, so they are represented by only one trajectory (dashed thick line). The interpretation is that they passed through the FTE core and observed the bipolar variation just in the V_N component. Furthermore, it was clearly observed the rotational flow in the FTE's core (in the V_N - V_L plane). The positive correlation between V_L and B_L implies Alfvén waves propagating against the local magnetic field line direction (KOROTOVA et al., 2009). Probe *thd* was a good candidate to see the rotation in V_N and V_M, but unfortunately there was no plasma

data available. The motion in the opposite sense was observed by *thb* as a bipolar variation in a V_N inward-outward flow combined with a V_M flow.
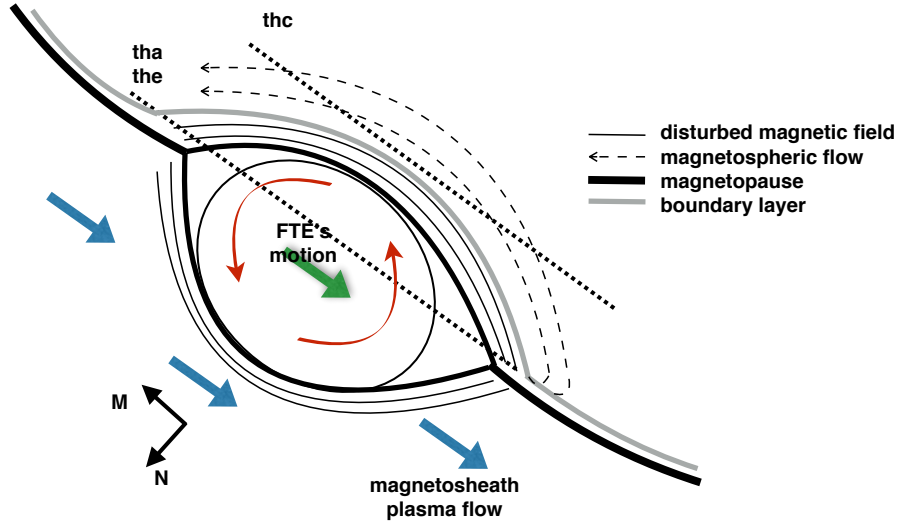
Figure 5.10 - Rotational Flow in an FTE's Core. The sketch is similar to Figure 5.3. In this case the red arrows represent the rotating flow in the FTE's core. *the* and *tha* are shown in the same trajectory because they were close to each other and observed the same features of plasma and magnetic field.

5.5 Summary and Discussion

In this Chapter it was discussed about plasma flows inside and outside the FTEs. Korotova et al. (2009) suggested that plasma flows associated with FTEs depend upon the relative FTE's motion and the plasma ambient velocity. Zhang et al. (2011) suggested plasma flow vortices inside the magnetosphere associated with FTEs. There were analyzed flow velocities inside and surrounding the FTE observed by THEMIS probes in 2007, and noted that plasma perturbations associated with FTEs are more easily observed in the magnetosphere than in the magnetosheath. Generally, FTEs move with the magnetosheath velocity when observed in the magnetosheath, whilst they move faster than the plasma velocity in the magnetosphere.

Three case presented include representative signatures observed in dataset in this thesis. The first case shows an FTE observed at both sides of the magnetopause, where the magnetosheath probe observed a perturbation in the magnetic field, the ion energy flux and the ion density, but they observed no flow velocity perturbation, which is consistent with an FTE moving with the same velocity of the magne-

tosheath plasma flow. The magnetic field and plasma signatures were more clear inside the magnetosphere. The probe in the boundary layer had a direct entry into the FTE core. The probe farthest from the magnetopause observed only a plasma parturbation.

The second case presented an FTE observed by all THEMIS probes located inside the magnetosphere, with velocity variations showing a clear inward/outward flow. These flow variations depend on the probe trajectory through the FTE structure. When the probe has a direct encounter with the FTE, as *tha*, the plasma flow is similar to the magnetosheath flow. For a more internal crossing, as *thc* and *thd*, it is possible to observe the inward/outward flow generated by the FTE motion, besides the flow inside the structure. The interesting fact is the high speed observed by *thd* outside the structure, this might be a hydrodynamic effect of a fluid passing by a rigid obstacle.

The last case study shows an FTE with a rotating flow inside its core. It was observed by two probes located in the boundary layer, close to each other. Within the FTE the flow was mainly in the antisunward direction. V_N and V_L present a rotation inside the structure. Korotova et al. (2009) observed such a feature in FTEs and suggested their relation with Alfén waves moving along the principal structure axis. They point out that the direction of wave propagation is related to the ΔB_N and ΔV_N signs. The Alfén waves propagating parallel (antiparallel) to the axial magnetic field produce anticorrelated (correlated) variations in B_N and V_N.

6 CONCLUSIONS AND FUTURE WORKS

6.1 Conclusions

In this thesis it has been studied a considerable number of flux transfer events in details. Although the techniques presented here had been employed in previous studies, the analysis of equatorial FTEs using multi-point observations and of its subsequent motion have a significant importance to better understand magnetic reconnection at the Earth's magnetopause. It was created a list of flux transfer events observed by THEMIS probes at the dayside of the magnetopause and characterized these events according to the solar wind parameters and magnetic reconnection locations.

In Chapter 4 it was presented solar wind related distribution of FTEs occurrence and location. It was found that FTEs can occur during a typical solar wind condition, including northward IMF orientation. For the spatial distribution it was observed that the FTEs spread along a large extension of Y_{GSM}. A fact that deserves to be emphasized is the large occurrence of FTE events for a B_{y-GSM}-dominant IMF, which is also observed in the clock angle analysis. Also the observation of a clockwise rotation of the reconnection line is consistent with model of magnetic reconnection by component.

In the FTE motion analysis the deHoffmann-Teller technique indicated that FTEs at the flanks of the magnetosphere tend to move antisunward as well as dawn or duskward. For FTEs at the dayside magnetopause the majority of the propagation velocity shows a combination of duskward (or dawnward) with a southward motion, the latter one becoming dominant at the subsolar region. The V_{z-GSM} values are small for direct FTEs.

Comparison between the observed velocities of FTEs with those predicted by the Cooling model presented a good agreement at the flanks. The discrepancies between predicted and observed velocities might be due to the assumption in which reconnection line should pass through the subsolar point. In other words, reconnection line is located in somewhere else of the equatorial region, e.g. the place in which the shear angle is maximized (TRATTNER et al., 2007). It was observed FTEs during northward IMF orientation, unlike previous works, the FTEs are located in low latitudes of the dayside magnetopause and the reverse FTEs are consistent with equatorial reconnection line. The reverse FTEs do not agree with reconnection in low latitudes.

In Chapter 5 case studies of FTEs observed at multi-point observations done outside of the FTE structures were presented. Those cases represent different features found in our dataset. They showed that it is more difficult to observe flow variation in the magnetosheath than in the magnetosphere. The flow signature inside the magnetosphere depends on the point at which the probe encounters the FTE. If the probe crosses directly through the core it will observe the internal FTE flow and a typical magnetosheath flow. Now, if the probe passes by the FTE further from the magnetopause it can observe an inward flow ahead and outward flow behind the FTE in the V_N component. One interesting observation showed that the flow at the FTE edges can be faster than that inside the structure. It was showed also that disturbances in plasma parameters is more significant than magnetic disturbance deep inside the magnetosphere.

An example of rotating flow inside the FTE was showed. It was observed by two probes located in the boundary layer, close to each other. Within the FTE the flow is mainly in the antisunward direction. The B_N and B_L components presented a rotation inside the structure. Korotova et al. (2009) observed such feature in FTEs and suggested that an Alfén wave is moving along the (opposite) sense of the principal structure axis.

6.2   Future Work

Flux transfer events (FTEs) are often observed in the vicinity of the Earth's magnetopause and are considered to be result of transient magnetic reconnection. Thus, study on magnetic reconnection is one of the important issues for the time-dependent solar wind-magnetospheric coupling process. Although previous studies have been elucidating several features about FTEs since its discovery, some fundamental questions still remain unsolved: Which model is the best to explain the FTE formation?; What is the influence of interplanetary conditions for the FTEs formation?

The formation of FTEs can be investigated with observational approaches as well as with numerical simulations and/or theoretical models. As mentioned above, the relation between observed FTEs and theoretical FTE models has not been clear yet. THEMIS mission can allow to observe FTEs at distinct points of the magnetosphere, magnetopause and magnetosheath. Therefore, in future works one can focus attention to comparing models of FTEs' formation with observed FTE information, verify the global effect of FTEs on the magnetospheric dynamics, and extend the FTEs list to the post-terminator magnetosphere.

Two facts that facilitates studying structures like FTEs are their frequent rate of occurrence and that they do not need extreme interplanetary condition to occur. Although the THEMIS mission is still providing awesome contributions to the understanding of magnetospheric dynamics, there is now a great expectation of more related research with the Magnetospheric Multiscale satellites - MMS mission, which will allow the study of magnetic reconnection down to the electron skin depth scale.

REFERENCES

ALEXEEV, I. I.; BELENKAYA, E. S.; BOBROVNIKOV, S. Y.; KALEGAEV, V. V. Modelling of the electromagnetic field in the interplanetary space and in the Earth's magnetosphere. **Space Science Reviews**, v. 107, p. 7–26, apr. 2003. 47

ANGELOPOULOS, V. The THEMIS mission. **Space Science Reviews**, v. 141, n. 1-4, p. 5–34, dec. 2008. 25, 26

AUSTER, H. U.; GLASSMEIER, K. H.; MAGNES, W.; AYDOGAR, O.; BAUMJOHANN, W.; CONSTANTINESCU, D.; FISCHER, D.; FORNACON, K. H.; GEORGESCU, E.; HARVEY, P.; HILLENMAIER, O.; KROTH, R.; LUDLAM, M.; NARITA, Y.; NAKAMURA, R.; OKRAFKA, K.; PLASCHKE, F.; RICHTER, I.; SCHWARZL, H.; STOLL, B.; VALAVANOGLOU, A.; WIEDEMANN, M. The THEMIS fluxgate magnetometer. **Space Science Reviews**, v. 141, n. 1-4, p. 235–264, dec. 2008. 25

BAUMJOHANN, W.; TREUMANN, R. A. **Basic space plasma physics**. London: Imperial College Press, 1996. 340 p. ISBN 1-86094-017-X. 3, 4, 6, 12

BERCHEM, J.; RUSSELL, C. T. Flux transfer events on the magnetopause - Spatial distribution and controlling factors. **Journal of Geophysical Research**, v. 89, n. A8, p. 6689–6703, aug. 1984. 18, 61

CHAPMAN, S.; FERRARO, V. C. A. A new theory of magnetic storms. **Terrestrial Magnetism and Atmospheric Electricity (Journal of Geophysical Research)**, v. 36, p. 171, 1931. 11

COLLADO-VEGA, Y. M. **The evolution and motion of transient events in the solar wind-magnetosphere interaction**. PhD Thesis (PhD) — The Catholic University of America, 2013. 23

COOLING, B. M. A.; OWEN, C. J.; SCHWARTZ, S. J. Role of the magnetosheath flow in determining the motion of open flux tubes. **Journal of Geophysical Research**, v. 106, p. 18763–18776, sep. 2001. 21, 22, 41, 46

COWLEY, S. W. H. Magnetosphere-ionosphere interactions: A tutorial review. In: _____. **Magnetospheric Current Systems**. American Geophysical Union, 2013. p. 91–106. ISBN 9781118669006. Available from: <http://dx.doi.org/10.1029/GM118p0091>. 13

COWLEY, S. W. H.; OWEN, C. J. A simple illustrative model of open flux tube motion over the dayside magnetopause. **Planetary and Space Science**, v. 37, p. 1461–1475, nov. 1989. 46, 47

DALY, P. W.; RIJNBEEK, R. P.; SCKOPKE, N.; RUSSELL, C. T.; SAUNDERS, M. A. The distribution of reconnection geometry in flux transfer events using energetic ion, plasma and magnetic data. **Journal of Geophysical Research**, v. 89, p. 3843–3854, jun. 1984. 18

DEHOFFMANN, F.; TELLER, E. Magneto-hydrodynamic shocks. **Physical Review Letters**, American Physical Society, v. 80, p. 692–703, Nov 1950. Available from: <http://link.aps.org/doi/10.1103/PhysRev.80.692>. 41

DUNGEY, J. W. Interplanetary Magnetic Field and the Auroral Zones. **Physical Review Letters**, v. 6, n. 2, p. 47–48, jan 1961. 1, 11

_____. The structure of the exosphere or adventures in velocity space. In: _____. **The Earth's Environment**. New York: Gordonand Breach, 1963. p. 505–550. 56

ELPHIC, R. C. Observations of Flux Transfer Events: A Review. In: _____. **Physics of the Magnetopause**. [S.l.]: the American Geophysical Union, 1995. p. 225–+. 17, 18

FARRUGIA, C. J.; ELPHIC, R. C.; SOUTHWOOD, D. J.; COWLEY, S. W. H. Field and flow perturbations outside the reconnected field line region in flux transfer events - Theory. **Planetary and Space Science**, v. 35, p. 227–240, feb. 1987. 63

FARRUGIA, C. J.; RIJNBEEK, R. P.; SAUNDERS, M. A.; SOUTHWOOD, D. J.; RODGERS, D. J. A multi-instrument study of flux transfer event structure. **Journal of Geophysical Research**, v. 93, n. A12, p. 14465–14477, dec. 1988. 18

FARRUGIA, C. J.; SOUTHWOOD, D. J.; COWLEY, S. W. H. Observations of flux transfer events. **Advances in Space Research**, v. 8, p. 249–258, 1988. 28

FEAR, R. C. **Cluster multi-spacecraft observations of flux transfer events**. PhD Thesis (PhD) — University of London, University College London (United Kingdom, 2006. 17, 35, 40, 61

FEAR, R. C.; FAZAKERLEY, A. N.; OWEN, C. J.; LUCEK, E. A. A survey of flux transfer events observed by Cluster during strongly northward IMF. **Geophysical Research Letters**, v. 32, p. L18105, sep. 2005. 21, 56, 59, 61

FEAR, R. C.; MILAN, S. E.; FAZAKERLEY, A. N.; OWEN, C. J.; ASIKAINEN, T.; TAYLOR, M. G. G. T.; LUCEK, E. A.; RÈME, H.; DANDOURAS, I.; DALY, P. W. Motion of flux transfer events: a test of the cooling model. **Annales Geophysicae**, v. 25, n. 7, p. 1669–1690, 2007. Available from: <http://www.ann-geophys.net/25/1669/2007/>. 46, 55

GONZALEZ, W. D.; JOSELYN, J. A.; KAMIDE, Y.; KROEHL, H. W.; ROSTOKER, G.; TSURUTANI, B. T.; VASYLIUNAS, V. M. What is a geomagnetic storm? **Journal of Geophysical Research**, v. 99, n. A4, p. 5771–5792, apr. 1994. 11, 12

GONZALEZ, W. D.; MOZER, F. S. A quantitative model for the potential resulting from reconnection with an arbitrary interplanetary magnetic field. **Journal of Geophysical Research**, v. 79, n. 28, p. 4186–4194, oct 1974. 13, 19, 34, 38, 39, 47, 64

HAERENDEL, G.; PASCHMANN, G.; SCKOPKE, N.; ROSENBAUER, H. The frontside boundary layer of the magnetosphere and the problem of reconnection. **Journal of Geophysical Research**, v. 83, p. 3195–3216, jul. 1978. 1, 14

HOILIJOKI, S.; SOUZA, V. M.; WALSH, B. M.; JANHUNEN, P.; PALMROTH, M. Magnetopause reconnection and energy conversion as influenced by the dipole tilt and the IMF B_x. **Journal of Geophysical Research (Space Physics)**, v. 119, p. 4484–4494, jun. 2014. 61

KAWANO, H.; RUSSELL, C. T. Cause of postterminator flux transfer events. **Journal of Geophysical Research**, v. 102, n. A12, dec. 1997. 19, 56, 57

_____. Survey of flux transfer events observed with the ISEE 1 spacecraft: Dependence on the interplanetary magnetic field. **Journal of Geophysical Research**, v. 102, n. A6, p. 11307–11313, jun. 1997. 19, 21, 34

KHRABROV, A. V.; SONNERUP, B. U. Ö. DeHoffmann-Teller Analysis. **Analysis Methods for Multi-Spacecraft Data / Götz Paschmann and Patrick Daly (eds.). ISSI Scientific Reports Series, ESA/ISSI, Vol. 1. ISBN 1608-280X, 1998, p. 221-248**, v. 1, p. 221–248, 1998. 41

KING, J. H.; PAPITASHVILI, N. E. Solar wind spatial scales in and comparisons of hourly wind and ace plasma and magnetic field data. **Journal of Geophysical Research: Space Physics**, v. 110, n. A2, p. n/a–n/a, 2005. ISSN 2156-2202. Available from: <http://dx.doi.org/10.1029/2004JA010649>. 33

KIVELSON, M. G.; RUSSELL, C. T. **Introduction to Space Physics**. New York: Cambridge University Press, 1995. 862 p. ISBN 0-521-45714-9. 10

KOBEL, E.; FLUCKIGER, E. O. A model of the steady state magnetic field in the magnetosheath. **Journal of Geophysical Research**, v. 99, p. 23617, dec. 1994. 47

KOROTOVA, G. I.; SIBECK, D. G.; ROSENBERG, T. Geotail observations of fte velocities. **Annales Geophysicae**, v. 27, n. 1, p. 83–92, 2009. Available from: <http://www.ann-geophys.net/27/83/2009/>. 63, 66, 67, 77, 78, 79, 82

KUO, H.; RUSSELL, C. T.; LE, G. Statistical studies of flux transfer events. **jgr**, v. 100, p. 3513–3519, mar. 1995. 19, 40

LAKHINA, G. S. Magnetic reconnection. **Bulletin of the Astronomical Society of India**, v. 28, p. 593–646, dec. 2000. 7, 8

LEE, L. C.; FU, Z. F. A theory of magnetic flux transfer at the Earth's magnetopause. **Geophysical Research Letters**, v. 12, n. 2, feb. 1985. 19, 20, 41

LOCKWOOD, M.; WILD, M. N. On the quasi-periodic nature of magnetopause flux transfer events. **Journal of Geophysical Research**, v. 98, p. 5935–5940, apr. 1993. 18

PAPAMASTORAKIS, I.; PASCHMANN, G.; BAUMJOHANN, W.; SONNERUP, B. U. O.; LUEHR, H. Orientation, motion, and other properties of flux transfer event structures on September 4, 1984. **jgr**, v. 94, p. 8852–8866, jul. 1989. 41

PARKS, G. K. **Physics of space plasmas**: an introduction. Boulder, Colorado: Westview Press, 2004. ISBN 0-8133-4129-9. 7

PASCHMANN, G.; HAERENDEL, G.; PAPAMASTORAKIS, I.; SCKOPKE, N.; BAME, S. J.; GOSLING, J. T.; RUSSELL, C. T. Plasma and magnetic field characteristics of magnetic flux transfer events. **Journal of Geophysical Research**, v. 87, n. A4, p. 2159–2168, apr. 1982. 16, 17, 75

PASCHMANN, G.; PAPAMASTORAKIS, I.; SCKOPKE, N.; HAERENDEL, G.; SONNERUP, B. U. O.; BAME, S. J.; ASBRIDGE, J. R.; GOSLING, J. T.; RUSSELL, C. T.; ELPHIC, R. C. Plasma acceleration at the Earth's magnetopause - Evidence for reconnection. **Nature**, v. 282, p. 243–246, nov. 1979. 1, 14

PHAN, T. D.; HASEGAWA, H.; FUJIMOTO, M.; OIEROSET, M.; MUKAI, T.; LIN, R. P.; PATERSON, W. Simultaneous Geotail and Wind observations of reconnection at the subsolar and tail flank magnetopause. **Geophysical Research Letters**, v. 33, p. 9104–+, may 2006. 46

PRIEST, E.; FORBES, T. **Magnetic Reconnection**: MHD theory and applications. Cambridge: Cambridge University Press, 2000. 1, 5, 14

RIJNBEEK, R. P.; COWLEY, S. W. H.; SOUTHWOOD, D. J.; RUSSELL, C. T. Observations of reverse polarity flux transfer events at the Earth's dayside magnetopause. **Nature**, v. 300, p. 23–26, nov. 1982. 16, 51

_____. A survey of dayside flux transfer events observed by ISEE 1 and 2 magnetometers. **Journal of Geophysical Research**, v. 89, n. A2, p. 786–800, feb. 1984. 18, 61

RUSSELL, C. T.; BERCHEM, J.; LUHMANN, J. G. On the source region of flux transfer events. **Advances in Space Research**, v. 5, p. 363–368, 1985. 34

RUSSELL, C. T.; ELPHIC, R. C. Initial ISEE magnetometer results - Magnetopause observations. **Space Science Reviews**, v. 22, p. 681–715, dec. 1978. 1, 14, 15, 16, 17, 19, 27, 41, 51, 63

_____. ISEE observations of flux transfer events at the dayside magnetopause. **Geophysical Research Letters**, v. 6, p. 33–36, jan. 1979. 15

SAUNDERS, M. A.; RUSSELL, C. T.; SCKOPKE, N. A Dual-satellite study of the spatial properties of FTEs. In: E. W. Hones Jr. (Ed.). **Magnetic Reconnection in Space and Laboratory Plasmas**. Washington, D.C.: AGU, 1984. p. 145–152. 18

SCHOLER, M. Magnetic flux transfer at the magnetopause based on single X line bursty reconnection. **Geophysical Research Letters**, v. 15, n. 4, p. 291–294, apr. 1988. 20, 41

SHUE, J.-H.; CHAO, J. K.; FU, H. C.; RUSSELL, C. T.; SONG, P.; KHURANA, K. K.; SINGER, H. J. A new functional form to study the solar wind control of the magnetopause size and shape. **Journal of Geophysical Research**, v. 102, n. A5, p. 9497–9512, may 1997. 28, 35, 47, 64

SHUE, J.-H.; SONG, P.; RUSSELL, C. T.; STEINBERG, J. T.; CHAO, J. K.; ZASTENKER, G.; VAISBERG, O. L.; KOKUBUN, S.; SINGER, H. J.;

DETMAN, T. R.; KAWANO, H. Magnetopause location under extreme solar wind conditions. **Journal of Geophysical Research**, v. 103, n. A8, p. 17691–17700, aug. 1998. 28, 29

SIBECK, D. G.; KUZNETSOVA, M.; ANGELOPOULOS, V.; GLASSMEIER, K.; MCFADDEN, J. P. Crater FTEs: Simulation results and THEMIS observations. **Geophysical Research Letters**, v. 35, p. L17S06, may 2008. 18

SIBECK, D. G.; LIN, R.-Q. Concerning the motion of flux transfer events generated by component reconnection across the dayside magnetopause. **Journal of Geophysical Research**, v. 115, p. 4209, apr. 2010. 46, 47

_____. Concerning the motion and orientation of flux transfer events produced by component and antiparallel reconnection. **Journal of Geophysical Research**, v. 116, p. 7206, jul. 2011. 22, 23

SONNERUP, B. U. Ö.; GUO, M. Magnetopause transects. **Geophysical Research Letters**, v. 23, n. 25, p. 3679–3682, 1996. 41

SONNERUP, B. U. Ö. Magnetopause reconnection rate. **Journal of Geophysical Research**, v. 79, n. 10, p. 1546–1549, 1974. ISSN 2156-2202. Available from: <http://dx.doi.org/10.1029/JA079i010p01546>. 13, 47

SOUTHWOOD, D. J. Theoretical aspects of ionosphere-magnetosphere-solar wind coupling. **Advances in Space Research**, v. 5, p. 7–14, 1985. 63

SOUTHWOOD, D. J.; FARRUGIA, C. J.; SAUNDERS, M. A. What are flux transfer events? **Planetary and Space Science**, v. 36, p. 503–508, may 1988. 20, 21

TRATTNER, K. J.; MULCOCK, J. S.; PETRINEC, S. M.; FUSELIER, S. A. Probing the boundary between antiparallel and component reconnection during southward interplanetary magnetic field conditions. **Journal of Geophysical Research**, v. 112, p. 8210, aug. 2007. 34, 61, 81

WALTHOUR, D. W.; SONNERUP, B. U. Ö. Remote Sensing of 2D Magnetopause Structures. **Washington DC American Geophysical Union Geophysical Monograph Series**, v. 90, p. 247, 1995. 41

WALTHOUR, D. W.; SONNERUP, B. U. O.; PASCHMANN, G.; LUEHR, H.; KLUMPAR, D.; POTEMRA, T. Remote sensing of two-dimensional magnetopause structures. **Journal of Geophysical Research**, v. 98, p. 1489–1504, feb. 1993. 41

ZHANG, H.; KIVELSON, M. G.; ANGELOPOULOS, V.; KHURANA, K. K.; WALKER, R. J.; JIA, Y. D.; MCFADDEN, J.; AUSTER, H. U. Flow vortices associated with flux transfer events moving along the magnetopause: Observations and an mhd simulation. **Journal of Geophysical Research**, v. 116, n. A8, p. n/a–n/a, 2011. ISSN 2156-2202. Available from: <http://dx.doi.org/10.1029/2011JA016500>. 63, 67, 73, 78

ZHANG, H.; KIVELSON, M. G.; KHURANA, K. K.; MCFADDEN, J.; WALKER, R. J.; ANGELOPOULOS, V.; WEYGAND, J. M.; PHAN, T.; LARSON, D.; GLASSMEIER, K. H.; AUSTER, H. U. Evidence that crater flux transfer events are initial stages of typical flux transfer events. **Journal of Geophysical Research**, v. 115, p. A08229, aug. 2010. 66

neglecting the electron pressure gradient